TWO CAUSALITY CORRELATION TECHNIQUES APPLIED TO JET NOISE

by

ROBERT RACKL

Dipl. Ing., Technische Hochschule Graz, Austria, 1969

A THESIS SUBMITTED IN PARTIAL FULFILMENT OF

THE REQUIREMENTS FOR THE DEGREE OF

DOCTOR OF PHILOSOPHY

in the Department

of

Mechanical Engineering

We accept this thesis as conforming to the

required standard

THE UNIVERSITY OF BRITISH COLUMBIA

April, 1973

In presenting this thesis in partial fulfilment of the requirements for an advanced degree at the University of British Columbia, I agree that the Library shall make it freely available for reference and study. I further agree that permission for extensive copying of this thesis for scholarly purposes may be granted by the Head of my Department or by his representatives. It is understood that copying or publication of this thesis for financial gain shall not be allowed without my written permission.

Department of Mechanical Engineering

The University of British Columbia
Vancouver 8, Canada

Date April 10, 1973

Supervisor: Dr. Thomas E. Siddon

ABSTRACT

The thesis describes two techniques for investigating experimentally the generation of noise by turbulent jets using a recently developed method of cross correlation (Siddon, 7th ICA, Budapest 1971). The work is motivated by the need to reduce further the exhaust noise of modern jet transport aircraft. The aim is to provide new information on noise generation mechanisms, to stimulate future theoretical research by finding the distribution and character of noise sources, and to provide diagnostic tools for making noise surveys of turbulent flows in general. Experiments were conducted in an anechoic chamber using a cold model air jet at a Mach number of about 0.32.

The first method used, the image technique, cross correlates the pressure on a surface close to the jet with the radiated sound in the far field. This enables the deduction of the acoustic source strength per unit surface area which in turn gives an indication of the approximate location of the sound sources in the jet. The method is shown to be self consistent. The technique can be used in the investigation of supersonic jets as well; this is where its real power may lie.

The second method directly cross correlates the hydrodynamic pressure fluctuation in the turbulent jet flow with the far field sound allowing the deduction of the local acoustic source strength per unit volume and the associated power spectral density. A specially designed foil type sensor is used to measure the pressure fluctuations. A distribution of source strength over the jet for radiation at 45° to the jet axis is obtained, and is,

not unexpectedly, similar to the distribution of mean velocity shear. The axial distribution from a "slice" of the jet results by radially integrating the source strengths; it is in qualitative agreement with the results of other researchers. However, difficulties are encountered in making the method self consistent, i.e., the radiated sound as predicted by integrating over all the sources in the jet differs widely from the directly measured sound. Reasons for this discrepancy are given and solutions to overcome it are proposed.

A Fourier transform technique allows the deduction of the contribution to the spectrum of the radiated pressure from a unit volume of turbulence. Thus, the spectral character of the sound sources in the jet is obtained, although the above difficulties are reflected here as well.

The number of independent acoustic sources in the jet was estimated by calculating the average correlationvolume. The number turns out to be of the order of 100 to 200; this lies between two widely different estimates of about 3 and about 2500 given by other researchers.

ACKNOWLEDGEMENTS

This work was undertaken at the suggestion and under the supervision of Dr. T.E. Siddon who guided the research with patience and on whose experience the author often heavily relied.

Thanks go to summer students N. Michailoff for helping construct the anechoic facility, and to R. Nanson and K.F. Phoon for helping with the data acquisition.

Thanks also to Mr. John Smith of Richmond, BC, for fibreglassing the jet nozzle.

This research was sponsored by the National Research Council of Canada, under Grant No. 67-7106. The development of the pressure sensor received support by the Defense Research Board of Canada under Grant No. 66-9603.

NOTATION

(Special notations of the appendices are not included)

A	axial flow error coefficient
B	cross flow error coefficient
c_o	ambient speed of sound
C_p	static pressure error coefficient
C_{p_u}	C_p for u-component only
C	probe contamination ratio
D	nozzle diameter
db	decibels
h	distance jet axis to surface S
L	integral length scale
ℓ_i	unit vector perpendicular to surface S
m	meters
mm	millimeters
M	Mach number
n	number of incoherent sources in the jet
P	total static pressure (subscripts have same meaning as below for lower case p's)
p	fluctuating part of static pressure
p_o	ambient pressure
$p^{(0)}$	"pseudosound" pressure
$p^{(1)}$	acoustically propagating part of the pressure p
p_m	measured pressure
p_t	true pressure
p_s	surface pressure
p_∞	static pressure at jet exit

r	$r=\|\underline{x}-\underline{y}\|$; or radial distance from jet center line
rms	root mean square = $\sqrt{\overline{\ldots^2}}$
S	surface
S_I	imaging surface
S_{UA}	source strength per unit area
S_{UV}	source strength per unit volume
t	time
$\hat{t}$	retarded time
T_{ij}	Lighthill's stress tensor
u	component of velocity in axial direction
u_i	velocity vector
U_o	nozzle exit velocity
$\bar{U}$	mean velocity
V	volume of source region
V_c	correlation volume
V_{jet}	volume of sound producing jet turbulence
v, w	components of velocity perpendicular to axis of probe
x	$x=\|\underline{x}\|$
$x_i, \underline{x}$	space coordinate (often indicating the point of sound detection in the far field)
x_o	distance from nozzle exit to far field microphone
$y_i, \underline{y}$	space coordinate (usually used in the source region and/or as integration variable)
δ_{ij}	Kronecker Delta
θ	angle between jet axis and far field direction
ν	frequency
ρ	density
ρ_o	ambient density
τ	time delay
$\hat{\tau}$	retarded time delay

τ_{ij} viscous stress tensor

$\underline{\xi}$ space separation vector (ξ_1, ξ_2, ξ_3)

∇^2 $\partial^2/\partial y_i^2$ or $\partial^2/\partial x_i^2$

$\dot{}$ a dot on a quantity indicates derivation with respect to real time

$\overline{\quad}$ an overbar denotes time averaging

[...] replace in the expression within the brackets t by $\hat{t}=t-r/c_o$, or τ by $\hat{\tau}=\tau+r/c_o$, whichever is appropriate.

The jet Strouhal number is defined by $\nu D/U_o$

TABLE OF CONTENTS

FIGURES

I. FOREWORD AND HISTORICAL BACKGROUND

In this section, a brief review of aerodynamic noise research with emphasis on subsonic jet noise will lead up to the present work. Section II will say more on why the present work was undertaken and establish its proper place in the overall research effort. As with most disciplines of science, theory and experiments go hand in hand. Here, for reasons of clarity in the historical development, they are separated.

It was primarily the advent of new, very noisy propulsion methods at the end of World War II - the jet engine and the rocket - that stimulated the development of a new discipline, the study of sound generated aerodynamically. In his book "Acoustics of a Nonhomogeneous Moving Medium," Blokhintsev (1946) gave a thorough account of the interrelationship between acoustic and aerodynamic motions of a fluid. References to this work are rare in the English literature, probably because it was translated into English only 10 years after it was first published in Russian. Lighthill (1952) combined the basic equations of fluid dynamics (conservation of mass and momentum) in such a way as to show how to formulate an inhomogeneous form of the wave equation for the case of fluids disturbed by larger than acoustic perturbations:

$$\frac{\partial^2 \rho}{\partial t^2} - c_o^2 \frac{\partial^2 \rho}{\partial x_i^2} = \frac{\partial^2 T_{ij}}{\partial x_i \partial x_j} \qquad (1.1)$$

where:

ρ = density, t=time, c_o=speed of sound, x_i=space variable, T_{ij} = a tensor representing externally applied stresses (external from the point of view of the acoustician).

The solution to Eq.(1.1) is in the form of retarded potentials [see Eq.(1.2)]. Lighthill himself and then many other workers applied, enlarged and simplified the theory: Lighthill found that the sound intensity from a free aerodynamic flow should vary with the eighth power of some characteristic velocity and the square of some characteristic dimension (U^8D^2-Law). He considered turbulence as a source of noise and suggested a model for jet noise in terms of convected acoustic quadrupoles, replacing the stresses in the fluid, in an ambient fluid at rest (Lighthill 1954). Proudman (1952) estimated the properties of noise generated by isotropic turbulence, mainly assuming Gaussian models for the stochastic processes. This is, however, an oversimplified model for subsonic jet noise because the turbulence in the mixing region, far from being isotropic (see for instance Ribner 1965 or Fuchs 1972), is characterized by a large mean velocity gradient. Proudman was also the first to show that the far field noise from any flow can be viewed as being generated by the components of the velocity fluctuations in the direction of observation. Curle (1955) included the effect of surfaces in the flow; such surfaces could be real or just

hypothetical (e.g., so as to exclude an uninteresting or excessively complicated region from the field). He obtained the most general solution of Eq. (1.1):

$$\rho(\underline{x},t) - \rho_o = -\frac{1}{4\pi c_o^2}\int_S \ell_i\left[\frac{\partial \rho u_i}{\partial t}\right]\frac{dS(\underline{y})}{r} +$$

$$+\frac{1}{4\pi c_o^2}\frac{\partial}{\partial x_i}\int_S \ell_j\left[\rho u_i u_j + p\delta_{ij} - \tau_{ij}\right]\frac{dS(\underline{y})}{r} +$$

$$+\frac{1}{4\pi c_o^2}\frac{\partial^2}{\partial x_i \partial x_j}\int_V \left[T_{ij}\right]\frac{dV(\underline{y})}{r} \qquad (1.2)$$

where:

$\underline{x}$ points to the point of observation, ρ_o = ambient density, S = surface, ℓ_i = vector perpendicular to S at $\underline{y}$, $\underline{y}$ = space variable in the source region, $r = |\underline{x}-\underline{y}|$, u_i = velocity, p = pressure, τ_{ij} = viscous stress tensor, V = volume of sound generating flow, [...] means replace time t by the earlier time $t - r/c_o$.

Many aerodynamic sound problems can be solved approximately by straightforward application of Eq. (1.2) if simplifying assumptions are admissible. Such may be: the receiver is many typical wavelengths away from the source; the receiver is many typical source dimensions away; the motions at the source are "coherent", i.e., the particles move in unison over a certain region; heat conduction and viscosity are negligible; the flow is quasi incompressible. In the general case, however, Eq. (1.2) is an integral equation which has not been solved in closed form. Additional difficulties arise from the indeterministic, random

character of turbulence.

Powell (1964) suggested a different model for aerodynamic noise generation: A vortex flow and an acoustic dipole have a similar streamline pattern. He replaces the flow field by an equivalent dipole field. Although this theory seems attractive in view of Taylor's interacting vortices model of turbulent transfer mechanisms (Tennekes & Lumley 1972, section 3.3), it has not had a significant impact on jet noise research.

Perhaps the simplest concept of flow noise was developed by Ribner (1962), at first in 1958, elaborating on ideas also arrived at independently by Meecham & Ford (1958): The flow field is regarded as an array of dilating and compressing eddies bumping into each other. The pressure is separated into three parts, the first representing the ambient pressure independent of time, the second the hydrodynamic pressure fluctuation (or the "pseudosound"), the third the pressure disturbance due to acoustic waves traveling through the fluid. Ribner shows that:

$$p(\underline{x},t) \cong -\frac{1}{4\pi c_o^2} \int_V \left[\ddot{p}^{(o)} \right] \frac{dV(\underline{y})}{r} \qquad (1.3)$$

where p is the far field radiated sound and $\ddot{p}^{(o)}$ is the second time derivative of the pseudosound pressure. Although it may not be evident at first sight, this theory of "Sound from Fluid Dilatations" is consistent with the quadrupole concept and has been acknowledged as such (Appendix B of Lighthill 1963). A monopole type of source necessarily changes its volume when radiating sound, a quadrupole does not. In a free turbulent flow the net change in volume of all monopoles combined is zero, the

net radiation is not. Thus, four neighbouring monopoles can be thought of as making up a quadrupole.

At moderate subsonic Mach numbers the pseudosound is very well approximated by the static pressure fluctuations within the turbulence. If the latter could be measured, Eq. (1.3) could be evaluated. Section IV of this paper describes such an attempt.

Lighthill's U^8D^2-Law has been experimentally confirmed for turbulent jets over a wide range of subsonic Mach numbers. Other semi-empirical laws dealing with jet noise (Ribner 1958; Lilley 1958; Powell 1958) were derived using the self preservation properties of the turbulence in the mixing region (the first 4 to 5 diameters downstream of the nozzle) and of the fully developed flow further downstream. (The extent of the transition between these two regions is not yet clearly defined). Thus it was predicted that the power spectral density of the far field pressure should first increase with the square and then decrease with the inverse square of frequency; measured spectra show a similar shape and locate the peak Strouhal number (based on exit velocity, exit diameter and frequency) between 0.2 and 0.3 (Mollo-Christensen, Kolpin & Martucelli 1963, section 5), depending on the direction of radiation. With respect to the spatial distribution of sound sources it was predicted that the acoustic source strength of "slices" of the jet remains approximately constant in the mixing region and falls off very rapidly with the inverse seventh power of axial distance in the fully developed region. Although there is some supporting evidence, (see discussion in section IV) conclusive experimental confirmation is lacking. The present research not only attempts

to make this confirmation but will go one step further and show a way to measure the local acoustic source strength distribution over the jet volume.

In the experimental field[1] efforts concentrated first on surveying the radiated sound field from turbulent jets. It was found that lower frequency sound is radiated more or less omnidirectionally and that higher frequencies follow a heart shaped pattern with the dip on the downstream axis - the higher the frequency the more pronounced the dip of the heart. Parallel to that, the properties of the jet turbulence were studied in detail, such as mean velocities, turbulence intensities, and correlation lengths, with the aim of predicting the noise radiation from this data. The properties of self preservation mentioned above were discovered, but a quantitative noise prediction was not possible to an acceptable degree of confidence.

Although theoretical formalisms relating the turbulence properties to the radiated sound abound, very few experimenters have tried to verify those theories. Chu's (1966) work was pioneering. Using the third integral of Eq.(1.2) he was able to convert it into a form such that the mean squared radiated pressure in the far field depended on the fourth derivative of a velocity space-time correlation. He measured this correlation at

[1] A list of references of early experimental and theoretical work can be found in Lighthill (1962) or Ribner (1964). The list of references of the present paper attempts to include many of the experimental papers published since 1963 in the open English literature; the citations are preceeded by a "*". A more recent list of references of theoretical work can be found in Doak (1972).

a point 4 diameters downstream for different angles of sound radiation and estimated the overall mean squared acoustic pressure; the agreement was reasonable but not totally satisfying for two reasons: 1) It would have been prohibitively time consuming to survey the complete jet (modern multi channel correlators were not available at the time); 2) taking the fourth derivative of an experimentally obtained function was subject to a considerable degree of uncertainty, as the results varied with the method of curve fitting used.

More recently, Siddon has introduced a means for tying together the far field and turbulence properties by implementing the "causality correlation technique" (Siddon 1970, 1971b). Any source fluctuation appearing in Eq. (1.2) or (1.3) can be viewed as the basic sound generator. If it can be measured and the resulting sound in the far field is monitored simultaneously, the two signals may be cross correlated; in this manner, the acoustic strength of the sources can be deduced quantitatively. The word "causality" is used because the process of the cause (the source fluctuation) giving rise to the effect (the radiated sound) provides the basis for the measurement. The technique has been applied to the acoustic radiation from small airfoils embedded in a flow (Clarke & Ribner 1969; Siddon 1970, 1973a) and to jet noise by Lee (1971) and the present work (see further discussion in section II).

Although the mathematical theories have not been able to give clear cut guidance for designing quiet jet engines, substantial noise reductions have been achieved, mainly by applying the U^8D^2-Law. Reductions of the jet exit velocity with

corresponding increase of the nozzle diameter and mass flow led to the evolution of high bypass ratio fan engines. Significant noise reductions with increased efficiency of performance resulted. A very large number of passive noise suppression devices were proposed and tried out. In many cases the insertion of a suppressor decreased the noise from the jet turbulence but not the overall noise. The interaction of the flow with the device generated additional dipole noise such that minimal net noise reduction resulted. Only two suppressor configurations were found to be acceptable, in terms of their acoustic benefit/ aerodynamic penalty ratio. These are the corrugated nozzle and the multitube nozzle. Even these, however, produce less than the expected noise reduction, if one defines noise in terms of subjectively weighted indices such as PNdb or dbA. They are designed with the notion of reducing the intensity of turbulence or the amount of velocity shear, i.e., to make the mixing process smoother, mainly by entraining air not only on the outside but also on the inside thereby breaking up the mixing region. Their exact functioning is still subject to speculation. It is felt that refractive shielding may play a significant role in their acoustical behaviour as well. The two methods presented in this paper may be used as tools both to further our understanding of the noise generation process and as aids in the design and improvement of such noise suppression devices.

Although the noise from commercial jet transport aircraft has been reduced by slightly more than 20 PNdb in the past two decades people continue to be annoyed in the vicinity of airports as the number of flyovers increases. We can expect this increase to continue and therefore cannot stop trying to reduce jet noise.

II. PRESENT TRENDS AND INTRODUCTION TO SECTIONS III AND IV.

Present theoretical efforts seem to be guided by the findings of the Aerodynamic Noise Symposium at Loughborough in September 1970 (Fisher & Lowson 1971; Lowson 1971). Effects of convection of the sources on the radiated sound field are adequately understood and can be cast into mathematical form. Effects of refraction are more difficult to deal with: We have to try to understand the mechanisms of sound generation and propagation in and through a shear layer. The reader is referred to Doak's excellent review article (1972) in which new approaches are suggested: He infers that Lighthill's theory was a big step forward, but "... was specifically designed to deliberately avoid all questions of the interdependencies among acoustic, turbulent and thermal types of motion ...". Recent theories by Crow, Doak and Lilley (among others) are discussed that go back to the origins of acoustics and aerodynamics, i.e., the works of Stokes, Kirchhoff and Rayleigh. In Doak's opinion, a combination of these theories will take us another big step forward.

The Loughborough Symposium also concluded "... it appears that the existence of a significant degree of order in jet turbulence is confirmed ..." (Fisher & Lowson 1971, p. 594). This statement was based on experimental evidence presented at the Meeting by Lau, Fisher & Fuchs, and by Crow & Champagne. However, opinions still diverge widely on this subject. The supporters of

the orderly structure hypothesis are making a strong case for their view by publishing substantial amounts of existential evidence (Crow & Champagne 1971; Davis 1971; Lau, Fisher & Fuchs 1972; Fuchs 1972; Fuchs & Michalke 1971). Visualization techniques and space correlations indeed seem to indicate that coherent large scale structures convect for many diameters downstream in the jet before losing their identities. This coherence is easily recognizable at small Reynolds numbers (after transition from the laminar shear layer); it is not so well recognizable as the Reynolds number increases but shows also for Reynolds numbers over $2*10^5$ which is of the order of the Reynolds number in the experiments described in this paper.

By analogy, one may consider the turbulence structure in a wake behind a bluff cylinder: At moderate Reynolds numbers the Karmann Vortex Street develops, resulting in a strong periodic contribution to the spectrum. When the Reynolds number is increased this periodicity gets buried in a broad band spectrum, characteristic of a wide range of turbulence scales. The turbulence in a jet may behave similarly; the shape of the pressure spectrum (Fig.4-27) does not show a discrete periodic component, but a broadly peaked energy distribution is evident.

Even though, there may exist an orderly structure in jet turbulence it is not necessarily of direct consequence to the radiated noise. It is well established that it is the rate of decay of the convecting velocity structure (whether turbulent or periodic) that controls the noise emission. In fact, the radiation depends on the second time derivative of the source fluctuation quantity and is thereby biased to higher frequency

content than the turbulence proper. In Lee's (1971) and the present work, for low speed jets, not only was no evidence discovered of an orderly structure pertinent to the jet noise radiation, but the results point to a contrary hypothesis of a large number of independently radiating sources.

A "Simple Pressure Source Model of Jet Noise" has been put forward by Scharton & White (1972). While the idea of more or less independent sources is retained the paper also draws some support from the orderly structure hypothesis by postulating a small number of large scale pressure sources (of the order of 3). These are presumed to develop close to the nozzle exit, then fluctuate and convect downstream. The present author feels that the resulting empirical model may be suited for prediction of the overall jet noise radiation, but that it does not provide detailed information on the noise generating mechanisms. A more thorough critique can be found in section IV.

The causality correlation technique as implemented by Lee (1971, also Lee & Ribner 1972) uses the velocity fluctuations as the basic emitter of sound. The velocity was measured with a hot film anemometer whose frequency dependent phase response was suspected to be quite different from that of the microphone measuring the sound in the far field. It was therefore necessary to perform the cross correlations in narrow frequency bands instead of in a broad band covering all frequencies of interest, thus increasing substantially the amount of experimental work. Citing from the abstract of Lee & Ribner (1972): (Their work) "... yielded the relative intensity and spectrum of the noise originating from unit volume of a jet (35 locations) and received

at a far field point ($r=96D, \theta=40°$); this in turn led to the relative emission of successive "slices" of a jet versus axial distance x over the measurement range ($1D \leq x \leq 7D$). Qualitative agreement was found with Ribner's x^0-Law, and the spectral peaks for each slice were located in frequency essentially as predicted by Powell (1959)." It was also reported that the total effective number of uncorrelated noise-producing eddies is on the order of 2500, in sharp contrast to the number 3 reported by Scharton & White (1972). In section IV of the present paper the number of incoherent sources is estimated to be on the order of 100 to 200. There, it is also discussed how extraneous acoustic or electronic noise and bandwidth can substantially increase or decrease the apparent value of this number, introducing a source of ambiguity.

Little recent progress has been made in the area of noise suppression devices. Arndt (Barefoot & Arndt 1972) is experimenting with screens perturbing the jet and Scharton & White (1972) have tested a suppressor consisting of five staggered concentric tubes filling the potential core of the jet. In both cases some noise reduction is reported, however, the associated performance penalty (e.g. thrust reduction) is not well documented, and indeed is expected to be rather high.

The techniques presented here do not have as their objective noise reduction as such. Rather, the aim is on the one hand to increase the knowledge of noise generating mechanisms in turbulent flows and maybe provide some stimulation for future theoretical work; on the other hand the techniques developed can be used as diagnostic tools in surveying more complicated flow noise phenomena and in designing and optimizing noise

suppressors.

The image technique described in section III cross correlates the pressure on a surface close to the jet with the far field noise allowing the deduction of the surface source strength distribution. This in turn gives an indication of the approximate location of the acoustical sources in the jet, at least in an axial sense. The advantage of having the flow undisturbed by a probe is traded off against a loss of spatial resolution. The technique is shown to be self consistent and may have applications as a quick and easy to use tool in the design of noise suppressors. Also, it is not limited to cold, subsonic flows and can be used in the investigation of hot and/or supersonic flows where it is quite difficult if not impossible to insert a probe.

The causality correlation technique described in section IV forms the main body of this thesis. It complements and extends Lee's (1971) work. Instead of the turbulent velocity fluctuations the fluctuating turbulent pressures are taken as the basic noise emitters. Pressure, being a nondirectional scalar quantity, is in principle more attractive to the experimenter than velocity. Difficulties arise when one tries to measure turbulent pressure fluctuations as the local velocity field produces additional pressures at the probe, thus creating a pressure error. The development of a unique airfoil type pressure sensor as a means of avoiding those errors is reported. The sensor is then used to perform the pressure causality correlations by scanning the jet radially at different downstream locations. Thus the local source strength per unit volume and the associated power spectral

density are deduced. The correlations are done in broad band as both transducers are condenser microphones with matched phase characteristics. Difficulties are encountered in making the technique self consistent, although results agree qualitatively with the results of Lee (1971) and other workers.

The thesis hopes to establish that the two methods presented have experimental advantages alluded to above and are worthwhile to be further developed.

III. IMAGE TECHNIQUE

This technique was born from a desire to avoid inserting probes of any kind into the flow. Instead, a rigid plane surface is placed in the near field of the flow. It will be shown that the sound reflected from the surface is exactly equivalent to the noise radiation from an identical "image" flow behind the surface if this surface were removed. The derivation follows the ideas of A. Powell (1960) who developed the imaging principle with boundary layer noise in mind. Here, it is applied to jet noise. In addition, the present work employs the causality principle by cross correlating the radiated sound in the far field with the pressure on the imaging surface. This pressure is thought of as a "cause" or source of the sound in the sense that it is representative of a certain limited region in the jet flow, the extent of which will be discussed. The acoustic source strength per unit surface area will be deduced. Looking at the "acoustic footprint" the flow leaves on the surface allows some conclusion on the distribution of noise sources in the image flow behind the surface.

3.1 Imaging System. We start with Lighthill's (1952) equation for aerodynamic noise [Eq. (1.1) rewritten]:

$$\nabla^2\rho - \frac{1}{c_o^2}\frac{\partial^2\rho}{\partial t^2} = -\frac{1}{c_o^2}\frac{\partial^2 T_{ij}}{\partial y_i \partial y_j} \qquad (3.1)$$

where $T_{ij} = \rho u_i u_j - \tau_{ij} + (p - c_o^2\rho)\delta_{ij}$

Using the isentropic assumption

$$p(\underline{x}) = (\rho(\underline{x}) - \rho_o)c_o^2 \qquad (3.2)$$

(which is good in the acoustic far field and in the source region as well, if entropic fluctuations are not present) and neglecting at the surface all but the pressure stresses, the solution for the radiated sound becomes:

$$4\pi\, p(\underline{x},t) = \frac{\partial^2}{\partial x_i \partial x_j}\int_{V_o}\frac{1}{x}\left[T_{ij}\right]d^3\underline{y} + \frac{\partial}{\partial x_i}\int_{S_1}\ell_i\frac{1}{x}\left[p_s\right]dS \qquad (3.3)$$

where the brackets indicate evaluation at the earlier time

$$t - |\underline{x}-\underline{y}|/c_o$$

The first integral is the direct contribution from the jet; the second integral represents the sound reflected from the surface. p_s is the surface pressure. ℓ_i is the outward normal to the surface S_1 (Fig.3-1). If S_1 were vibrating or translating a third integral would appear [as indicated in the more general Eq.(1.2)], but this is not the case for the rigid wall assumed here.

In order to establish the image system we add a jet which is the exact instantaneous mirror image of the first jet (Fig.3-1). The surface S_1 is the plane of symmetry. Whether S_1 is a real rigid surface or a hypothetical plane does not matter because the adding of the instantaneous mirror image with S_1 removed will

produce exactly the same boundary conditions by symmetry, as with S_1 in place as a real rigid boundary. Therefore the sound field radiated from the image jet is exactly equal to the sound field reflected from S_1. With the quantities associated with the image system denoted by primes we can write:

$$\frac{\partial}{\partial x_i}\int_{S_1} \ell_i \frac{1}{x}\left[p_s\right] dS = \frac{\partial^2}{\partial x_i \partial x_j}\int_{V_o'} \frac{1}{x}\left[T_{ij}'\right] d^3\underline{y} \qquad (3.4)$$

If x is large (far field approximation) terms like

$$\frac{\partial}{\partial x_i}\int \frac{1}{x}\left[\cdots\right] \quad \text{are replaced by} \quad -\frac{x_i}{c_o x^2}\int \frac{\partial}{\partial t}\left[\cdots\right] \qquad (3.5)$$

(see Lighthill 1952 or Ribner 1964)

Eq. (3.3) becomes:

$$4\pi\, p(\underline{x},t) = \frac{x_i\, x_j}{c_o^2\, x^3}\int_{V_o}\left[\frac{\partial^2 T_{ij}}{\partial t^2}\right] d^3\underline{y} - \frac{x_i}{c_o x^2}\int_{S_1}\ell_i\left[\frac{\partial p_s}{\partial t}\right] dS \qquad (3.6)$$

where we can say that the second integral represents either the sound reflected from the surface S_1, or [by Eq. (3.4)] the sound radiated from the image jet. In what follows it is shown how information on the noise sources in the image jet (approximate spatial distribution and spectral character) can be obtained. Since the image jet is an instantaneous mirror image the same information is good for the real jet. However the results may not be identically valid for a single isolated jet radiating into unbounded space as the insertion of the surface S_1 may slightly change the structure of the jet (see second paragraph of section 3.3).

3.2 Cross Correlation Formalism. Equation (3.6) is multiplied by the far field sound pressure p at a different time t', and then a time average is performed. Under the assumption of statistical stationarity the result will be independent of the absolute time and depend only on the time delay $\tau = t - t'$ (Crandall & Mark 1963, section 1.5). The overbar denotes a time average:

$$4\pi\,\overline{pp}(\tau) = \frac{x_i\,x_j}{c_o^2 x^3}\int_{V_o}\overline{\left[\frac{\partial^2 T_{ij}}{\partial t^2}\right]p}\;d^3\underline{y} - \frac{x_i}{c_o x^2}\int_{S_1}\ell_i\overline{\left[\frac{\partial p_s}{\partial t}\right]p}\;dS \qquad (3.7)$$

where, again, the second integral could be replaced by

$$\frac{x_i\,x_j}{c_o^2 x^3}\int_{V_o'}\overline{\left[\frac{\partial^2 T_{ij}'}{\partial t^2}\right]p}\;d^3\underline{y} \qquad (3.8)$$

the contribution from the image. This is the part we are interested in:

$$\overline{pp}(\tau)_{\text{image only}} = \frac{\cos\theta}{4\pi c_o x}\int_{S_1}\left[-\frac{\partial}{\partial\tau}\,\overline{p_s p}\right]dS \qquad (3.9)$$

where $x_i\,\ell_i = -x\cos\theta$ (Fig.3-1). Use is made of the fact that differentiation with respect to time under the time average can be converted into differentiation with respect to time delay if the processes are statistically stationary (Crandall & Mark, 1963, section 1.6). The brackets now mean evaluation at the retarded time delay (Siddon 1973a)

$$\tau = \hat{\tau} = |\underline{x}-\underline{y}|/c_o \qquad (3.10)$$

where $\underline{y}$ indicates the point where p_s is detected.

Notice that the Lighthill stress tensor T_{ij} has disappeared. Its complicated structure does not concern us here.

Writing Eq. (3.9) in differential form and setting $\tau = 0$:

$$\frac{d\overline{p^2}}{dS} = \frac{-\cos\theta}{4\pi c_o x} \left[\frac{\partial}{\partial \tau} \overline{p_s p} \right]_{\tau = \hat{\tau}} \qquad (3.11)$$

Eq. (3.11) gives the portion of the radiation from the image jet associated with a unit area of the surface S_i at the point where p_s is detected. We can regard this as a measure of the "local" acoustic source strength in the image jet. Section IV will describe a method of determining the actual distribution of source strength in the flow by measuring an approximation of T_{ij}. Here we are content with a loss of spatial resolution but gain three advantages:

1) It is not necessary to insert a probing device into the flow, a simple measurement of surface pressure p_s is sufficient.

2) Only one time derivative is involved in Eq. (3.11); Eq. (3.7) indicates two time derivatives and the work of Chu (1966) required taking a fourth derivative of a correlation. Numerical errors increase with the order of the derivative whether the differentiation is done by analog circuitry before the correlating process or afterward by digital methods.

3) No further assumptions have been made about the nature of the flow, the isentropic assumption (3.2) pertains only to the radiated sound in the far field. The method could therefore be used for instance in the investigation of noise from hot and/or supersonic jets. At higher than low subsonic Mach numbers or with large differences between the densities of the source fluid and the ambient air, the far field microphone would have to be placed

such that the sound reflected from the surface towards the microphone would not pass again through the flow field where it would be refracted or even shielded, as could be the case with supersonic jets.

3.3 Experiments. The experiments were conducted in an anechoic room. The setup was as shown in Fig.3-1. The jet diameter was 38.1 mm (1.5 inches), the Mach number at the nozzle exit about 0.32. Fig.3-2 shows spectra of the acoustic pressure in the far field at θ=45° to the jet axis; one for the jet alone (a), the other with the wall installed behind the jet (b). They peak at a Strouhal number of about 0.2 (corresponding to about 700 Hertz). The "bumpy" nature of (a) is thought to be due to the room not being completely anechoic at all frequencies. (b) is of course larger as it represents both the direct and the reflected jet noise. That (b) contains more than one pronounced peak is expected as the direct and the reflected sound waves will - depending on their frequency - tend to enhance or cancel each other. This is a well known difficulty arising when jet engines are tested near a hard ground plane.

The distance from the jet center line to the surface was a compromise between conflicting requirements: On the one hand the surface should be close to the flow in order to increase the spatial resolution. On the other hand the surface has to be far enough away from the flow in order to avoid the Coanda effect; i.e., the tendency of the jet to attach to nearby surfaces because the fluid between the jet and the surface is being dragged along by entrainment, decreasing the pressure and thereby

drawing the jet towards the surface. A very close surface may also interfere with the entrainment of air into the jet so that its developed structure may differ substantially from that of a single isolated jet. Furthermore, direct interaction of the flow with the surface must be avoided; this would introduce unwanted noise by violating the assumption that surface shear stresses are unimportant [this assumption is implicit in Eq.(3.3)]. In recognition of these limiting factors the distance between the surface and the jet center line was chosen to be 197 mm (little more than 5 nozzle diameters).

Most of the surface S_1 consisted of a 0.5 inch thick sheet of plexiglass. The surface pressure p_s was measured using a Bruel & Kjaer 1/4-inch microphone (type 4136) connected to the surface by a short 0.020 inch diameter hole (Fig.3-3). The resonant frequency of the Helmholtz resonator formed by the hole and the small cavity in front of the microphone diaphragm was sufficiently high above the frequencies of interest in the jet noise.

The far field microphone was placed for most of the experiments at 45° to the jet axis at a distance of about 1.9 meters from the jet orifice. Some data was also obtained at 60° and 90°.

The surface pressure p_s was measured at many points on the surface and cross correlated with the signal from the far field.

The signal processing equipment and the anechoic room were the same as will be described in section 4.4.

Fig.3-4 shows an example of a correlation function $\overline{p_s p}(\tau)$. Eq. (3.11) requires taking the derivative of this function at the delay time $\tau=|\underline{x}-\underline{y}|/c_o$ which was done on a digital computer. The curve also exhibits a "precursor" the existence of which is explained as follows:

The flow noise radiates in all directions, including to the point where the field microphone is located and to the point on the wall where p_s is measured; in the vicinity of the time delay corresponding to the difference in sound travel times from the source flow to these two points the signals are somewhat coherent and a secondary correlation "blip" results. In order to separate this precursor from the part of the correlation function we are interested in (the vicinity around $\tau=|\underline{x}-\underline{y}|/c_o$) one must not put the surface S_1 too close to the flow; the further the surface is from the flow the smaller the difference in sound travel times, and the more the precursor is moved to the left on the time delay axis. However, the presence of the precursor does not violate the theory and, in principle, can be ignored.

3.4 Nondimensionalization. (See also Appendix B) In order to make the results independent of the particular experimental setup chosen and to make them comparable with the results of other workers the measured quantities are nondimensionalized using characteristic lengths, density, and velocities. It is well established (Lighthill 1952) that the far field acoustic pressure of a subsonic air jet issuing into a medium of identical gas

properties obeys the following dimensional similarity:

$$p \propto \rho U_o^4 D c_o^{-2} x^{-1} \tag{3.12}$$

Therefore the acoustic pressure p was nondimensionalized by

$$2(0.5\rho U_o^2) M^2 D/x \tag{3.13}$$

M is the jet exit Mach number, x is the distance to the field point.

p_s is a near field pressure at the plane surface; its variation with U_o was determined by experiment. A point six jet diameters downstream from the intersection of the exit plane with the rigid surface was chosen as representative. In Fig.3-5 H is the dynamic head at the nozzle exit in meters of water. H is proportional to U_o^2. At the chosen location it turned out that p_s varied as H^2 or U_o^4, i.e. it obeyed the same similarity relation given in Eq.(3.12) as does p. Therefore p_s was nondimensionalized by the same quantity (3.13) except that x was replaced by h, the distance of the surface from the jet center line. Time was nondimensionalized by D/U_o. More details are to be found in Appendix B.

3.5 Results. Fig.3-6 shows the nondimensional source strength distribution on the rigid surface. The actual quantity plotted is: (for rationale see Appendix B)

$$S_{UA} = \frac{-\cos 45^\circ \left[\frac{\partial}{\partial \tau} \overline{p_s p} \right]_{\tau=\hat{\tau}}}{\left\{ 2(0.5\rho U^2) M^2 \right\}^2 \frac{U_o}{D} \frac{D}{x_o} \frac{D}{h}} \tag{3.14}$$

The strongest sources appear to be concentrated in an area 4

to 14 diameters downstream of the nozzle exit. It would be convenient to be able to use the reflection principle from acoustic ray theory, as indicated in Fig.3-9, in order to trace back where the sound has emanated from the jet. Strictly speaking, the reflection principle can only be applied if the reflecting surface is much larger than a typical wavelength, if it is truly rigid, and if the incident acoustic disturbance has far field character (i.e., if the wave fronts are approximately plane). The first two requirements are well fulfilled by the present experimental setup. The third is not so well fulfilled as the surface pressures p_s are measured in the transition region between near field and far field. (Fig.4-18 shows how the pressure fluctuations vary with distance from the jet center line; h~5D is in an area where the near field changes into the far field.) At 6 diameters, p_s behaves quite like a far field pressure, as mentioned before (Fig.3-5), but there is some scatter in the data.

Fig.3-7 and Fig.3-8 show equal source strength contours for angles θ (far field direction to jet axis) of 90° and 60°. This data was taken early in the research before certain refinements in the electronics were introduced. It is however useful in a qualitative way supporting the ray acoustic argument: The location of the strongest sources apparently moves from 2 diameters to 12 diameters as θ goes from 90° to 60°. Such a shift is what would be expected if ray theory were applicable.

It appears therefore that one can "borrow" the ray acoustics argument when discussing the problems of spatial resolution afforded by the image method. Fig.3-9 illustrates the

hypothetical "zone of influence": the region of the jet that will predominantly contribute to the source strength on the surface where p_s is measured. The zone of influence is cone shaped; the angle of aperture of the cone is however left to speculation. The angle will be smaller for higher frequencies since the reflection argument becomes more and more valid as the wavelength decreases. This pertains both to the reflection mechanism itself and to the far field condition. The jet noise spectrum peaks at about 700 Hertz. This corresponds to a wavelength of about 0.5m which is larger than h=0.197m. For this frequency one could therefore not expect a very narrow angle of aperture. Supersonic flows generally produce much higher frequencies. There, the reflection argument should be much more applicable.

Using the reflection argument regardless of whether it is strictly applicable or not, the actual sound producing region will be found to be 2 to 8 diameters downstream of the exit plane. This is consistent with the findings of other researchers (Ribner 1958, Lee 1971, Dyer 1959, Powell 1959, Lilley 1958, et al.). This statement does not, however, add much new insight into the character of noise production from turbulent jets. The method described here is presented in order to show its feasibility in the study of flow noise. In particular, as already mentioned above, the derivation of the image system does not contain any assumption about Mach number except an implicit disregard of refractive effects due to temperature or velocity gradients along the path of the sound. The method could therefore be used to study the noise generation from supersonic flows where it is still more difficult if not impossible to locate the noise

sources by probing the jet itself.

Maestrello & McDaid (1970) have advanced a different image technique for determining jet noise characteristics. There, a means is shown of locating sound sources by determining the directions where sound waves are coming from by a complex Fourier analysis of two point space-time-correlations of the surface pressure on a rigid surface in the vicinity of the jet. The theory is quite complicated, and so are the computations to process the data. Some results are presented but not enough to enable a conclusion on the distribution of sound sources. The paper reads as if the authors first expected to obtain detailed information on sound source distribution in the jet but later encountered problems of spatial resolution similar to the ones in the present work. The following quote from the Maestrello & McDaid paper (1970) equally applies to the technique developed here: "... sound undergoes convection and scattering between the time it is generated and the time it leaves the turbulence of the jet. Thus the point of generation could be farther upstream ..." Only a technique probing the flow [such as Chu (1966), Lee (1971), section IV of the present paper] can shed more light on this problem. All an image technique can determine at the most is the direction from where the sound waves are coming when they impinge on the reflecting surface.

An advantage of Maestrello & McDaid's (1970) approach is that spectral information is not only obtained very easily, but is implicit in the method. However, in order to gain some significant insight, the amount of experimental work required is quite large. In the present approach one would think it is easy

to obtain spectral information by computing the Fourier transform of Eq.(3.9) resulting in the contribution to the overall power spectral density from a unit surface area at the point where the surface pressure is measured. Unfortunately, the precursor (discussed in section 3.3 and shown in Fig.3-4) superposes itself on the cross correlation function and makes the Fourier transform difficult to interpret: Eq.(3.11) gives the contribution from the image only. The precursor does not affect significantly the derivative of $\overline{p_s p}(\tau)$ at $\tau=r/c_o$ because it lies far enough to the left on the time delay axis. The operation of Fourier transforming involves the complete record of $\overline{p_s p}(\tau)$, including the precursor. Attempts to perform this Fourier operation showed that the transform became negative for some frequency ranges. This occurs because of the constructive and destructive interference effects at certain frequencies as already discussed in section 3.3. In view of this ambiguity ways of obtaining quantitative spectral information were not further explored in the image technique.

Nevertheless, some qualitative spectral information can be obtained by inspecting the cross correlations: Fig.3-10 shows how they change in shape as one moves downstream in the jet. It can be seen that the characteristic frequencies are higher closer to the nozzle exit (the correlation has high curvatures at the peaks and the distance between zero crossings is small) and becomes lower further downstream (lower curvature and larger distance between zero crossings). This behaviour is of course expected as the turbulence scales grow in the downstream direction.

Fig.3-11 shows the distribution of the root mean squared

near field pressure over the surface. It shows a peak in the same area as Fig.3-6, but the tails decrease much less rapidly, both in the direction of the jet flow and perpendicular to it. An attempt to identify sound sources that way would be much less successful. The zone of influence on p_s alone is the whole hemisphere and not the narrow cone shaped region of the image cross correlation technique (which sort of "points" to the source of sound).

When the source strength per unit area is integrated over transverse "strips" of the surface, i.e., in the direction perpendicular to the jet axis at each axial location, Fig.3-12 results. It has a pronounced peak. Using the reflection argument, by tracing back from the peak location of 10 diameters, the strongest acoustic sources would be located between 4 and 5 diameters from the nozzle exit. This is in close agreement with other results (e.g. Ribner 1958, 1962; Dyer 1959).

3.6 Check. Eq.(3.9) can be used as a check of the method: When the "stripwise" source strength of Fig.3-12 is integrated along the axis, the surface integral of Eq.(3.9) can be evaluated, for $\tau=0$. The left hand side is calculated from a direct measurement of the jet noise without the reflecting surface. In order to represent the radiation from the image jet a correction was made for the difference in distance to the far field microphone between the real and the image jet. The integration on the right hand side was carried out graphically. With the nondimensionalization done as indicated in section 3.4 and in Appendix B, the directly measured value (left hand side) becomes

$$\frac{\overline{p^2}}{\left\{2\,(0.5\rho U_o^2)\,M^2\,D/x\right\}^2} = 0.177 \times 10^{-5} \qquad (3.15)$$

and the integrated value (right hand side) is $0.147*10^{-5}$. This corresponds to a difference of only 0.8 db. Apart from numerical errors in the computation of the correlation functions and their derivatives, sources of uncertainty are the finite extent of the surface and its imperfect rigidity (recalling that most of the surface consists of a 0.5 inch thick sheet of plexiglass). This check on internal consistency lends further confidence in the use of causality correlation techniques to spatially resolve complex source distributions (see also Siddon 1973a).

IV. CAUSALITY CORRELATION TECHNIQUE

4.1 Introduction

This technique was developed in order to probe the jet flow in such a way as to obtain the spatial distribution and characteristics of the elementary acoustic sources. Use is made of a recently developed causality correlation technique (Siddon 1966, 1970, 1971b, 1973a; Clarke & Ribner 1969; Lee 1971; Lee & Ribner 1972; Siddon & Rackl 1971; Rackl 1972b). As mentioned in section I the fluctuating pressures are taken as the basic noise emitters. By computing the cross correlation between these pressures and the radiated acoustic pressure in the far field quantitative information on the acoustic source distribution can be obtained.

Section 4.2 summarizes the underlying theory and treats the concept of causality correlations, spectrum from a unit volume, and correlation volume.

The experimental setup was as shown in Fig.4-1: As in section III, a cold, circular (1.5 inch diameter), subsonic jet (Machnumber about 0.32) discharged into an anechoic room. The turbulent pressures were measured by a specially developed airfoil type pressure sensor (described in detail in section 4.3). The far field pressure was monitored by a 1/2-inch microphone. The cross correlations of the two signals were computed on a hybrid signal correlator. Typical correlation

functions are shown in Fig.4-22a. More details will be found in section 4.4.

The remaining sections after 4.4 show how the data was reduced and discuss the results. Comparisons are made with results of other researchers. At least qualitative agreement is achieved. Difficulties are encountered in trying to make the method quantitatively self consistent. Possible explanations are given. Once the viability of the method has been demonstrated it becomes a diagnostic tool for the investigation of other flows. It could, for instance, be used in the study of the effectiveness of various jet quietening devices.

4.2 Theory

4.2.1 Fluid Dilatations. The theory is based on Ribner's (1962) ideas on viewing the turbulent flow as an array of acoustic monopoles generated by a quasi-incompressible and isentropic flow. For subsonic flows, Lighthill's wave equation (1.1) can be re-written in the approximate form:

$$\frac{1}{c_o^2}\frac{\partial^2 p}{\partial t^2} - \nabla^2 p = \frac{\partial^2 \rho u_i u_j}{\partial y_i \partial y_j} \qquad (4.1)$$

The right hand side of Eq.(4.1) may be regarded as a forcing term of the wave equation for p. Acoustically, it represents a distribution of acoustic quadrupoles embedded in a medium at

rest. It can be converted into a corresponding monopole field ("dilatations") by splitting the pressure disturbance into two parts:

$$p - p_o = p^{(0)} + p^{(1)} \tag{4.2}$$

where:

p = instantaneous static pressure

p_o = local time average static pressure

$p^{(0)}$ is defined by

$$-\nabla^2 p^{(0)} = \frac{\partial^2 \rho u_i u_j}{\partial y_i \partial y_j} \tag{4.3}$$

It has been shown that $p^{(0)}$ is the actual perturbation pressure within an exactly incompressible flow and is a good approximation for $M^2 \ll 1$ (see Kraichnan 1956 and Ribner 1962).

$p^{(1)}$ is the part of the pressure associated with the propagation (not the generation) of acoustic waves. The relationship of $p^{(0)}$ and $p^{(1)}$ is expressed in the "dilatation equation" which results after combining Eq. (4.1), Eq. (4.2), Eq. (4.3):

$$\frac{1}{c_o^2} \frac{\partial^2 p^{(1)}}{\partial t^2} - \nabla^2 p^{(1)} = -\frac{1}{c_o^2} \frac{\partial^2 p^{(0)}}{\partial t^2} \tag{4.4}$$

The right hand side of Eq. (4.4) can be regarded as the forcing

term of the wave equation for the acoustic pressure $p^{(1)}$. The solution for the radiated sound in terms of Kirchhoff's retarded potentials becomes:

$$p^{(1)}(\underline{x},t) = -\frac{1}{4\pi c_o^2}\int_V \frac{1}{|\underline{x}-\underline{y}|}\left[\frac{\partial^2 p^{(0)}(\underline{y},t)}{\partial t^2}\right]_{\hat{t}} d^3\underline{y} \qquad (4.5)$$

where, again, the brackets indicate evaluation at the earlier time

$$\hat{t}=t-|\underline{x}-\underline{y}|/c_o$$

(See Fig.4-2 for geometry).

In the geometric far field, and if the origin is chosen in or close to the source region, the term $1/|\underline{x}-\underline{y}|$ may be approximated as $1/x = 1/|\underline{x}|$. Then:

$$p^{(1)}(\underline{x},t) = -\frac{1}{4\pi c_o^2 x}\int_V \left[\frac{\partial^2 p^{(0)}(\underline{y},t)}{\partial t^2}\right]_{\hat{t}} d^3\underline{y} \qquad (4.6)$$

In the acoustic far field (many typical wavelengths away), $p^{(1)}$ approximates the total pressure fluctuation $p(\underline{x},t)$. Fig.4-18 shows the typical variation of the pressure fluctuation with distance from the jet. Starting at a position on the centerline 4 diameters downstream of the nozzle and moving at right angles to the center line, the far field condition of a 6 db drop in the rms pressure per doubling of distance is reached at about 10 diameters (the cross correlation measurements were made about 50

diameters away).

The straight line indicating the 6 db drop per doubling of distance represents the variation of $p^{(1)}$ alone. If the line is extended backward into the source region one can estimate the magnitude of an equivalent point source representing the radiation of the whole jet. As shown on Fig.4-18 its pressure field would be about 20 to 40 db weaker than the actual measured jet pressure, i.e., the approximation of $p^{(0)}$. In fact, the jet is composed of many incoherent sources each of which will of course be weaker than the single equivalent point source. In the source region therefore $p^{(1)}$ is very much smaller than $p^{(0)}$. This means that we do not expect the sound to have any significant back reaction on the flow or to disturb the measurement of $p^{(0)}$ which arises purely from incompressible turbulent momentum exchanges.

In order to obtain the mean squared radiated pressure Ribner proceeds to square and time average Eq.(4.6), involving a space-time correlation of $p^{(0)}$ under a double integral with four time derivatives. This operation is similar to the one employed by Chu (1966).

4.2.2 Causality Correlation. In the present formalism, we obtain the mean squared radiated pressure by multiplying both sides of Eq.(4.6) by its left hand side, evaluated at a new time $t+\tau$. After time averaging:

$$\overline{p(\underline{x},t)\,p(\underline{x},t+\tau)} = -\frac{1}{4\pi c_o^2 x}\int_V \overline{\left[\ddot{p}^{(0)}(\underline{y},t)\right]_{\hat{t}}\,p(\underline{x},t+\tau)}\;d^3\underline{y} \qquad (4.7)$$

$p(\underline{x},t+\tau)$ can be taken under the integral sign because it is independent of $\underline{y}$. Also, in this case time averaging and integration over V are interchangeable operations. Under the assumption of statistical stationarity the left hand side is a function of τ only; similarly on the right hand side:

$$\overline{pp}(\underline{x},\tau) = -\frac{1}{4\pi c_o^2 x}\int_V \left[\overline{\ddot{p}^{(0)}(\underline{y})\,p(\underline{x})}\right]_{\hat{\tau}}\,d^3\underline{y} \qquad (4.8)$$

where $\hat{\tau}=t+\tau-\hat{t}=t+\tau-t+|\underline{x}-\underline{y}|/c_o=\tau+|\underline{x}-\underline{y}|/c_o$

$\overline{p^2}$ is obtained by setting $\tau=0$. The integrand in Eq. (4.8) establishes the causative relationship between the source fluctuation and the radiated sound.

According to a property of stationary random variables (Crandall & Mark 1963) this integrand can be written in different ways:

$$\overline{\ddot{p}^{(o)}p}(\tau) = -\frac{\partial}{\partial\tau}\,\overline{\dot{p}^{(o)}p} = \frac{\partial^2}{\partial\tau^2}\,\overline{p^{(o)}p} \qquad (4.9)$$

The second form turned out to be the most convenient in most of the experiments described herein. Fig.4-22a shows typical cross correlations $\overline{\dot{p}^{(o)}p}$. Their shape is very close to antisymmetric. Appendix C treats an extension of the theory that allows the prediction of the shape of the correlation functions; good agreement is achieved with actual measured functions.

Note that only one probe has to be inserted into the flow (Fig.4-1) instead of two as have been normally employed in the more classical approach; only a single integral is to be evaluated; only two time derivatives are involved.

4.2.3 Local Source Strength and Spectrum. Writing Eq.(4.8) in differential form gives the radiation from unit volume:

$$\frac{\partial\,\overline{pp}(\underline{x},\tau)}{\partial V} = -\frac{1}{4\pi c_o^2 x}\left[-\frac{\partial}{\partial\tau}\,\overline{\dot{p}^{(o)}p}\right]_{\tau=\hat{\tau}} \qquad (4.10)$$

Again, the contribution to the total mean squared pressure from the point where $p^{(o)}$ is detected is obtained by setting $\tau=0$.

The contribution to the spectrum $\Phi(\nu)$ of $p(\underline{x},t)$ from the point of $p^{(o)}$-detection is obtained by taking the real part of the Fourier Transform of Eq.(4.10):

$$\int_{-\infty}^{\infty} \frac{\partial \overline{pp}(\tau)}{\partial V} e^{i2\pi\nu\tau} d\tau = \frac{1}{4\pi c_o^2 x} \int_{-\infty}^{\infty} \left[\frac{\partial}{\partial \tau} \overline{\dot{p}^{(o)} p} \right]_{\hat{\tau}} e^{i2\pi\nu\tau} d\tau$$

$$\frac{\partial \Phi(\nu)}{\partial V} = \frac{\nu}{2 c_o^2 x} \mathcal{F}_s \left\{ \left[\overline{\dot{p}^{(o)} p}(\tau) \right]_{\hat{\tau}} \right\} \qquad (4.11)$$

where $\mathcal{F}_s\{\ldots\}$ means Fourier Sine Transform. (See Appendix A for a more detailed derivation.)

4.2.4 Correlation Volume.

The correlation volume is defined by analogy to the integral length scale in turbulence. The latter is defined by

$$L(\underline{x}) = \frac{1}{\overline{u^2}} \int_0^{\infty} \overline{u(\underline{x})\, u(\underline{x}+\underline{\xi})}\, d\xi \qquad (4.12)$$

where u is a velocity component and $\underline{\xi}$ is a space separation vector. Fig.4-3 shows that the integrand will contribute to the integral only over a certain distance, the correlation length L. L gives an indication of the typical lengths involved in the turbulent energy exchange. Similarly, we would like to define a correlation volume giving an indication of the typical sizes of volumes or eddies associated with the radiation of sound. To this end we follow, for a moment, the more common method of squaring and time averaging Eq.(4.6):

$$\overline{p\dot{p}}(\underline{x},\tau) = \frac{1}{16\pi^2 c_o^4 x^2} \int_{V'}\int_{V''} \overline{\left[\ddot{p}^{(0)}\right]_{\hat{t}'} \left[\ddot{p}^{(0)}\right]_{\hat{t}''}}\, d^3\underline{y}''\, d^3\underline{y}' \qquad (4.13)$$

where $t'=t-|\underline{x}-\underline{y}'|/c_o$ and $t''=t-|\underline{x}-\underline{y}''|/c_o+\tau$. The integrand will contribute significantly to the inner integral only over the correlation volume V_c. Thus V_c is defined by

$$V_c = \frac{1}{\overline{\ddot{p}^{(0)2}}} \int_{V''} \overline{\left[\ddot{p}^{(0)}\right]_{\underline{y}'} \left[\ddot{p}^{(0)}\right]_{\underline{y}''}}\, d^3\underline{\xi} \qquad (4.14)$$

where $\underline{y}''=\underline{y}'+\underline{\xi}$ and the time delay τ is set to zero. Therefore, differentiating Eq. (4.13) with respect to volume results in the mean squared pressure from unit volume:

$$\frac{\partial \overline{p^2}(\underline{x})}{\partial V} \simeq \frac{V_c}{16\pi^2 c_o^4 x^2}\, \overline{\ddot{p}^{(0)2}} \qquad (4.15)$$

By a consideration similar to the one in Eq. (4.9) we can write down the alternative forms

$$\overline{\ddot{p}^{(0)2}} \equiv \left\{-\frac{\partial^2}{\partial\tau^2}\, \overline{\dot{p}^{(0)}\dot{p}^{(0)}}\right\}_{\tau=0} = \left\{\frac{\partial^4}{\partial\tau^4}\, \overline{p^{(0)}p^{(0)}}\right\}_{\tau=0} \qquad (4.16)$$

and use whichever form is the most convenient. Combining Eq. (4.15) and Eq. (4.10) and using Eq. (4.16) we get

$$V_c \simeq 4\pi c_o^2 x \frac{\left[\frac{\partial}{\partial \tau}\ \overline{\dot{p}^{(o)} p}\right]_{\hat{\tau} = r/c_o}}{\overline{\ddot{p}^{(o)2}}} \qquad (4.17)$$

The usefulness of this correlation volume V_c suffers slightly in that it is dependent upon the choice of the direction of $\underline{x}$, the location of detection of the radiated sound p. It indicates the average size of an eddy radiating in the $\underline{x}$-direction.

The jet is often thought of being composed by a number of incoherent sources, in essence turbulent eddies, compressing and dilating as they bump into each other. If V_c is evaluated at a point such that it represents the average size of all sound producing eddies in the jet, then a rough estimate of the number of eddies in the whole jet can be obtained from the quotient $n=V_{jet}/V_c$, where V_{jet} is the volume occupied by the jet turbulence contributing significantly to the noise. Substituting Eq. (4.14) into Eq. (4.13), with $\tau=0$ and V_c =const, gives:

$$\overline{p^2}(\underline{x}) \simeq \frac{1}{16\pi^2 c_o^4 x^2} \left[\frac{\partial^4}{\partial \tau^4}\ \overline{p^{(o)} p^{(o)}}\right]_{\tau=0} V_c V_{jet} \qquad (4.18)$$

on the other hand, from Eq. (4.8), the following approximation results:

$$\overline{p^2}(\underline{x}) \simeq \frac{1}{4\pi c_o^2 x}\left[\frac{\partial}{\partial\tau}\,\overline{\dot{p}^{(o)}p}\right]_{\hat{\tau}=r/c_o} V_{jet} \qquad (4.19)$$

Therefore, combining Eq.(4.18) and Eq.(4.19) gives, as a rough estimate:

$$n = \frac{V_{jet}}{V_c} \simeq \frac{\overline{p^2}\left\{\frac{\partial^4}{\partial\tau^4}\,\overline{p^{(o)}p^{(o)}}\right\}}{\left[\frac{\partial}{\partial\tau}\,\overline{\dot{p}^{(o)}p}\right]^2} \qquad (4.20)$$

Here, n is a coarse measure of the number of incoherent sources in the jet. If the spectra are peaky [as they are for jet pressure (see Fig.4-27)]differentiation with respect to time t or time delay τ can be approximated by multiplying by a characteristic frequency $2\pi\nu$:

$$n \simeq \frac{\overline{p^2}(2\pi\nu)^4\left\{\overline{p^{(o)}p^{(o)}}\right\}}{\left[(2\pi\nu)^2\,\overline{p^{(o)}p}\right]^2} = \left\{\frac{\left[\overline{p^{(o)}p}\right]}{p_{rms}p^{(o)}_{rms}}\right\}^{-2} \qquad (4.21)$$

Eq.(4.21) shows that n can be roughly estimated by calculatingthe inverse square of the correlation coefficient.

4.3 Development Of The Pressure Sensor.

4.3.1 Limitations on Conventional Cylindrical Probes.

In order to evaluate experimentally Eq.(4.10) it is necessary to measure $p^{(0)}$. As mentioned in section 4.2.1 $p^{(0)}$ approximates the actual total perturbation pressure in the flow for $M^2<<1$. In the present experiments the Mach number at the exit was about 0.32. The Mach numbers of the convecting eddies will be smaller; of the order of 0.2. Therefore the condition $M^2<<1$ appears to be well satisfied. The difficulties inherent in the accurate measurement of pressure fluctuations in turbulence are well recognized. For a probe of the classical cylindrical configuration (Fig.4-4) the measured instantaneous pressure p_m is generally lower than the true instantaneous pressure p_t (i.e. for no probe in the flow) by an amount which depends on the fluctuating components v and w of cross flow normal to the axis of the probe (Siddon 1969). The empirical equation,

$$p_m - p_t \simeq -B\rho(v^2+w^2-\overline{v^2}-\overline{w^2}) \qquad (4.22)$$

where $B \simeq 0.5$

gives a good approximation to the instantaneous error. Siddon (1971a) estimated that the rms value of this instantaneous error can be quite large. In a turbulent jet (where turbulence intensities are typically of the order of 0.2) this rms instantaneous error is approximately 0.025 or higher when nondimensionalized by the dynamic pressure of the flow $0.5\rho U_o^2$; the instantaneous error will be larger, maybe of the order of 0.04. Although the rms value of the instantaneous error can be large, the difference between the rms values of the true and the

measured pressures often turns out to be much smaller. In the present application where cross correlation techniques are employed it is the instantaneous error we are concerned with. It will be necessary to substantially reduce it as the measured pressure fluctuation in a turbulent jet attains maximum values of about 0.05 when nondimensionalized by $0.5\rho U_o^2$. Therefore, using a conventional cylindrical probe the instantaneous error could be of the same magnitude as the pressure fluctuation itself.

Siddon (1969) also showed a way of building an error compensating probe by measuring simultaneously the pressure p_m, and the velocity components v and w, and instantaneously evaluating Eq. (4.22) thereby correcting the measured pressure and arriving at the true pressure p_t.

Even if the accuracy could be improved in this way another problem appears. During the early part of the research it was found that cylindrical probes interacting with the turbulence generate significant extraneous noise as indicated in Fig. 4-5. Imagine a patch of turbulence convecting past the probe. Interacting with the nose of the probe a localized fluctuating side force is induced, sending a dipole pulse to the field microphone. A short time later the same patch of turbulence interacts with the stem of the probe sending off another dipole pulse. These dipole pulses are coherent with the basic source fluctuation and therefore make an extraneous contribution to the correlation $\overline{p^{(o)}p}$. Because these pulses leave the probe earlier and later than the true signal, the result is a tendency for the correlation to be broadened in a rather peculiar way near the correct value of acoustic travel time $|\underline{x}-\underline{y}|/c_o$. Shortening the

nose makes the three contributing effects even less distinguishable as shown by the dashed line on Fig.4-5.

It must be stressed at this point that, although the overall noise in the far field increases by only one decibel or so when inserting the cylindrical probe, the effect on the cross correlation is very prominent because of the discriminatory power of the method: It singles out the contribution to the overall noise from a very localized region in the flow which is more appropriately called 'correlation volume'. If the overall jet noise arises from many independent (separately correlated) source regions, the extraneous dipole effect can contribute substantially to the apparent radiation from such a localized source region, without noticeably altering the overall decibel value.

4.3.2 Airfoil Probe.

The best prospect for suppressing the dipole radiation rests in the possibility of reducing the surface area of the pressure sensor in the direction of the field microphone to something much smaller than the correlation area of the turbulence. A flat airfoil-like probe satisfies this requirement. It is inserted into the flow such that the plane of the foil contains the direction of the mean flow and of the radiation to the far field microphone as shown in Fig.4-6. The thin structure ensures that dipole radiation in the plane of the foil is virtually eliminated.

In order to put the above statements on a more quantitative basis it is helpful to introduce the "Probe Contamination Ratio"

C. C gives the ratio between the mean squared acoustic pressure due to dipole radiation from the probe surface and the mean squared acoustic pressure due to quadrupole radiation from the eddy or correlation volume surrounding the probe. Of course we would like to keep C as small as possible. Appendix D shows how C is defined mathematically, how it can be estimated, and gives some estimates of interest in the present problem. It would appear from these rough estimates that the foil type pressure probe built during the present research has a small enough probe contamination ratio that dipole noise should not be a problem.

By giving the foil a certain shape and strategically locating the pressure sensing holes the probe can be made insensitive to pressure errors of aerodynamic origin (Fig.4-7). For example in the subsonic case (Fig.4-8), the pressure distributions for a thin airfoil suggest that by locating the pressure sensing holes close to the trailing edge, the probe can be made almost insensitive to angle of attack fluctuations both normal to and along the span of the airfoil. This of course presupposes that the scale of the turbulence structure is large compared to the characteristic airfoil dimensions.

The correlation plots on Fig.4-9 show that the effects of extraneous dipole radiation can be eliminated. Curve "a" is a cross correlation between $p^{(o)}$ (as measured by a foil shaped probe) and the radiated sound p, while curve "b" was obtained by using a cylindrical B&K 1/8-inch microphone with a short nosecone, all other conditions being kept the same as for curve "a". The microphone was mounted on a B&K type 2618 preamplifier via an adaptor type UA0160 modified into a right angle connector.

The irregularities in curve "b" are attributed to dipole radiation from the cylindrical probe, particularly the nosecone, and from the probe support. Curve "c" is the Fourier Sine transform of curve "a" or the cross-spectrum. Curve "d" represents the cross-spectrum as calculated from curve "b". It does not have as "nice" a shape as the one calculated from curve "a", and even becomes negative for some frequencies. A negative going cross-spectral density function does not seem possible for a situation wherein the source distribution consists of a random array of uncorrelated phenomena: The power spectral density from a unit volume of source flow should always be positive. It is, however, possible to hypothesize situations where localized spectra may exhibit peaks and valleys arising from constructive and destructive interference at critical frequencies if spatially separated sources are to some degree coherent. Such a situation was seen in the image experiment (section 3.3). For the case of probe generated dipole noise, the dipole source and the corresponding turbulent (eddy) source are somewhat coherent. They radiate at different times, the difference being given by the convection speed and the distance from the nose of the probe to the sensing holes. A further investigation of this phenomenon is left for future work.

Great care was devoted to developing the foil type pressure sensor. An early type with a sensing hole at the trailing edge of the wing tip (Siddon & Rackl 1971) did not exhibit satisfactorily low sensitivity to angle of attack fluctuations in the plane of the foil and to fluctuations in the chordwise direction. To have low sensitivity to angles of attack in the direction normal to

the plane of the airfoil is desirable but not necessary in the present application as the following argument will show:

Remember that the field microphone is placed in the same plane that contains the foil probe (Fig.4-6). The far field pressure in Proudman's (1952) form is

$$p(\underline{x},t) = \frac{1}{4\pi c_o^2 x} \int_V \left[\frac{\partial^2(\rho u_x^2)}{\partial t^2} \right]_{\hat{t}} d^3\underline{y} \qquad (4.23)$$

(conf. Fig.4-10)

This clearly shows that only the velocity component u_x in the direction $\underline{x}$ of the field microphone contributes to p. Pressure measurement errors are due to the turbulent velocities interacting with the probe. u_x lies in the plane of the foil probe. Errors due to turbulent velocities u,v in this plane are minimized by the probe design. Errors dependent on the velocity component w perpendicular to this plane will not, in principle, contribute to the cross correlation $\overline{\dot{p}(o)p}$ because w does not contribute to the radiation of p.

4.3.3 Static Pressure Calibration.

Various configurations of foil type pressure probes were tried out, some typical examples being shown in Fig.4-11. They consist of a stainless steel tube embedded in balsa wood with an airfoil type cross section. The end of the tube connects to the lower and upper surface of the foil. Pressure errors due to changing inclination of the onset flow were determined statically in the potential core of a 1.5 inch diameter jet about 0.5 diameter from

the exit plane, using a Pitot static tube as a reference. The probe configuration that gave the most satisfactory performance is the wedge shaped sensor of Fig.4-12. Fig.4-13 gives the deviations from true static pressure, in the form $C_p = (P-P_\infty)/(0.5\rho U_o^2)$. For angles of attack less than ±12° (equivalent to turbulence intensities less than 0.2) the C_p error in the plane of the foil (v-component) varies by less than .008. By way of comparison, the incidence error for a cylindrical probe in 20% turbulence could attain an instantaneous C_p value of about 0.04 (section 4.3.1). The out of plane error curve (w-direction) has a marked anti-symmetry. This is most probably due to one or both of 2 reasons: 1) the airfoil section and the pressure taps lack symmetry due to an imperfect manufacturing process; 2) the jet flow development itself was influenced by the probe not being on the centerline at different angles of attack. In order to minimize the static pressure measurement error due to fluctuations in the u-component (direction of mean flow) the sensing holes are located in a dip, immediately forward of the thickening trailing edge. The resulting pressure recovery offsets a tendency for negative C_p due to the finite thickness (Fig.4-14).

The C_p error due to u-component fluctuations can be estimated from Fig.4-13. We define:

$$A = (P_m - P_\infty)/(0.5\rho U_o^2) \qquad (4.24)$$

where P_m is the measured static pressure for 0° angle of attack, P_∞ is the static pressure that would occur without the probe in

the flow. At 0° angle of attack, the deviation from the true pressure is shown to be C_p =-0.006. However, P_∞ was not exactly known. By varying the configuration of the foil probe and the reference Pitot static tube in the jet it was found that the uncertainty of where the C_p=0-line lies is of the order of 0.003. In the worst case:

$$C_p = -0.009 = (P_m - P_\infty)/(0.5\rho U_o^2) = A \qquad (4.25)$$

If, as discussed in the next paragraph, the static calibration remains valid in the turbulent flow we can write (Siddon 1969):

$$C_{pu} = \frac{p_m(t) - p_\infty(t)}{0.5\rho U_o^2} \simeq A\frac{2u\bar{U}}{\bar{U}^2} \simeq 2\times(-0.009)(\frac{u}{\bar{U}}) \qquad (4.26)$$

In 20% turbulence $u/\bar{U}$ = 0.2. The C_{pu}-error will therefore be at the most -0.0036.

The suggestion that static incidence calibrations remain valid in the real, time-varying flow implies a quasi-steady assumption. Such an assumption holds if the sensor dimensions are small compared with the scales of the approaching flow. In other words, the ratio $\nu L/U$ must be small, where L is the characteristic chord length of the foil. For the present probe L≃10 mm. Thus the upper limiting frequency will be about $\nu_u \simeq U/4L \simeq 2500$ Hz in a 100 m/sec flow. This is quite a severe restriction. In the zone of maximum shear the mean velocity is even smaller (about 70 m/sec), and we are interested in frequencies up to about 5 kHz although the jet noise peaks at 700 Hz (Fig.3-2). We may therefore expect to run into difficulties of

resolution. This may be one of the reasons why the final check (section 4.5.2) does not work out. As this is the first pressure probe of an airfoil type it should be looked upon as a prototype. It is hoped that further development will follow, in particular with regard to miniaturization.

4.3.4 The Complete Pressure Sensor as shown in Fig.4-12 and Fig.4-15 consists of the foil probe mounted to a B&K 1/8-inch microphone which is connected via an adaptor type UA0160 to a type 2618 preamplifier. The adaptor was filled with paraffin and the preamplifier-adaptor combination was coated with paraffin to eliminate mechanical resonances. The cavity connecting the foil to the microphone combines with the small pressure sensing holes to form a Helmholtz resonator. The resulting resonant response at about 2500 Hz was damped out with a cotton insert. Fig.4-16 shows the resulting frequency response of the pressure sensor. It is essentially flat at the frequencies contributing predominantly to the acoustic spectrum.

4.4 Experiments

The experiments were conducted in an anechoic chamber with dimensions 2.7m*2.7m*1.8m (measured from the tip of the wedges) with a lower cutoff frequency of about 300 Hz. The jet nozzle was placed near one corner of the room; the nozzle exit diameter was 38.1mm (1.5 inches).

4.4.1 Air Supply, Settling Chamber, and Nozzle.

(Fig.4-17) A reciprocating compressor was used as the air supply. It fed into a large recieving tank. The air then flowed through a flexible hose to the settling chamber. Most of the settling chamber was packed with loose fibreglass of the type used for heat and sound insulation. This eliminated noise propagation from upstream, especially from the valve and the entry into the settling chamber. Immediately upstream of the nozzle were placed a cotton wool filter to retain dust and a set of screens with diminishing mesh size to ensure a uniform velocity distribution at the nozzle entry. The nozzle itself was designed such that a uniform velocity distribution would result at the nozzle exit by analogy to the magnetic flux through a ring current (Smith & Wang 1944). The shape of the nozzle was generated on a computer. The mould was produced on a numerical milling machine, the nozzle itself being made of fibreglass using gel coat as the first layer to obtain a smooth inside surface.

4.4.2 The Far Field Microphone.

A B&K 1/2-inch microphone was used as the field microphone located at 45° from the jet axis at a distance of about 50 diameters (1.9 meters) from the nozzle exit. That the far field

condition was met is shown in Fig.4-18: It presents the variation of the rms pressure fluctuation from inside the flow region across the near field to the far field (the latter being characterized by the 6 db drop for every doubling of distance). The traverse was done perpendicular to the jet axis and starting at an axial location of 4 diameters from the nozzle exit.

4.4.3 Signal Processing.

(Fig.4-19) The signal $p^{(o)}(t)$ from the pressure sensor was amplified, filtered (passband 270 - 22500 Hz), differentiated, and fed into channel A of a PAR Model 101 Signal Correlator. The signal p(t) from the far field, measured by a 1/2-inch B&K microphone, was amplified, filtered the same way, and fed into channel B of the correlator. An x-y plotter was used to record the resulting correlation functions $\overline{p^{(o)}p}$. The raw correlation functions contained some noise from the signal correlator and acoustic contamination from reflections off the probe support and traversing mechanism. The latter manifests itself by weak secondary peaks occurring some time after the source-reciever delay time $\tau=r/c_o$. Some subjective judgement was used in eliminating the acoustic contamination in the tails of the correlation functions. This measure affects only the cross-spectra resulting from Fourier Transformation of the complete correlation function. The unfiltered local source strength, equal to the derivative at $\tau=r/c_o$ (vertical line in Fig.4-9, curve "a"), is the principal quantity extracted from the data as indicated by Eq.(4.10). In order to process the data on a computer the plotted correlation functions were digitized using a graphical digitizer. The derivative was calculated by least

square fitting a polynomial to the correlation function in the vicinity of $\tau=r/c_o$. The Fourier Sine Transform according to Eq.(4.11) was estimated using a Fourier transform utility package (Rackl 1972a). (Fig.4-22a and Fig.4-22b).

Keeping the field microphone always at the same location of 45° to the jet axis the pressure sensor was moved around in the jet on the side opposite to the microphone, in order to minimize interference of the probe support with the sound field (Fig.4-1). Radial traverses were done at various downstream locations.

4.5 Data Reduction

4.5.1 Source Strength Distribution.

The procedure described in the previous section results in the distribution of source strength per unit volume shown in Fig.4-20. Nondimensionalization was effected as shown in Appendix B. The nondimensionalized source strength plotted is:

$$S_{UV} = \frac{-\left[\frac{\partial}{\partial\tau}\,\overline{\dot{p}^{(0)}p}\,(\tau)\right]_{\hat{\tau}=r/c_o}}{2(0.5\rho U_o^2)^2 M^2\, D/x_o\,(U_o/D)^2} \qquad (4.27)$$

where:

U_o = nozzle exit velocity,

$M = U_o/c_o$ = Mach number,

D = nozzle exit diameter,

x_o = distance nozzle exit - field microphone.

It is not surprising that the distribution of S_{UV} bears some similarity to the distribution of mean shear in a jet. It has traditionally been argued that sound generation from turbulent flows should be strongest in the regions of most intense turbulence occurring where the gradients of mean velocity are largest. Thus, over the first few diameters, S_{UV} is strongest half a diameter from the jet axis; further downstream the peak shifts toward the axis and decreases rapidly in amplitude. At this point it should be emphasized that this distribution does not indicate the sound power radiated from unit volume, but the contribution to the mean squared pressure in the far field at 45° to the jet axis.

For each downstream location the radial distribution was integrated resulting in the distribution of source strength from a "slice" of the jet:

$$S_{slice} = \int_{r=0}^{\infty} S_{UV} 2\pi r \, dr \qquad (4.28)$$

Fig. 4-21 shows the present result and compares it qualitatively only with results of other workers (Lee & Ribner 1972; Ribner 1958, 1962; Dyer 1959; Jones 1968; see also Chu, Laufer & Kao 1972). The present and H.K. Lee's works use similar techniques (causality correlations); Lee's data were taken for a far field location of 40° to the jet axis and at a Mach number of about 0.3. The other curves are not experimental data; they are based on semi-empirical techniques and indicate the sound power radiated from a slice, without consideration of directionality. It is known that higher frequencies are radiated more

preferentially in directions in the vicinity of 45°, this being due to source convection and refraction by the shear layer affecting the higher frequencies more than the lower ones. Higher frequencies are generated closer to the exit than lower frequencies: One might therefore expect the axial source distribution for 45° radiation to peak earlier (i.e. between 2 and 3 diameters downstream) than would be expected for the overall power distribution. The restrictions discussed in section 4.3.3 must however be born in mind. The general trend is to support Ribner's prediction from similarity considerations except very close to the nozzle exit where the flow has to readjust very rapidly from a boundary layer inside the nozzle to a freely growing shear layer. One must also point out that it is not known accurately where the assumptions of similarity become valid downstream of the potential core, i.e. the axial location where the x^{-7}-Law takes over is uncertain.

4.5.2 Check, Closure Difficulty.

Further integration of S_{slice} along the jet axis should recover the $\overline{p^2}$ as measured directly at $\underline{x}$, according to Eq. (4.8). This provides a check of the procedure. However, the $\overline{p^2}$ as obtained by integration is nearly 10 times as large as the measured one. The possibility of a numerical mistake is ruled out as the calculations were checked many times, also by different persons. Numerous possibilities explaining this discrepancy were considered and many were discarded. Among the latter were: Vortex shedding from the probe trailing edge (the shedding frequency is of the order of 14 Kilohertz), mechanical shaking of the microphone. Possibly valid explanations are:

1) The derivative of $\overline{p^{(0)}p}$ is to be evaluated according to Eq.(4.10) at $\tau=r/c_o$, the time delay that corresponds to the travel time of the sound from the source to the far field microphone. This "geometrical" time delay is in fact not equal to the real sound travel time as the probe is inserted from the far side of the jet (Fig.4-1) and the sound must travel through the jet flow where it is accelerated and refracted. The "effective" time delay is therefore slightly smaller. The typical $\overline{p^{(0)}p}$ shown in Fig.4-24 is quite antisymmetrical. According to the geometrical time delay the derivative would have to be calculated at a point slightly to the right of the point of symmetry (here called the "center"), but still on the portion with positive slope. The effective time delay would move this point toward the center where the slope is steepest. Experimental evidence was collected showing that the effective time delay should be shorter:

Some experiments were performed with the pressure sensor inserted from the near side. In this case the geometric time delay was very close to the "center" as one would expect since the sound does not travel through the jet exhaust stream. In another set of experiments, a point source with a diameter of about 0.1 inches was placed immediately under the pressure probe (inserted from the far side) and driven by random noise and by pure tones. The cross correlation was computed in the usual manner with and without the jet flow. In the latter case a peak in the correlation function was observed very close to the calculated geometrical time delay. When the jet flow was turned on this peak shifted to the left toward a shorter time delay.

This shift varied somewhat for random noise and for pure tones of different frequency; it was impossible to determine the exact shift with the simple setup used. A third experiment was performed on the computer only: The Fourier Sine transform was calculated for a selected $\overline{p^{(o)}p}$ "centered" at a varying $\hat{\tau}$, i.e. the amount of origin shift on the τ-axis {indicated in Eq. (4.11) by $[\ldots]_{\hat{\tau}}$} before Fourier transforming was varied in the vicinity of $\tau=\hat{\tau}=r/c_o$. As may be expected, when $\overline{p^{(o)}p}$ was centered on the point of symmetry a sine transform resulted that remained positive for all frequencies. If centered before or after the point of symmetry the transform showed negative going parts, which does not seem possible as already mentioned in section 4.3.2. It was therefore decided to assume that the effective time delay is given by the point of steepest slope. This decision may not have been the best. The slope at the geometrical time delay is smaller and would result in a smaller integrated $\overline{p^2}$, but the change would fall far short of accounting for the total observed discrepancy.

2) The calculations in Appendix D indicate that dipole noise should not be a problem with the present pressure sensor. However, Appendix D deals only with gross turbulence properties for x/D=4. Maybe one should give more consideration to the smaller turbulence scales especially when they are of the order of the probe size. This will be the case closer to the exit plane; there, dipole noise could indeed become dominant.

3) The insertion of the probe into the flow will, of course, change the flow. The smaller the probe the less this disturbance. The discussion of section 4.3.3 shows that the probe may indeed

be too large to adequately resolve the turbulent pressure at a point in the present jet, especially further upstream (closer than about 2 diameters from the exit) where scales are small and frequencies are high. The quasisteady assumption for the pressure error would no longer be valid.

4) It was pointed out to the author that there is a strong mean velocity gradient across the surface of the probe when it is inserted from the far side as shown in Fig.4-1. This may lead to an additional flow distortion and pressure error. However, when the probe was inserted at a point 1/2 a diameter directly above the axis (not behind as in Fig.4-1) where there would hardly be any velocity gradient across the probe, the correlation $\overline{\dot{p}^{(o)}p}$ was not significantly different.

5) The dynamic calibration of the pressure sensor was done acoustically only. It may be that flow over the pressure sensing holes substantially alters the frequency response of the probe.

4.5.3 Spectra. The upper part of Fig.4-9 shows a typical pair of cross-functions: 9a the experimentally obtained cross correlation function in the time domain, 9c the cross spectrum function in the frequency domain calculated from 9a according to Eq.(4.11), i.e., the spectral density of the source strength per unit volume. Fig.4-22b shows some typical cross spectrum functions for various downstream locations. Again integrating radially one obtains the spectra from slices of the jet. Their peak frequencies are plotted against downstream distance from the nozzle exit in Fig.4-23 (full circles) together with other results available. (Lee & Ribner 1972; Chu, Laufer and Kao 1972).

The empty squares of Fig.4-23 were arrived at by a very simple argument: We know that the radiated sound depends on the second derivative of the source fluctuation. Bearing this in mind, the spectral density of $p^{(o)}$ as measured with the stationary foil probe (Fig.4-27) was multiplied by the square of frequency and the peak frequencies entered into Fig.4-23. Although this does not account for directionality and is not amenable to quantitative analysis of source strength the curves fall close together.

It is interesting to note that none of the curves in Fig.4-23 attains the value of about 0.2 which corresponds to the peak Strouhal number of the overall noise at 45° from the jet axis. Lee(1971) has commented that this is "... due to the omitted contribution of that part of the jet extending beyond X=7D, which must dominate the low frequency sound emission." In the present case the measurements were done as far downstream as 10 diameters; the curve still does not show much tendency to bend down to lower Strouhal numbers. This can be interpreted in different ways:

1) The low frequency sound is emitted still further downstream. Looking at Fig.4-21 however, all available data suggests that there is hardly any sizable contribution to the jet noise from regions beyond 10 diameters.

2) The low frequency sound is generated upstream of the exit plane, i.e. in the nozzle and the settling chamber acting as acoustic resonators. If this were true one may expect to see in the spectrum a low frequency hump above the jet noise which would

vary markedly from one jet to another; but this is not the case.

3) Some of the points discussed in section 4.5.2 will, of course, be reflected in the spectra. In particular point 2): The smaller turbulence scales are associated with higher frequencies. Therefore, if dipole contamination were a problem it would enhance the high frequency contents and thus make the spectra peak at higher Strouhal numbers. In addition, far downstream, where scales are large, interaction of the flow with the stem of the probe may produce a signal which is coherent with the measured pressure signal and again contaminate the cross correlation.

The directly measured sound spectrum in the far field at 45° from the jet axis and the one that results by integrating all elementary spectra over the jet volume should, theoretically, be the same [Eq.(4.11) integrated over volume]. As for the mean squared pressure this check does not work out. Fig.4-28 compares the directly measured and the integrated nondimensionalized spectra. The reconstructed spectrum apparently includes an excess of high frequency energy.

4.5.4 Number of Incoherent Sources.

The correlation coefficient of Eq.(4.21) at a location 3 diameters downstream and 1/2 a diameter from the jet axis turned out to be approximately 0.08. Therefore, a rough estimate of the number of incoherent sources in the jet n is

$$n \simeq (0.08)^{-2} \simeq 150$$

It would appear reasonable to infer from this number that n is of the order of 100 to 200. One must however investigate what

external influences may increase or decrease the correlation coefficient:

1) Dipole noise off the probe can significantly increase the magnitude of the correlation function and of the correlation coefficient: In Eq. (4.21) both $\overline{p^{(0)}p}$ and p_{rms} will be affected by the dipole radiation. However, $\overline{p^{(0)}p}$ will increase much more than p_{rms} because p_{rms} is the noise coming from the whole jet, while $\overline{p^{(0)}p}$ represents the contribution from the small volume where the probe is inserted. (This was already discussed in section 4.3.1). Thus n may be considerably underestimated. The low value of $n \simeq 3$ given by Scharton and White (1972) was arrived at using a 1/8-inch microphone in a 5/8-inch diameter jet with Mach number equal to one. The probe contamination ratio (Appendix D) for this configuration is of the order of 1.8. This high value would indicate that dipole noise from the probe not only plays a significant role, but that it is dominant.

2) Filtering may have an influence on the magnitude of the correlation coefficient if a significant amount of the energy of one or both of the two signals being correlated is filtered out. In the present case, for instance, one may wish to increase the signal to noise ratio by using an octave band filter centred on the peak frequency of the jet noise spectrum. If $p^{(0)}(t)$ is measured at a point in the jet where the spectrum of $p^{(0)}$ peaks in the same octave band, the correlation $\overline{p^{(0)}p}$ may be left essentially uninfluenced by filtering. On the other hand, p(t) contains a significant amount of energy outside this octave band which is contributed from other parts of the jet. Therefore the filtered p_{rms} will be smaller than the unfiltered one, again

increasing the correlation coefficient and leading to an underestimation of n [octave band filtering was employed by Scharton & White (1972) which may have contributed to their low value of $n \simeq 3$].

3) External acoustic noise can significantly decrease the correlation coefficient (but leaving the correlation function unaffected): In Eq. (4.21), the acoustic pressure p_{rms} can contain other signals than the one radiated from the jet. This would decrease the correlation coefficient and thereby overestimate n. Care must therefore be taken to eliminate external noise sources. In the present work for instance, low frequency noise from the compressor supplying the air had to be filtered out by a 4th order high pass filter with a cutoff frequency of about 270 Hz.

4) Electronic noise may also substantially decrease the correlation coefficient by superposing itself on the $p^{(o)}(t)$ and $p(t)$ signals thereby increasing p_{rms} and $p^{(o)}_{rms}$ in Eq. (4.21). Again, n would be overestimated. Electronic noise has high frequency character and can usually be eliminated by a suitable low pass filter.

Lee & Ribner (1972, p. 1289) roughly estimated n to be of the order of 2500. Although this may come close to the truth it is not known if it may have been overestimated as described in points 3) and 4) above.

V. SUMMARY CONCLUSIONS, RECOMMENDATIONS.

Two experimental techniques were developed with the aim of learning more about the distribution of sound sources in a turbulent jet. They both use the causality principle in that they measure a source fluctuation and relate it to the radiated sound by a cross correlation method.

In the image technique a rigid surface is put close to the jet. The pressure on the surface is taken as a fluctuation representative of a certain limited region of the jet. The resulting distribution of source strength over the surface allows some conclusion on the noise sources in the jet using the ray acoustics reflection principle. For the low speed subsonic jet used the strongest sources appear to be located between 4 and 6 diameters downstream.

If this technique is employed in the future it would probably be of advantage to replace the rigid surface by a hypothetical plane as the presence of the real surface influences the development of the flow (Siddon 1973b). It may, however, be necessary to measure both velocity and pressure, as the boundary condition of no normal velocity on the surface would then disappear [terms containing u_i in the surface integrals of Eq. (1.2) would not vanish, but may be negligibly small in some cases].

In the direct turbulence probing technique the fluctuating

pressure is measured by an airfoil type sensor and is cross correlated with the far field radiated sound. Using Ribner's (1962) dilatation theory leads to a volume distribution of acoustic source strength in the jet which looks somewhat similar to the distribution of mean velocity shear. Radial integration gives the acoustic strength from "slices" of the jet; this is in qualitative agreement with results of other researchers. However, an attempt to regain the total radiated pressure by integrating over all sources in the jet failed. Reasons for this failure are given. From these the following recommendations result:

1) To further develop the pressure sensor: the shape of the present sensor was arrived at by "educated guessing". A theoretical investigation in the pressure distribution over the foil surface using a three dimensional theory [for instance Smith's method (Smith & Hess 1967)] should lead to an optimum foil shape which also takes into account the presence of the probe support. The analysis could even be carried further to include time varying incident flow. However, the computing time required using a modified Smith's method would be very large. - Miniaturization of the pressure sensor is very desirable both from the point of view of dipole noise contamination and of flow disturbance. The feasibility of using transducers other than condenser microphones should be explored. Such could be of the piezoelectric type or Kulite semiconductors which could be embedded directly into the airfoil surface. - The dynamic calibration should be done in a known unsteady flow such as an inclined rotating nozzle which generates a flow with sinusoidally varying angle of attack.

2) The larger the jet and the smaller the probe, the less problems will arise from extraneous disturbances. Also, tests run at higher Mach numbers would not only be more realistic models of jets used in modern aircraft but reduce the probe contamination ratio in proportion to M^{-2} as shown in Appendix D, Eq. (D.12).

3) The uncertainty regarding the correct time delay of the "center" of the causality correlation function should be reduced [section 4.5.2, point 1)]: The exact sound travel time from the transducer measuring the source fluctuation to the far field microphone has to be measured or calculated in some way. For instance, a point source of sound in the jet could be used at the location of the transducer, without the latter in place. Since it is next to impossible to build a strong point source with a uniform phase response, this phase response must at least be known and corrected for later.

The thesis established the feasibility of exploiting Ribner's pressure source model of flow noise using the causality correlation technique. The difficulties inherent in the method were uncovered; some were solved, for others viable solutions were proposed. Since the correlations can be performed in the broad band it is an efficient method. In its present state it gives a good picture of the relative source distribution. If the above recommendations are implemented highly accurate quantitative measurements of the source distribution should be possible.

REFERENCES

(Alphabetically according to the first author. A citation preceded by a "*" indicates an experimental work published since 1963.)

* J. Atvars, "Refraction of Sound by a Jet Velocity Field," M.A.Sc. Thesis (unpublished), UTIAS, 1964.

D.I. Blokhintsev, "Acoustics of a Nonhomogeneous Moving Medium," in Russian 1946. Translated as NACA Tech. Memor. No. 1399 (1956).

* A.J. Bowen, J.H. Dunmore, and D.C. Stevenson, "An Investigation of the Noise Field Produced Near a Half-Inch Diameter Steam Jet," J. Sound Vib. 5, 113 (1967).

* P. Bradshaw, D.H. Ferriss, R.F. Johnson, "Turbulence in the Noise Producing Region of a Circular Jet," J. Fluid Mech. 19, p. 591, 1964.

* W.T. Chu, "Turbulence Measurements Relevant to Jet Noise," UTIA S Report No. 119, November, 1966.

* W.T. Chu, J. Laufer, and K. Kao, "Noise Source Distribution in Subsonic Jets," Inter-Noise 72 Proceedings, p. 472.

* P.J.F. Clark & H.S. Ribner, "Direct Correlation of Fluctuating Lift with Radiated Sound for an Airfoil in Turbulent Flow," J. Acoust. Soc. Am. 46(3), part 2, p. 802-805, 1969.

S.H. Crandall & W.D. Mark, "Random Vibration in Mechanical Systems," Acad. Press N.Y. & London, 1963.

* S.C. Crow & F.H. Champagne, "Orderly Structure in Jet Turbulence," J. Fluid Mech. 48(3), pp. 547-591, 1971.

N. Curle, "The Influence of Solid Boundaries Upon Aerodynamic Sound," Proc.Roy.Soc. A, 231, 505-514, 1955.

* P.O.A.L. Davies, M.J. Fisher, M.J. Barrat, "The Characteristics of the Turbulence in the Mixing Region of a Round Jet," J. Fluid Mech. 15, pp. 337-367, 1963.

* M.R. Davis, "Measurements in a Subsonic Turbulent Jet Using a Quantitative Schlieren Technique," J. Fluid Mech. 46(4), pp.631-656, 1971.

P.E. Doak, "Analysis of Internally Generated Sound in Continuous Materials: 2. A Critical Review of the Conceptual Adequacy and Physical Scope of Existing Theories of Aerodynamic Noise, with special Reference to Supersonic Jet Noise,"

J. Sound Vib. 25(2), pp. 263-335, 1972.

I. Dyer, "Distribution of Sound Sources in a Jet Stream," J. Acoust. Soc. Am. 31, 1016 (1959).

* M.J. Fisher & F.R. Krause, "The Crossed-Beam Correlation Technique," J. Fluid Mech. 28(4), pp. 705-717, 1967.

M.J. Fisher & M.V. Lowson, "Aerodynamic Noise (Symposium at Loughborough University, September 1970)," J. Fluid Mech. 48(3),pp.593-603, 1971.

H.V. Fuchs and A. Michalke, "Four Introductory Lectures on Aerodynamic Noise Theory," Deutsche Luft- und Raumfahrt Mitteilung 71-20. 1971.

* H.V. Fuchs, "Space Correlations of the Fluctuating Pressure in Subsonic Turbulent Jets," J. Sound Vib. 23(1), pp. 77-99, 1972.

Ian S.F. Jones, "Scales Pertinent to Noise Prediction from the First Few Diameters of a Jet," AFOSR-UTIAS Symposium on Aerodynamic Noise 1968, Book of Abstracts, p. 8.

R.H. Kraichnan, "Pressure Field within Homogeneous Anisotropic Turbulence," J. Acoust. Soc. Am., 28(1), pp. 64-72, January, 1956.

* J.C. Lau, M.J. Fisher & H.V. Fuchs, "The Intrinsic Structure of Turbulent Jets," J. Sound Vib. 22(4), pp. 379-406, 1972.

J.C. Laurence, "Intensity, Scale and Spectra of Turbulence in Mixing Region of Free Subsonic Jet," Lewis Flight Prop. Lab. Report # 1292, 1957.

* H.K. Lee, "Correlation of Noise and Flow of a Jet," UTIAS Rep. 168 (1971); also AFOSR-TR-71-2572 (1971).

* H.K. Lee and H.S. Ribner, "Direct Correlation of Noise and Flow of a Jet", J.Acoust.Soc.Am., Vol. 52, Number 5(Part 1),p. 1280, 1972.

A.W. Liepmann, "On the Application of Statistical Concepts to the Buffeting Problem," J. Aeron. Sc. 19 (12), December, 1952.

M.J. Lighthill, "On Sound Generated Aerodynamically 1. General Theory," Proc.Roy.Soc. A, 211, 564-587, 1952.

M.J. Lighthill, "On Sound Generated Aerodynamically, II. Turbulence as a Source of Sound," Proc.Roy.Soc. A 222, 1-32;1954.

M.J. Lighthill, "The Bakerian Lecture, 1961, Sound Generated Aerodynamically," Proc.Roy.Soc. A, 267, 147-182, 1962.

M.J. Lighthill, "Jet Noise," AIAA Journal, 1(7), pp. 1507-1517, July, 1963.

G.M. Lilley, "On the Noise from Air Jets," ARC 20, 376-N40-FM 2724 (Sept. 1958).

M.V. Lowson, "Concluding Discussion at the Aerodynamic Noise Symposium, Loughborough, September 1970," J. Sound Vib. 17(1), pp. 1-4, 1971.

* P.A. Lush, "Measurement of Subsonic Jet Noise and Comparison with Theory," J. Fluid Mech. 46(3), pp. 477-500, 1971.

* L. Maestrello & E. McDaid, "Acoustic Characteristics of a High Subsonic Jet," AIAA Paper No. 70-234, Jan. 1970.

W.C. Meecham & G.W. Ford, "Acoustic Radiation from Isotropic Turbulence," J. Acoust. Soc. Am. 30(4), pp. 318-322, April 1958.

* E. Mollo-Christensen, M.A. Kolpin, and J.R. Martucelli, "Experiments on Jet Flows and Jet Noise Far Field Spectra and Directivity Patterns," J.Fluid Mech. 18, pp. 285-301, 1964.

* E. Mollo-Cristensen, "Jet Noise and Shear Flow Instability Seen from an Experimenter's Viewpoint," ASME J. of Appl. Mech. 34, pp. 1-7, 1967.

* R.C. Potter and J.H. Jones, "An Experiment to Locate the Acoustic Sources in a High Speed Jet Exhaust Stream," Abstract, 74th Meeting of the Acoust.Soc.Am., JJ4, 1967.

A. Powell, "Similarity Considerations of Noise Production from Turbulent Jets, Both Static and Moving," Douglas Aircraft Company Rep. SM-23246 (July 1958); also abridged in J.Acoust.Soc.Am. 31, pp. 812-813 (1959).

A. Powell, "Aerodynamic Noise and the Plane Boundary," J.Acoust.Soc.Am. 32, p. 982, 1960.

A. Powell, "Theory of Vortex Sound," J.Acoust.Soc.Am. 36, 177-195, 1964.

I. Proudman, "The Generation of Noise by Isotropic Turbulence," Proc.Roy.Soc. A, Vol. 214, p. 119, 1952.

* R. Rackl and T.E. Siddon, "Jet Noise Study Using Image Technique," CANCAM 1971, Calgary, Proceedings p. 473.

R. Rackl, "Correlation Function Processing with Fourier Transform," Dept. Mech. Eng., UBC, May 1972a.

* R. Rackl, "Further Studies on Cross Correlations between Fluid Dilatations and Flow Noise," 84th Meeting of Acoust. Soc. Am., paper XX8, 1972b.

H.S. Ribner, "On the Strength Distribution of Noise Sources Along a Jet," UTIA Rep. 51 (April 1958); also abridged in J. Acoust. Soc. Am. 30, p. 879 (1958).

H.S. Ribner, "Aerodynamic Sound From Fluid Dilatations," UTIA Rep. No. 86,July 1962. Also AFOSR TN 3430.

H.S. Ribner, "The Generation of Sound by Turbulent Jets," Advances in Applied Mechanics, Vol. 8, Academic Press Inc., New York, 1964.

* T.D. Scharton and P.H. White, "Simple Pressure Source Model of Jet Noise," JASA Vol. 52, No 1 (Part 2) July 1972, p. 399.

* L.K. Schubert, "The Role of Jet Temperature and Sound Source Position in Refraction of Sound from a Point Source Placed in an Air Jet," M.A.Sc. Thesis (unpublished), UTIAS, 1965.

W.R. Sears, "Some Aspects of Nonstationary Airfoil Theory and its Practical Application," J. Aeron. Sc. 8(2), p. 104, February 1941.

* T.E. Siddon, "On the Response of Pressure Measuring Instrumentation in Unsteady Flow," UTIAS Rep. No. 136, January 1969. Also AFOSR 68-2466.

* T.E. Siddon, "Correlation Study of Surface Interaction Noise," Trane Co. Research Dept. Report, La Crosse, Wisc., Dec. 1970.

T.E. Siddon, "Fluctuating Pressure Probe/Design and Calibration," Bolt, Beranek and Newman Report, July 1971a.

* T.E. Siddon & R. Rackl, "Crosscorrelation Analysis of Flow Noise with Fluid Dilatations as Source Fluctuation", H12, 82nd Meeting of ASA, Denver 1971.

T.E. Siddon, "New Correlation Method for Study of Flow Noise", 25 N 12, 7th ICA, Budapest 1971b.

* T.E. Siddon, "Surface Dipole Strength by Cross Correlation Method", JASA Vol. 53 No.2, pp.619-633, Feb. 1973. Also available as Siddon 1970. 1973a.

T.E. Siddon, "Noise Source Diagnostics Using Causality Correlations," abstract submitted for Specialists' Meeting 'Noise Mechanisms', AGARD Fluid Dynamics Panel, Belgium, Sept., 1973b.

A.M.O. Smith & J.L. Hess, "Calculation of Potential Flow about Arbitrary Bodies," Prog. Aeron. Sc., Vol 8, pp.1-138, 1967.

R.H. Smith & C.T. Wang, "Contracting Cones Giving Uniform Throat Speeds," J.Aeron.Sc., Oct. 1944, p. 356.

H. Tennekes & J. L. Lumley, "A First course in Turbulence," The MIT Press, Cambridge, Massachusetts, and London, England, 1972.

* R.B. Webster, "Jet Noise Simulation on Shallow Water," J. Fluid Mech. 40(2), pp. 423-432, 1970.

APPENDICES

Appendix A

Mathematical Details Concerning Eq. (4.7) Through Eq. (4.11).

Eq. (4.7) is repeated:

$$\overline{p(t)\,p(t+\tau)} = -\frac{1}{4\pi c_o^2 x}\int_V \overline{\left[\ddot{p}^{(0)}\right]_{\hat{t}}\, p(t+\tau)}\; d^3\underline{y} \qquad (A.1)$$

where $[\ldots]_{\hat{t}}$ means: Replace the argument (t) by argument-$|\underline{x}-\underline{y}|/c_o$ $(t-|\underline{x}-\underline{y}|/c_o)$. $p(t)$ can be taken under the integral sign because it is independent of $\underline{y}$. Time averaging and integration over V are independent, interchangeable operations. Under the assumption of statistical stationarity the time averages are functions of the time delay τ only. The left hand side of Eq. (4.7) becomes the autocorrelation of the far field sound $\overline{pp}(\tau)$. The right hand side can be put into a more convenient form:

Consider: $\frac{\partial}{\partial t} = \frac{\partial}{\partial \tau}\frac{d\tau}{dt}$

Put: $t'=t+\tau \rightarrow \frac{d\tau}{dt}=-1$

$$\overline{\left[\frac{\partial^2 p^{(0)}(t)}{\partial t^2}\right]_{\hat{t}}\, p(t+\tau)} = \overline{\left[\ddot{p}^{(0)}(t'-\tau)\right]_{\hat{t}'}\, p(t')} =$$

$$= \overline{\frac{\partial}{\partial \tau}\left[\dot{p}^{(0)}\right] p}\,(-1) = -\frac{\partial}{\partial \tau}\overline{\left[\dot{p}^{(0)}\right] p} =$$

$$= -\left[\frac{\partial}{\partial \tau}\,\overline{\dot{p}^{(0)} p}\right]_{\hat{\tau}} \qquad (A.2)$$

where $[\ldots]_{\hat{\tau}}$ again means: replace the argument (τ) by

argument+$|\underline{x}-\underline{y}|/c_o$ ($\hat{\tau}=\tau+|\underline{x}-\underline{y}|/c_o$). Eq. (4.7) therefore becomes in differential form:

$$\frac{\partial \overline{pp}(\tau)}{\partial V} = \frac{1}{4\pi c_o^2 x}\left[\frac{\partial}{\partial \tau}\overline{\dot{p}^{(o)}p}\right]_{\hat{\tau}} \qquad (A.3)$$

Now take the Fourier Transform

$$\int_{-\infty}^{\infty} \ldots e^{i2\pi\nu\tau} d\tau = \mathcal{F}\{\ldots\} \qquad (A.4)$$

of Eq. (A.3). The right hand side becomes:

$$\text{r.h.s.} = \frac{1}{4\pi c_o^2 x}\int_{-\infty}^{\infty}\left[\frac{\partial}{\partial \tau}\overline{\dot{p}^{(o)}p}\right]_{\hat{\tau}} e^{i2\pi\nu\tau}\, d\tau \qquad (A.5)$$

By partial integration:

$$\text{r.h.s} = \frac{-i2\pi\nu}{4\pi c_o^2 x}\int_{-\infty}^{\infty}\left[\overline{\dot{p}^{(o)}p}\right]_{\hat{\tau}} e^{i2\pi\nu\tau}\, d\tau \qquad (A.6)$$

By definition, the real part of the Fourier transform of the autocorrelation $\partial pp(\tau)/\partial V$ is the power spectral density. Therefore, taking the real part on both sides results in the spectral density of p per unit volume:

$$\frac{\partial \Phi_p(\nu)}{\partial V} = \mathcal{F}_c\left\{\frac{\partial \overline{pp}(\tau)}{\partial V}\right\} = \frac{\nu}{2c_o^2 x}\mathcal{F}_s\left\{\left[\overline{\dot{p}^{(o)}p}(\tau)\right]_{\hat{\tau}}\right\} \qquad (A.7)$$

where $\mathcal{F}\{\ldots\} = \mathcal{F}_c\{\ldots\} + i\mathcal{F}_s\{\ldots\}$,

$\mathcal{F}_c$ = cosine transform, $\mathcal{F}_s$ = sine transform.

When the Fourier transform is estimated by a numerical method it is usually necessary to correct the result

("smoothing") because a numerical integration cannot be extended to infinity. In the present case, however, the correlation functions $\overline{\dot{p}^{(o)}p}$ decrease sufficiently rapidly to zero within the length of the record available so that such a correction was not made.

Appendix B

Nondimensionalization of Correlation Functions

There are two reasons for nondimensionalizing data: 1) Fluctuations in ambient conditions will have less degradating effect on the final data. 2) Results are more general and easier to compare with results of other workers.

Lengths are measured in general in meters [m], sometimes in inches [in], pressures in N/m^2 (N=Newton), time in milliseconds [msec], and voltages in Volts [V].

B.1 Causality Correlation Technique

The signal flow is shown in Fig.4-19. The correlator computes $\overline{e_A e_B}(\tau)$, where e_A and e_B are the voltages applied to the two input channels; the dimension of $\overline{e_A e_B}$ is [V^2]. The output $C_c(\tau)$ of the correlator consists of voltages the values of which are numerically identical to the values of $\overline{e_A e_B}$. The sensitivity S_c of the correlator is therefore $S_c = 1[1/V]$.

What we are interested in is $\overline{\dot{p}^{(o)} p}$. Tracing through the electronics we get:

$$e_A(t) = RC\ G_{CA}\ G_{MA}\ S_A\ \dot{p}^{(o)}(t)$$

$$e_B(t) = G_{CB}\ G_{MB}\ S_B\ p(t)$$

where:

RC = time constant of the differentiator [msec],

G_C = input gain of correlator,

G_M = gain of measuring amplifier,

S = microphone sensitivity [V/N/m²].

$C_c(\tau)$ is recorded on an x-y-plotter (sensitivity S_{xy} [V/in]), the plotted function $C(\tau)$ is measured in inches. Then: $S_{xy}\ C(\tau) = \overline{e_A e_B}\ S_c$,

$$\overline{\dot{p}^{(0)}p}(\tau) = \frac{S_{xy}\ C(\tau)}{(S_A\ G_{MA}\ RC\ G_{CA})(S_B\ G_{MB}\ G_{CB})\ S_C}$$

Nondimensionalization is effected by dividing the far field acoustic pressure by

$$2(0.5\rho U_o^2)\,M^2 D/x_o ,$$

the hydrodynamic pressure fluctuation by

$$0.5\rho U_o^2 ,$$

time and time delay by D/U_o.

Using the second form of Eq. (4.9), Eq. (4.8) is nondimensionalized:

$$\frac{\overline{pp}(\tau)}{\left\{2(0.5\rho U_o^2)\,M^2\,D/x_o\right\}^2} =$$

$$= \frac{(U_o/D)^2}{4\pi c_o^2 x_o 2\,M^2\,D/x_o} \int_V \left[\frac{\partial}{\partial(\tau \frac{U_o}{D})} \overline{\frac{\partial \frac{p^{(0)}}{0.5\rho U_o^2}}{\partial(t\,U_o/D)} \frac{p}{\left\{2(0.5\rho U_o^2)\,M^2\,D/x_o\right\}}} \right]_{\hat{\tau}} d^3\underline{y}$$

The nondimensional integrand $[\ldots]_{\hat{\tau}}$ is extracted from the measured cross correlation data.

B.2 Image Technique

The signal flow is nearly the same as in Fig.4-19; we substitute a quarter inch microphone for the foil pressure sensor and omit the differentiator. Then:

$$\overline{p_s p}(\tau) = \frac{S_{xy}\, C(\tau)}{S_A\, G_{MA} G_{CA}\, S_B\, G_{MB} G_{CB}\, S_C}$$

Since it was determined that p_s scales much the same way as p, p_s is nondimensionalized by the same quantity (3.13) except that x_o is replaced by h, the distance of the surface from the jet axis. Equation (3.10) becomes:

$$\frac{\overline{p^2}}{\left\{2(0.5\rho U_o^2)\, M^2\, D/x_o\right\}^2} =$$

$$= \frac{\cos\theta\,(U_o/D)}{4\pi c_o\, x\, h/x_o} \int_S \left[\frac{\partial}{\partial(\tau U_o/D)} \frac{\overline{p_s}}{2(0.5\rho U_o^2)M^2 D/h} \frac{p}{2(0.5\rho U_o^2)M^2 D/x_o} \right]_{\hat{\tau}} dS$$

M = 0.325 (typical), $\theta \simeq 55°$, h/D = 5.17. (See Fig.B-1.)

The nondimensional integrand $[\ldots]_{\hat{\tau}}$ was extracted from the measured cross correlation data by a computer program. The integration was done by hand.

Appendix C

Prediction Of The Shape Of The Cross Correlation Function.

The procedure is similar to the one outlined by Siddon (1970, 1973a). Eq. (4.6) is rewritten:

$$p^{(1)}(\underline{x},t') = -\frac{1}{4\pi c_o^2 x}\int_{V'} \ddot{p}^{(0)}(\underline{y}',t'-r'/c_o)\, d^3\underline{y}' \qquad (C.1)$$

Eq. (4.7) was obtained by multiplying both sides of Eq. (4.6) by $p(\underline{x},t)$. Here, we are interested in predicting the shape of the function $\overline{\ddot{p}^{(0)}p}(\tau)$, so we multiply Eq. (C.1) by $p^{(0)}(\underline{y},t-r/c_o)$ and time average. On the right hand side the factor can be taken under the integral sign because the integration is with respect to $\underline{y}'$:

$$\overline{p^{(0)}(\underline{y},t-r/c_o)\, p(\underline{x},t')} =$$

$$= -\frac{1}{4\pi c_o^2 x}\int_{V'} \overline{p^{(0)}(\underline{y},t-r/c_o)\, \ddot{p}^{(0)}(\underline{y}',t'-r'/c_o)}\, d^3\underline{y}' \qquad (C.2)$$

Retarded time differences due to $r \neq r'$ can be neglected in low speed flows, since the acoustic wavelengths are generally large compared with correlation scales (Lighthill 1962), i.e., we set $r=r'$.

Assuming that all variables are stationary random functions and with $\tau=t'-t$ we get:

$$\overline{p^{(o)}(\underline{y},t-r/c_o)\,p(\underline{x},t')} = \overline{p^{(o)}p}\,(\underline{x},\underline{y},\tau+r/c_o) \qquad (C.3)$$

$$\overline{p^{(o)}(\underline{y},t-r/c_o)\,\ddot{p}^{(o)}(\underline{y}',t'-r'/c_o)} = \frac{\partial^2}{\partial\tau^2}\,\overline{p^{(o)}\,p^{(o)'}}(\underline{\xi},\underline{y},\tau) \qquad (C.4)$$

where $\underline{\xi}=\underline{y}'-\underline{y}$

Hence

$$\overline{p^{(o)}p\,(\tau+r/c_o)} = -\frac{1}{4\pi c_o^{\,2}\,x}\int_V \frac{\partial^2}{\partial\tau^2}\,\overline{p^{(o)}p^{(o)'}}(\underline{\xi},\underline{y},\tau)\;\;d^3\underline{\xi} \qquad (C.5)$$

We select a functional form for the correlation $\overline{p^{(o)}p^{(o)'}}$ which exhibits the property of convecting decay as space separation and time delay are increased:

$$\overline{p^{(o)}p^{(o)'}} = \overline{p^{(o)2}}\;f\left\{(\xi_1-U_c\tau)/L_1,\xi_2/L_2,\xi_3/L_3,\tau/T\right\} \qquad (C.6)$$

(the 1-direction is the direction of motion for the turbulence structure with convection velocity U_c). The function f has the properties:

(1) $f(\underline{\xi}=0,\tau=0) = 1$

(2) $f, \frac{\partial f}{\partial\,\mathrm{arg}} \to 0$ for arg $\to \infty$, sufficiently rapidly for all integrals to converge.

(3) $|f(\mathrm{arg}=0)| \geq |f(|\mathrm{arg}|>0)|$

(4) $f(\mathrm{arg}) = f(-\mathrm{arg})$

(5) f and $\frac{\partial f}{\partial \text{arg}}$ are continuous,

where arg stands for any of the 4 arguments of f. Now put $x_i = \xi_i/L_i$, $\tilde{t}=\tau/T$, $\alpha=U_c T/L_1$. T is some suitable time scale of no further concern here. $\tilde{t}$ is a nondimensional time delay, not the real time. Eq.(C.6) becomes:

$$\overline{p^{(0)}p^{(0)'}} = \overline{p^{(0)2}}\, f(x_1-\alpha\tilde{t},\, x_2,\, x_3,\, \tilde{t}) \qquad (C.7)$$

The convection of the turbulence is allowed for in the x_1-direction which is parallel to the jet axis. There is also some convection in the x_2- and x_3-directions due to spreading of the jet; this effect is very small and neglected here.

Now consider:

$$\frac{\partial}{\partial\tau} = \frac{\partial}{\partial\tilde{t}}\,\frac{d\tilde{t}}{d\tau} = \frac{1}{T}\,\frac{\partial}{\partial\tilde{t}} \qquad (C.8)$$

$$\frac{\partial^2}{\partial\tau^2}\,\overline{p^{(0)}p^{(0)'}} = \frac{1}{T^2}\,\overline{p^{(0)2}}\,\frac{\partial^2}{\partial\tilde{t}^2}\, f(x_1-\alpha\tilde{t},\, x_2,\, x_3,\, \tilde{t}) \qquad (C.9)$$

Put $x_1' = x_1 - \alpha t$. In what follows $\frac{d}{d\,\text{arg}}$ means partial differentiation with respect to one of the 4 arguments of f, the others being held constant. Then:

$$\frac{\partial f}{\partial \tilde{t}} = \frac{df}{dx_1'}\frac{dx_1'}{d\tilde{t}} + \frac{df}{dx_2}\frac{dx_2}{d\tilde{t}} + \frac{df}{dx_3}\frac{dx_3}{d\tilde{t}} + \frac{df}{d\tilde{t}} =$$

$$= -\alpha\frac{df}{dx_1'} + \frac{df}{d\tilde{t}} \qquad \text{(C.10)}$$

$$\frac{\partial^2 f}{\partial \tilde{t}^2} = -\alpha\frac{d}{dx_1'}\left(-\alpha\frac{df}{dx_1'} + \frac{df}{d\tilde{t}}\right) + \frac{d}{d\tilde{t}}\left(-\alpha\frac{df}{dx_1'} + \frac{df}{d\tilde{t}}\right) =$$

$$= \alpha^2\frac{d^2 f}{dx_1'^2} - 2\alpha\frac{d^2 f}{dx_1' d\tilde{t}} + \frac{d^2 f}{d\tilde{t}^2} \qquad \text{(C.11)}$$

It is mathematically convenient to assume that f is separable:

$$f = f_1(x_1')\, f_2(x_2)\, f_3(x_3)\, f_4(\tilde{t}) \qquad \text{(C.12)}$$

and define:

$$\int_{-\infty}^{\infty} f_i\, dx_i = F_i \qquad \text{(C.13)}$$

Then:

$$\overline{p^{(0)}p}\,(\tau+r/c_o) = -\overline{p^{(0)^2}}\,\frac{L_1 L_2 L_3 F_2 F_3}{4\pi c_o^2 x T^2} \times$$

$$\times \left\{\alpha^2 f_4 \int_{-\infty}^{\infty} \frac{d^2 f_1}{dx_1^{\gamma 2}}\, dx_1 - 2\alpha \frac{df_4}{d\tilde{\tau}} \int_{-\infty}^{\infty} \frac{df_1}{dx_1^{\gamma}}\, dx_1 + \frac{d^2 f_4}{d\tilde{\tau}^2} \int_{-\infty}^{\infty} f_1(x_1^{\gamma})\, dx_1 \right\} \qquad (C.14)$$

The first integral is zero by property (2) and (5). Because of property (4) the second integral vanishes. With $dx_1 = dx_1^{\gamma}$ finally

$$\overline{p^{(0)}p}\,(\tau+r/c_o) = -\overline{p^{(0)^2}}\,\frac{L_1 L_2 L_3 F_1 F_2 F_3}{4\pi c_o^2 x T^2}\,\frac{d^2 f_4}{d\tilde{\tau}^2} \qquad (C.15)$$

$\overline{p^{(0)}p}$ is independent of convection for any f_1 satisfying properties (1)-(5). It depends very strongly on T and the function f_4 which together describe the decay properties of the turbulence. For a nondecaying frozen convected pattern f_4 is a constant; no sound would be radiated. For a flow to produce acoustic output it is necessary that patterns are generated and then decay.

If we make the rather special assumption of a convected Gaussian for f:

$$f = \exp\{-(x_1 - \alpha\tilde{t})^2 - x_2^2 - x_3^2 - \tilde{t}^2\} \qquad (C.16)$$

$$\int_{-\infty}^{\infty} f_1\, dx_1 = \int_{-\infty}^{\infty} f_2\, dx_2 = \int_{-\infty}^{\infty} f_3\, dx_3 = \sqrt{\pi} \qquad (C.17)$$

$$\overline{p^{(0)}p}(\tau + r/c_o) = \frac{\sqrt{\pi}}{2}\,\overline{p^{(0)^2}}\,\frac{L_1 L_2 L_3}{c_o^2 \times T^2}\, e^{-\left(\frac{\tau}{T}\right)^2}\left\{1 - 2\left(\frac{\tau}{T}\right)^2\right\} \qquad (C.18)$$

The total area under $e^{-\tilde{\tau}^2}(1-2\tilde{\tau}^2)$ is zero. This means there is no dc-component in $\overline{p^{(0)}p}$ as one might expect since p is an acoustic pressure. This is true for any f_4 satisfying properties (1) - (5).

The shape of the cross correlation $\overline{\dot{p}^{(0)}p}$ can now easily be predicted:

$$\overline{\dot{p}^{(0)}p} = -\frac{\partial}{\partial\tau}\,\overline{p^{(0)}p} = -\frac{\partial}{\partial\tilde{\tau}}\,\overline{p^{(0)}p}\,\frac{d\tilde{\tau}}{d\tau} =$$

$$= \frac{\sqrt{\pi}}{2}\,\overline{p^{(0)^2}}\,\frac{L_1 L_2 L_3}{c_o^2 \times T^3}\; 2\, e^{-\tilde{\tau}^2}(3\tilde{\tau} - 2\tilde{\tau}^3) \qquad (C.19)$$

Fig.4-24 shows a typical measured cross correlation $\overline{\dot{p}^{(0)}p}$ and fitted to it by least squares a function of the type

$$A\, e^{-\left(\frac{\tau}{T}\right)^2}\left\{3\left(\frac{\tau}{T}\right) - 2\left(\frac{\tau}{T}\right)^3\right\} \qquad (C.20)$$

It appears that the convected Gaussian for f is a good assumption as the agreement is good. Knowing the appropriate coefficients from the fitted function one could empirically estimate the radiation from unit volume. The Fourier transform (equal to the cross spectral density) could be obtained in closed form without recourse to numerical transform techniques.

Appendix D

Probe Contamination Ratio

When a probe is inserted into a turbulent flow the interaction of the flow with the probe surface creates noise of a dipole nature. It superposes itself on the quadrupole sound radiated from the flow itself. For the cross correlation measurements using the causality principle it is necessary to minimize this dipole radiation. The reader may recall that dipoles are more efficient emitters than quadrupoles of similar strength, i.e., even a small probe surface may be able to considerably distort acoustic measurements. The probe contamination ratio C to be defined here is a number by which the acoustical performance of a probe in a turbulent flow with given properties can be evaluated.

D.1 Radiation from One Coherent Eddy with correlation volume V_c (no probe in the flow). It follows from Eq. (4.15) and Eq. (4.23) that:

$$\overline{p_{V_c}^2} = \frac{\partial \overline{p^2}}{\partial V} \dot{V}_c = \frac{V_c^2}{16\pi^2 c_o^4 x^2} \overline{\ddot{p}^{(0)2}} = \frac{V_c^2}{16\pi^2 c_o^4 x^2} \overline{\left\{\frac{\partial^2(\rho u_x^2)}{\partial t^2}\right\}^2} \qquad (D.1)$$

D.2 Probe Interaction Noise. Assuming that the probe does

not move and that shear stresses radiate negligible sound (see section D.5), and using Eq.(3.2) and Eq.(3.5), only the second integral of Eq.(1.2) is left. It becomes in the far field:

$$p_d = -\frac{\cos\beta}{4\pi c\, x} \int_S \left[\dot{p}_s\right] dS \qquad (D.2)$$

where the subscript "d" indicates dipole type radiation, β is the angle between the normal to the surface S and the direction of radiation, and p_s is the surface normal pressure. After squaring and time averaging, and setting $\cos\beta = 1$ for the worst case, Eq.(D.2) becomes:

$$\overline{p_d^2} = \frac{1}{16\pi^2 c_o^2 x^2} \overline{\int_S \left[\dot{p}_s\right] dS \int_{S'} \left[\dot{p}_s\right]' dS'} \qquad (D.3)$$

If the process is statistically stationary and the surface is small compared with a typical wavelength, the brackets [...] indicating evaluation at retarded time can be dropped in this case.

Assuming that p_s is well correlated over the surface of the probe (i.e. it is at least contained in a correlation volume), the integrals in Eq.(D.3) represent nothing else but the mean squared derivative of the fluctuating lift force exerted on the probe. We can use unsteady airfoil theory to estimate the lift L if the disturbance velocities are small compared to the mean flow U, and if the probe shape comes close to a slender body shape. The requirements are not too stringent as the probe contamination ratio is only a rough estimate designed to gain some feeling for the amount of dipole "poisoning". C_L is the unsteady lift

coefficient, α is the instantaneous angle of attack:

$$L(t) \simeq 0.5\rho U^2 S_p C_L \simeq 0.5\rho U^2 S_p \frac{dC_L}{d\alpha}\alpha(t) \qquad (D.4)$$

It is well known that the lift curve slope $\frac{dC_L}{d\alpha}$ depends on the wavenumber of the incident disturbance [Sears (1941) function, see also Liepmann 1952, p. 796; and see Fig.4-25]. Most probes can be generally regarded as low aspect ratio finite wings for which the variation of $\frac{dC_L}{d\alpha}$ with the wave number is only moderate, as indicated typically by the dashed line in Fig.4-25. A value of 2 is therefore used for the lift curve slope in the subsequent calculations. With

$$\alpha(t) \simeq v(t)/U \qquad (D.5)$$

(v is the component of the velocity disturbance perpendicular to U in the plane that contains the direction of radiation) Eq. (D.4) becomes after differentiating with respect to time, squaring, and time averaging:

$$\overline{L^2} \simeq (\rho U^2)^2 S_p^2 \frac{1}{U^2} \overline{\left(\frac{\partial v}{\partial t}\right)^2} \qquad (D.6)$$

which is an estimate of the product of the two integrals in Eq. (D.3). Therefore:

$$\overline{p_d^2} \simeq \frac{\overline{L^2}}{16\pi^2 c_o^2 x^2} \qquad (D.7)$$

D.3 Definition of Probe Contamination Ratio. We now define the probe contamination ratio as the ratio between the mean squared acoustic pressure due to dipole type radiation from the probe surface to the mean squared acoustic pressure due to quadrupole type radiation from the adjacent eddy of fluid:

$$C = \overline{p_d^2}/\overline{p_{V_c}^2} \qquad (D.8)$$

Combining Eq.(D.1), Eq.(D.6), and Eq.(D.7):

$$C = \left(\frac{U}{c_o}\right)^2 \left(\frac{\rho c_o^2 S_p}{V_c}\right)^2 \frac{\overline{\dot{v}^2}}{\overline{(\rho u_x^2)^{\cdot\cdot 2}}} \qquad (D.9)$$

For low speed flows the density ρ can be regarded constant and then cancels out in Eq.(D.9).

D.4 Estimates for a Low Speed Turbulent Jet. The point 4 diameters downstream and half a diameter from the axis is chosen as representative. There, the mean velocity U is about $0.6U_o$, where U_o is the exit velocity. It is assumed that $v_{rms} \simeq u_{rms} \simeq 0.15U_o$, and that differentiation with respect to time can be replaced by multiplying by $2\pi\nu \simeq 2\pi 0.2U/L_c$, where L_c is the correlation length, and is given by $L_c \simeq 0.13x$ (x is measured in diameters from the exit) (from Laurence 1957). If the correlation volume is imagined as an ellipsoid with minor axes 1/3 of the major then $V_c \simeq L_c^3$. Therefore Eq.(D.9) becomes:

$$C \simeq \left(\frac{0.6U_o}{c_o}\right)^2 c_o^4 \frac{S_p^2}{L_c^6} \frac{(2\pi\nu)^2 \overline{v^2}}{(2\pi\nu)^4 \overline{v^4}} \qquad (D.10)$$

Also (from Siddon 1969): $\overline{v^4} \simeq 2\overline{v^2}$ (D.11)

(note that for a Gaussian: $\overline{v^4} = 3\overline{v^2}$)

$$C \simeq (0.6M)^2 \frac{S_p^2}{L_c^6} \frac{c_o^4}{(2\pi\, 0.2\; 0.6U_o/L_c)^2\, 2(0.15U_o)^2} =$$

$$= \frac{14}{M^2} \left(\frac{S_p}{L_c^2}\right)^2 \qquad (D.12)$$

If we desire that C be less than 0.1 for good accuracy, we must

require that

$$\left(\frac{S_p}{L_c^2}\right)^2 < \frac{M^2}{140}$$

For $x=4D$, $L_c \simeq D/2$. Then we need

$$S_p < D^2M/48$$

In the experiments described in this thesis: D=38.1 mm, M=0.32:

$$S_p < 9.7 \text{ mm}^2 \qquad (D.13)$$

For cylindrical probes S_p can be replaced by an "effective" area because the pressure fluctuations due to the turbulent cross velocities are concentrated near the nose of the probe as shown in Fig.4-26. Assuming that S_p is equal to $2d^2$ (where d is the diameter of the probe) d would have to be 2.2 mm or less, a very small size for a dynamic pressure sensor. In addition, the 90° bend downstream of the sensing elements would create additional noise by flow separation and vortex shedding.

The pressure probe described in section IV of this thesis has a cross sectional area of about 10 mm², thus barely satisfying Eq. (D.13). However, the calculations here are done for x=4D. Closer to the jet exit the requirements become more stringent and the present probe may be radiating a significant amount of dipole noise.

D.5 Is the Skin Friction Indeed Unimportant for the Foil Probe? The radiated sound due to skin friction or shear stress is obtained by considerations similar to the ones arriving at Eq. (D.3):

$$\overline{p_{fr}^2} = \frac{1}{16\pi^2 c_o^2 x^2} \overline{\int_S \left[\dot{\tau}\right] dS \int_{S'} \left[\dot{\tau}\right]' dS'} \qquad (D.14)$$

[from the third term in the second integral of Eq.(1.2)] Under the same assumptions as for the lift force case the 2 integrals result in $\overline{\dot{W}^2}$, the mean square derivative of the drag force W. The Reynolds number Re is based on the chord length of the probe b=9.85 mm, the mean velocity $U=0.6U_o$= 66 m/sec, and the kinematic viscosity of the air at 20°C $\nu=14.9*10^{-6}$ m²/sec:

$$Re = bU/\nu = 4.36*10^4 < 5*10^5 = Re_{tr} \qquad (D.15)$$

where Re_{tr} is the Reynolds number for transition, i.e. the boundary layer is laminar. For a rough estimate of the quasi steady drag fluctuation we use Blasius' Law for the laminar skin friction coefficient c_w, although it is strictly applicable only to a flat plate:

$$c_w = 1.328/\sqrt{Re} \qquad (D.16)$$

then, the instantaneous drag force becomes:

$$W \cong c_w S_{p_f} 0,5\rho(U+u)^2 = \frac{1.328}{\sqrt{Re}} S_{p_f} 0.5\rho(U^2+2Uu+\sim 0) \qquad (D.17)$$

where S_{p_f} is now the upper surface area of the foil; u is the velocity fluctuation in the mean flow direction. Eq.(D.17) becomes after differentiating, squaring, and time averaging:

$$\overline{\dot{W}^2} \simeq \frac{(1.328\, S_{p_f} \rho U)^2}{Re} \overline{\dot{u}^2} \qquad (D.18)$$

We now define the probe contamination ratio for skin friction fluctuations by analogy to Eq. (D.8):

$$C_{fr} = \overline{p_{fr}^2} / \overline{p_{V_c}^2} \qquad (D.19)$$

Combining Eq. (D.19) and Eq. (D.1):

$$C_{fr} = \left(\frac{U}{c_o}\right)^2 \left(\frac{\rho c_o^2 S_{pf}}{V_c}\right)^2 \frac{\overline{\dot{u}^2}}{(\rho u_x^2)^{\cdot\cdot 2}} \frac{1.76}{Re} \qquad (D.20)$$

Assuming $\overline{\dot{u}^2} \simeq \overline{\dot{v}^2}$, using Eq. (D.9), and putting $S_{p_f} \simeq 10 S_p$ for the present probe:

$$C_{fr} \simeq \frac{176}{Re} C \qquad (D.21)$$

Eq. (D.21) shows that the probe contamination ratio for skin friction is very much smaller than the one for sound radiated due to forces normal to the surface. Shear stresses are therefore unimportant in the dipole noise calculations affecting the present foil type pressure sensor. Since C_{fr} is about 2 orders of magnitude smaller than C, dipole noise due to shear stresses is probably hardly ever of any importance in low speed turbulent air flows.

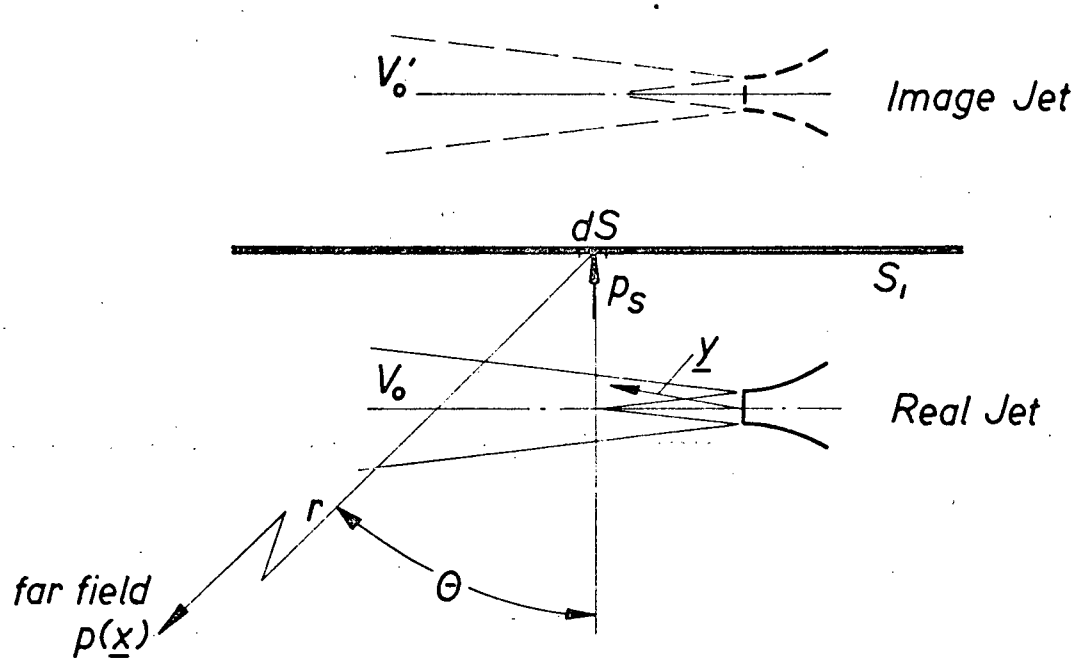

Fig.3-1 Image geometry

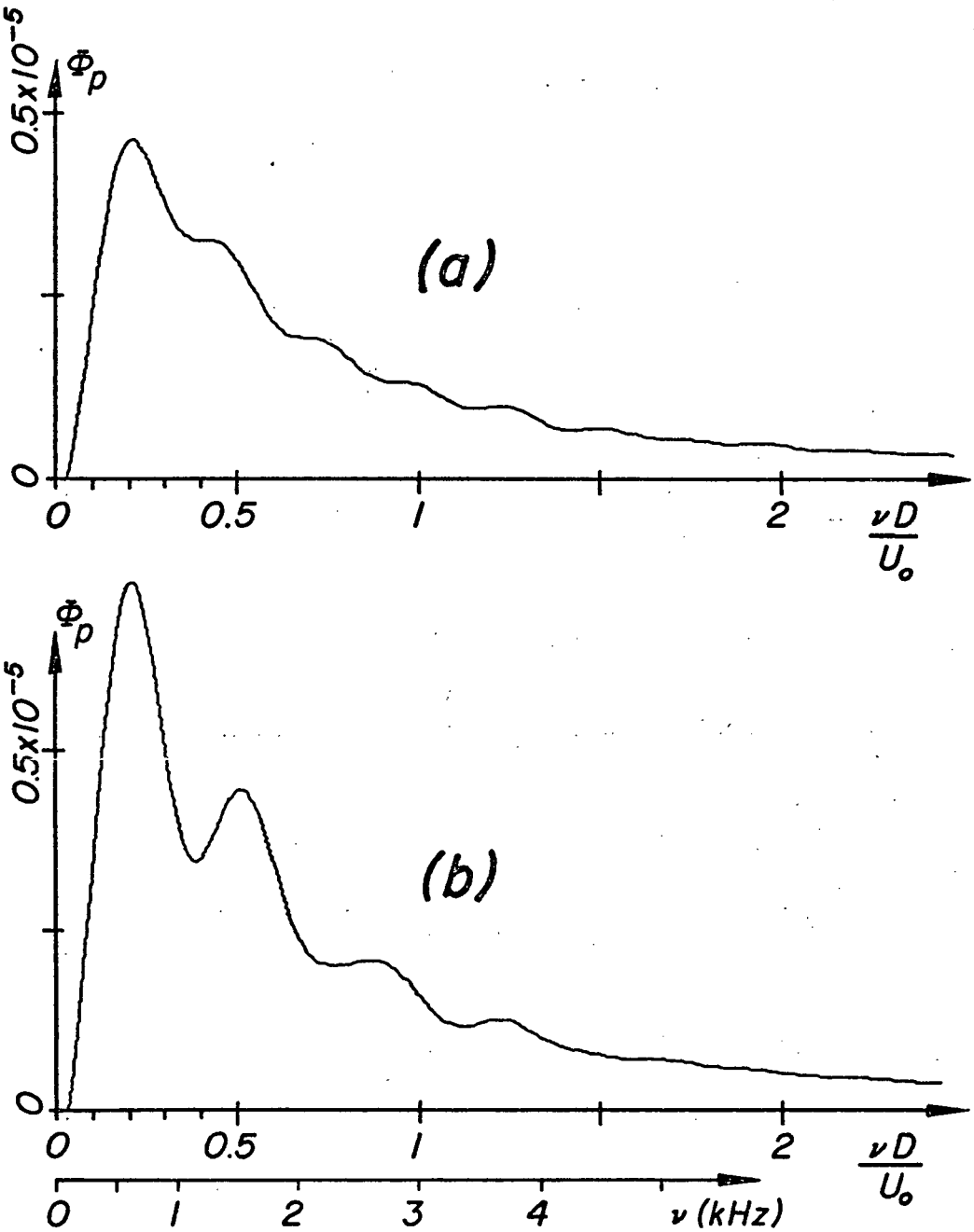

Fig.3-2 Nondimensional spectrum of jet noise at 45^{o} to jet axis. (a) isolated jet, (b) with surface S_1 behind the jet. (computer plot)

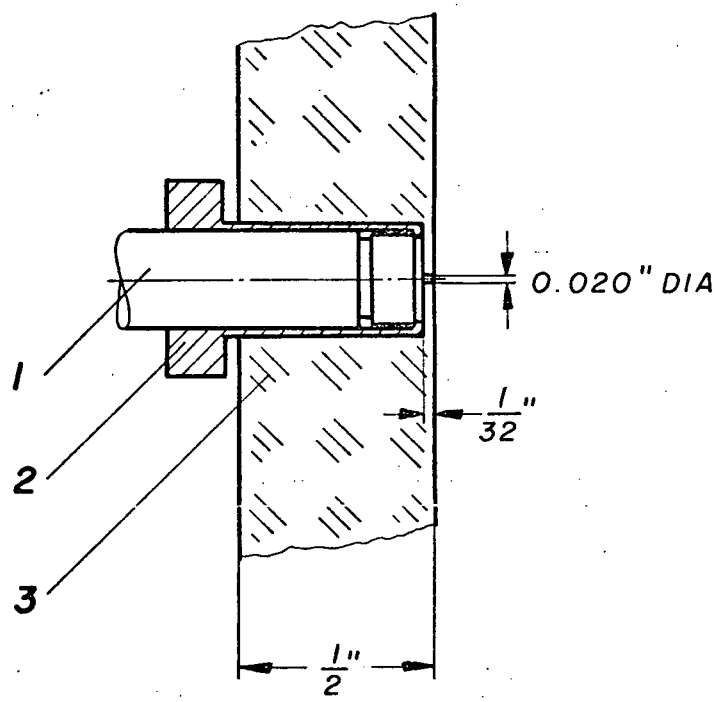

Fig.3-3 Microphone mounting. 1: ¼-inch Bruel & Kjaer microphone, 2: brass sleeve, 3: ½-inch thick plexiglass panel.

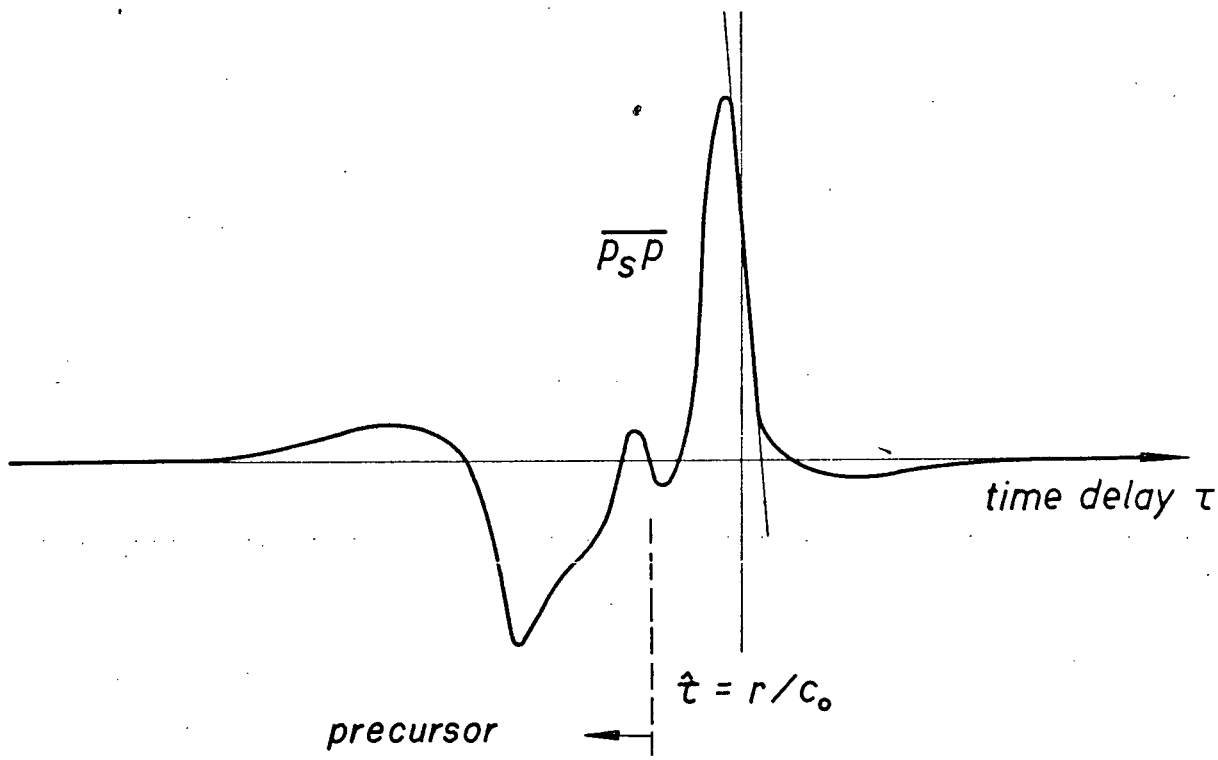

Fig.3-4 Typical cross correlation function between surface pressure p_s and far field pressure p. Derivative to be evaluated at $\tau=r/c_o$. Notice precursor to the left.

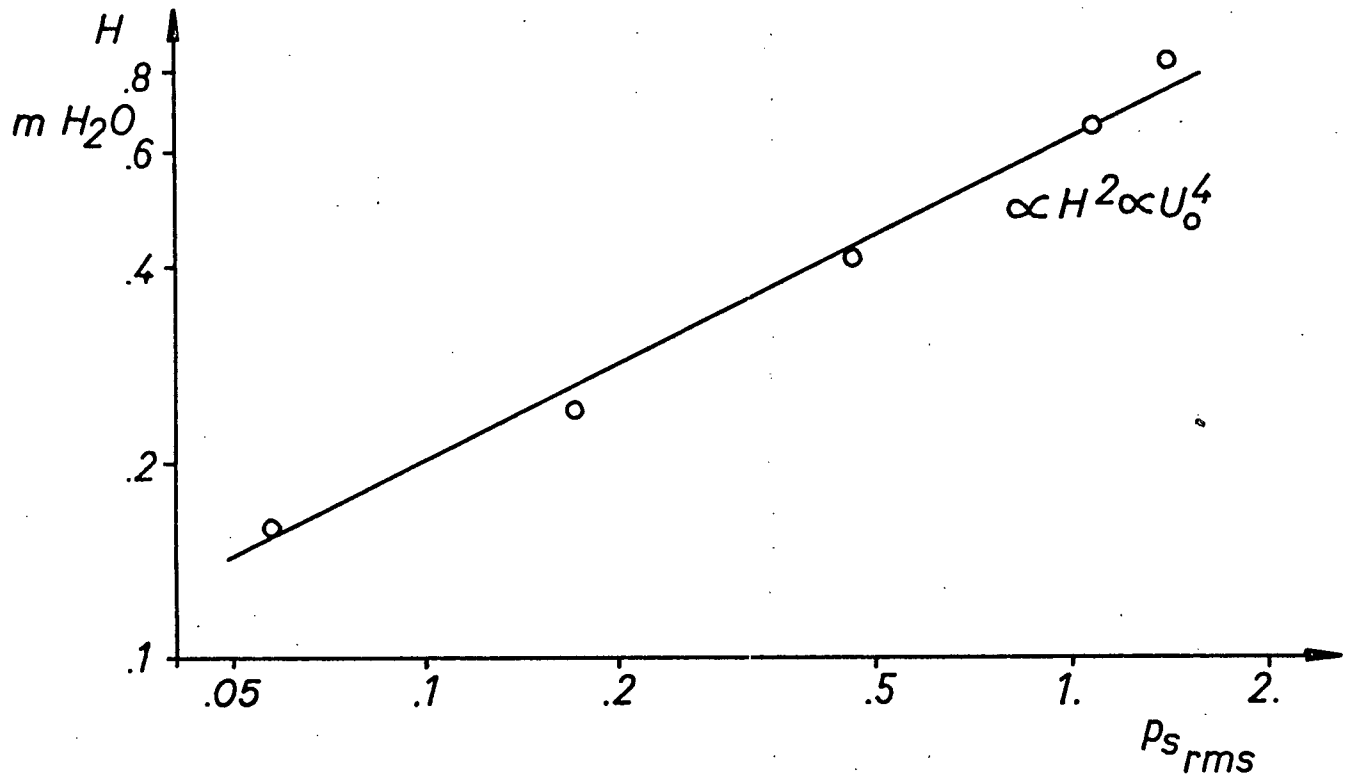

Fig.3-5 Relationship between surface pressure p_s and exit velocity U_o.
H = settling chamber pressure in meters of water.

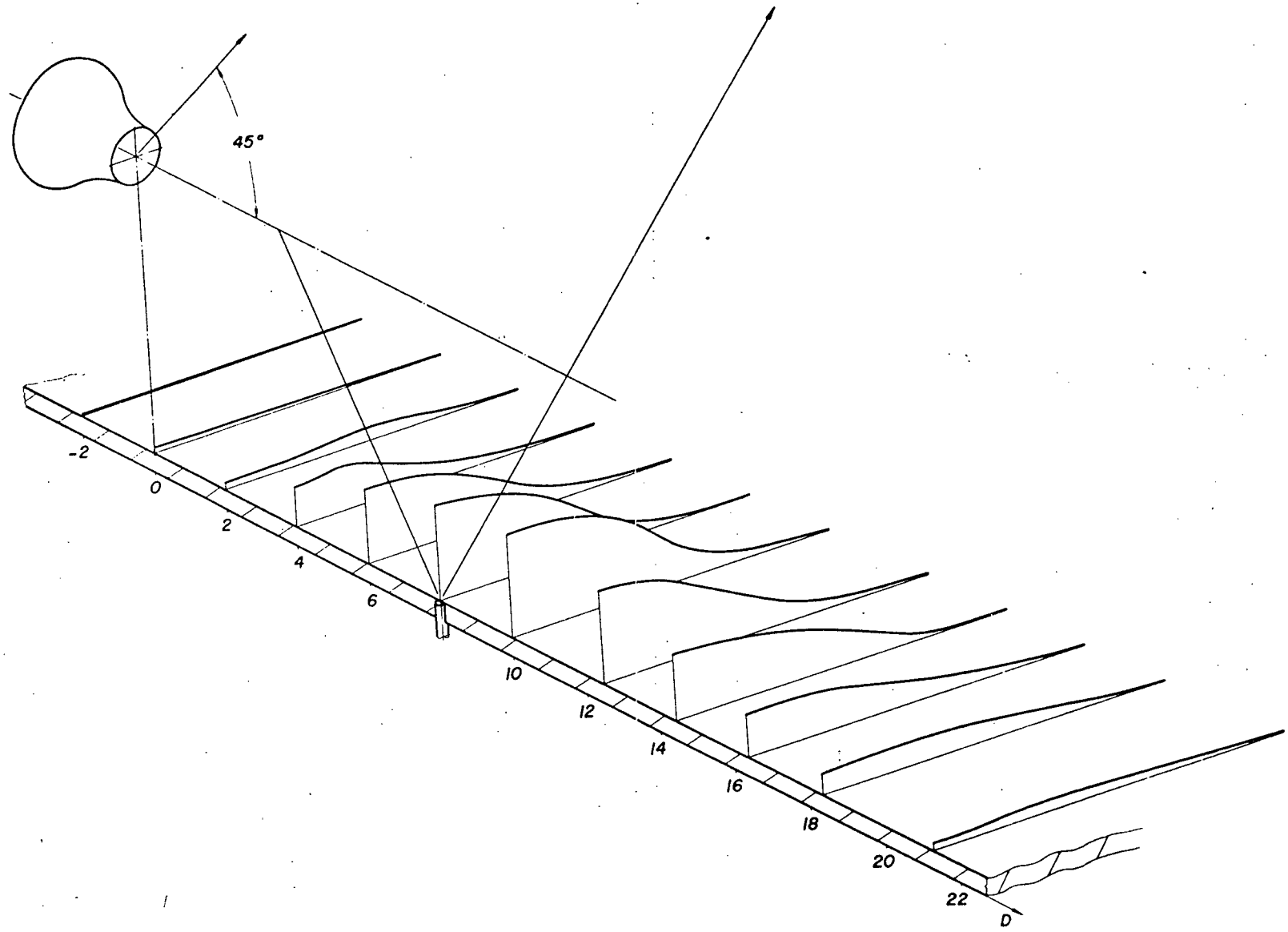

Fig.3-6 Distribution of source strength over surface S_1. Reflection path.

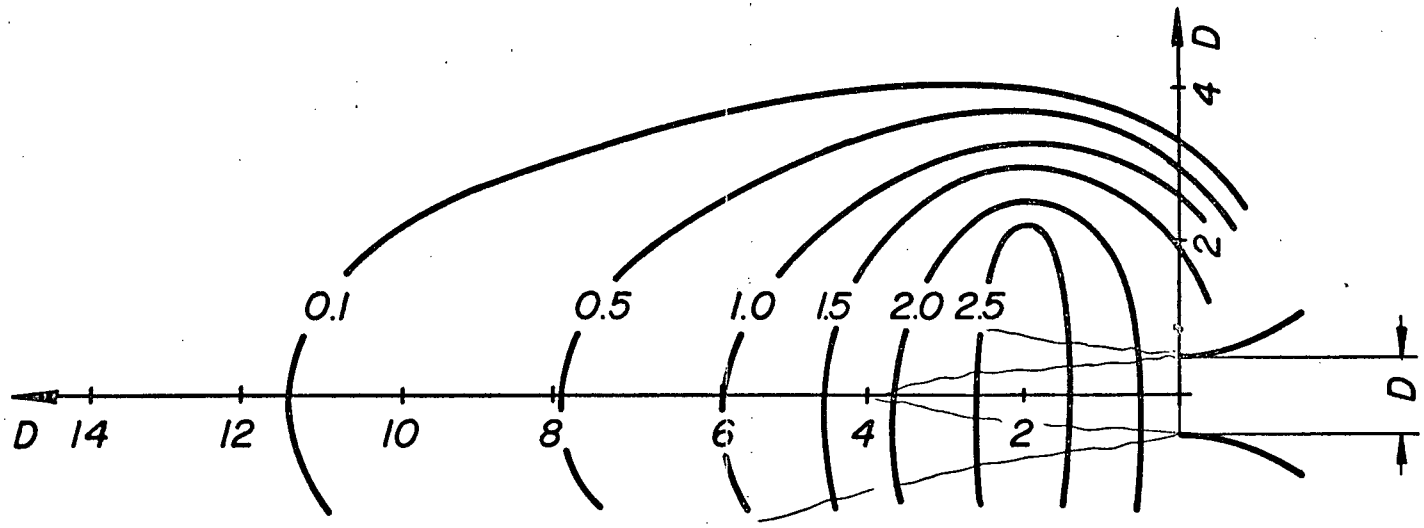

Fig.3-7 Equal source strength contours for $\theta=90^{o}$.

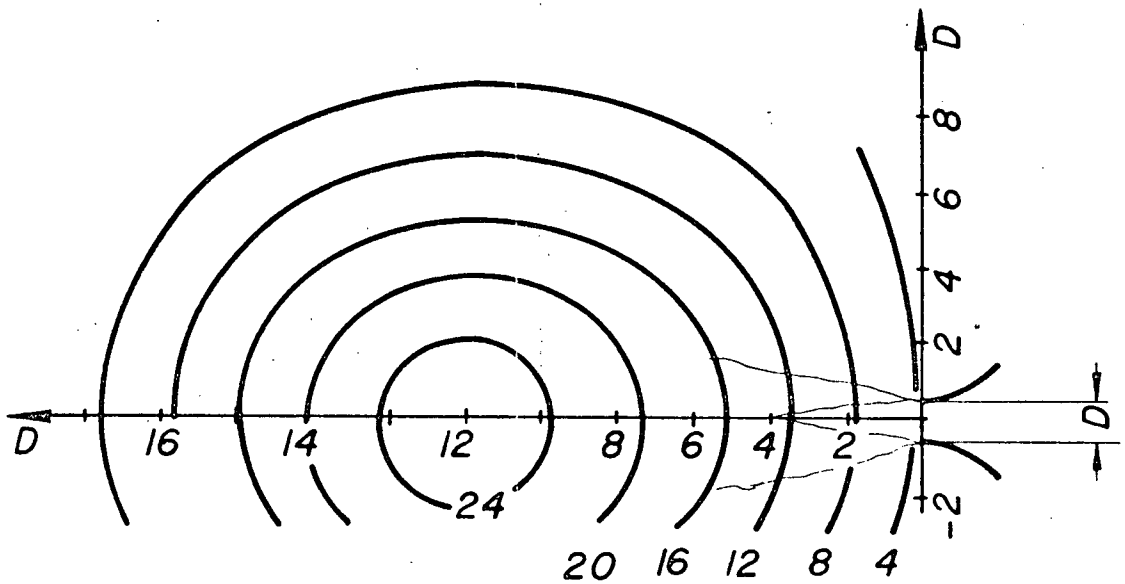

Fig.3-8 Equal source strength contours for $\theta=60^{o}$

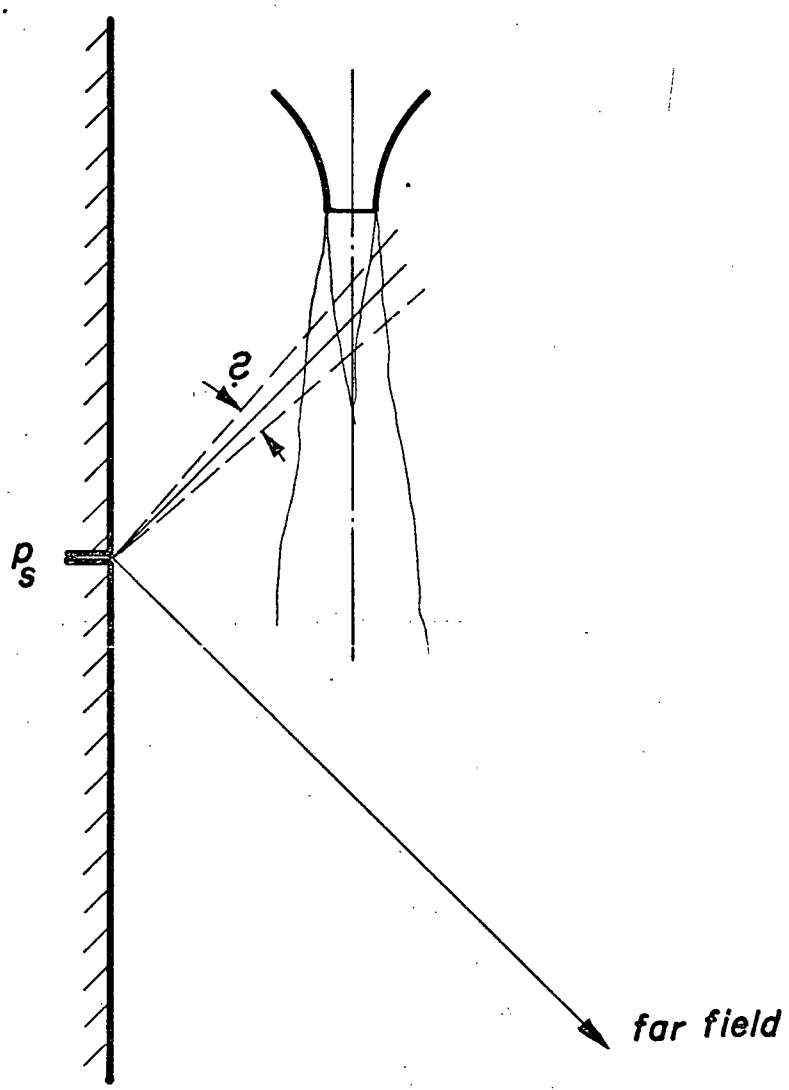

Fig.3-9 Zone of Influence. Angle of aperture of the dashed cone not known.

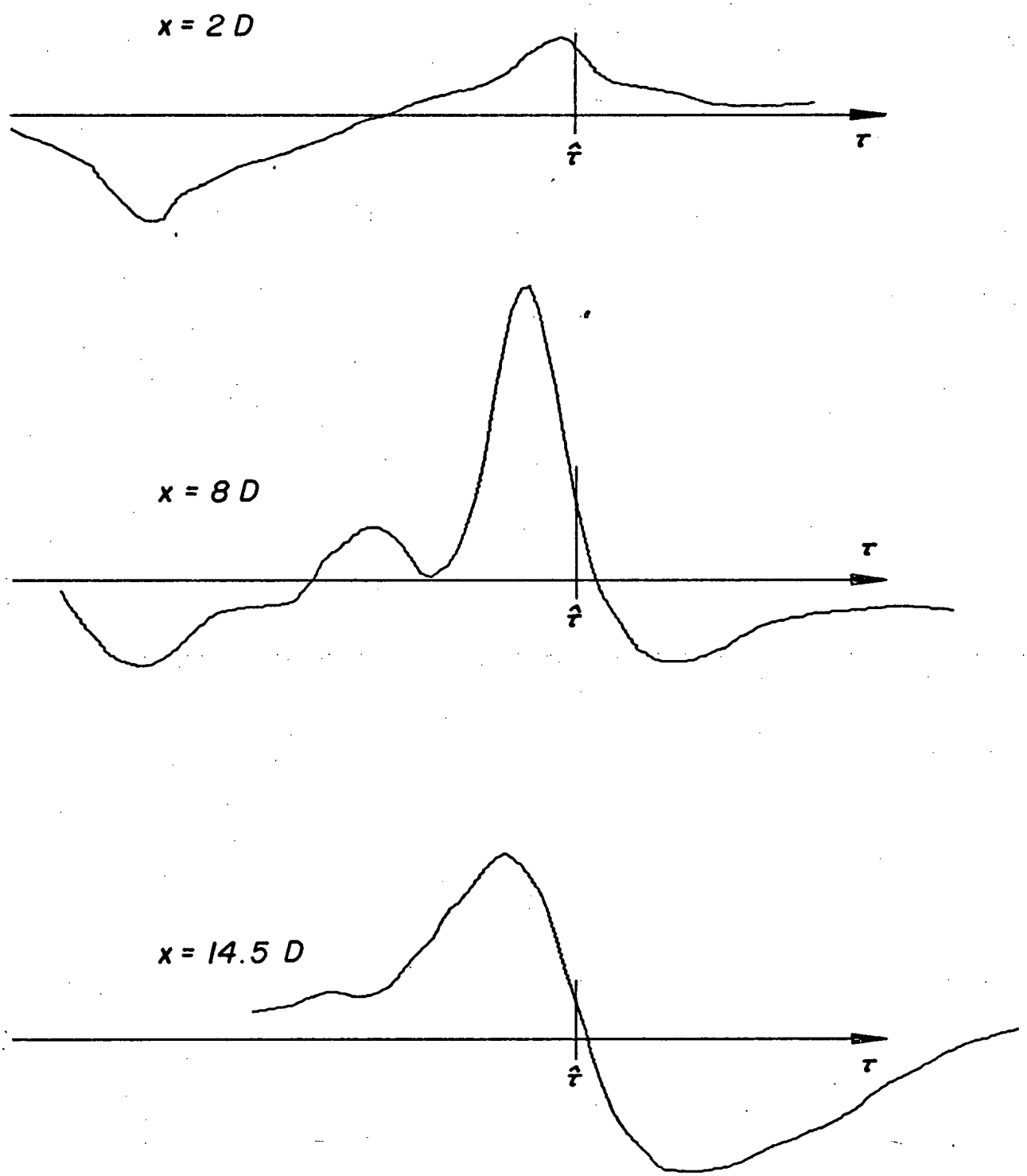

Fig.3-10 3 typical $\overline{p_s p}(\tau)$ at different downstream positions x. Distance jet axis to surface S_1 is 5.17D. p_s measured directly opposite of jet axis. p measured in far field at 45^o to jet axis. (computer plot)

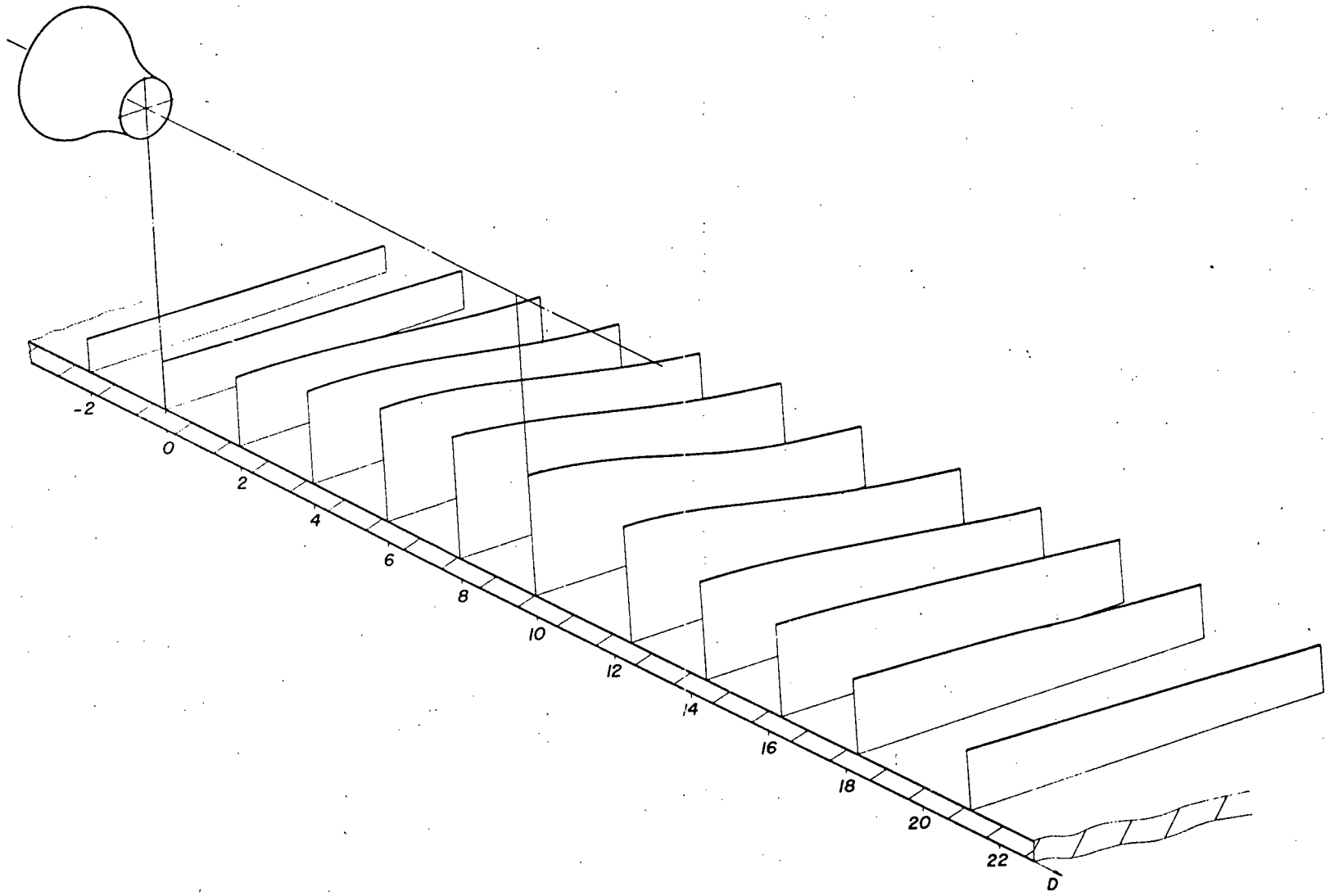

Fig.3-11 Distribution of root mean squared surface pressure over the surface S_1

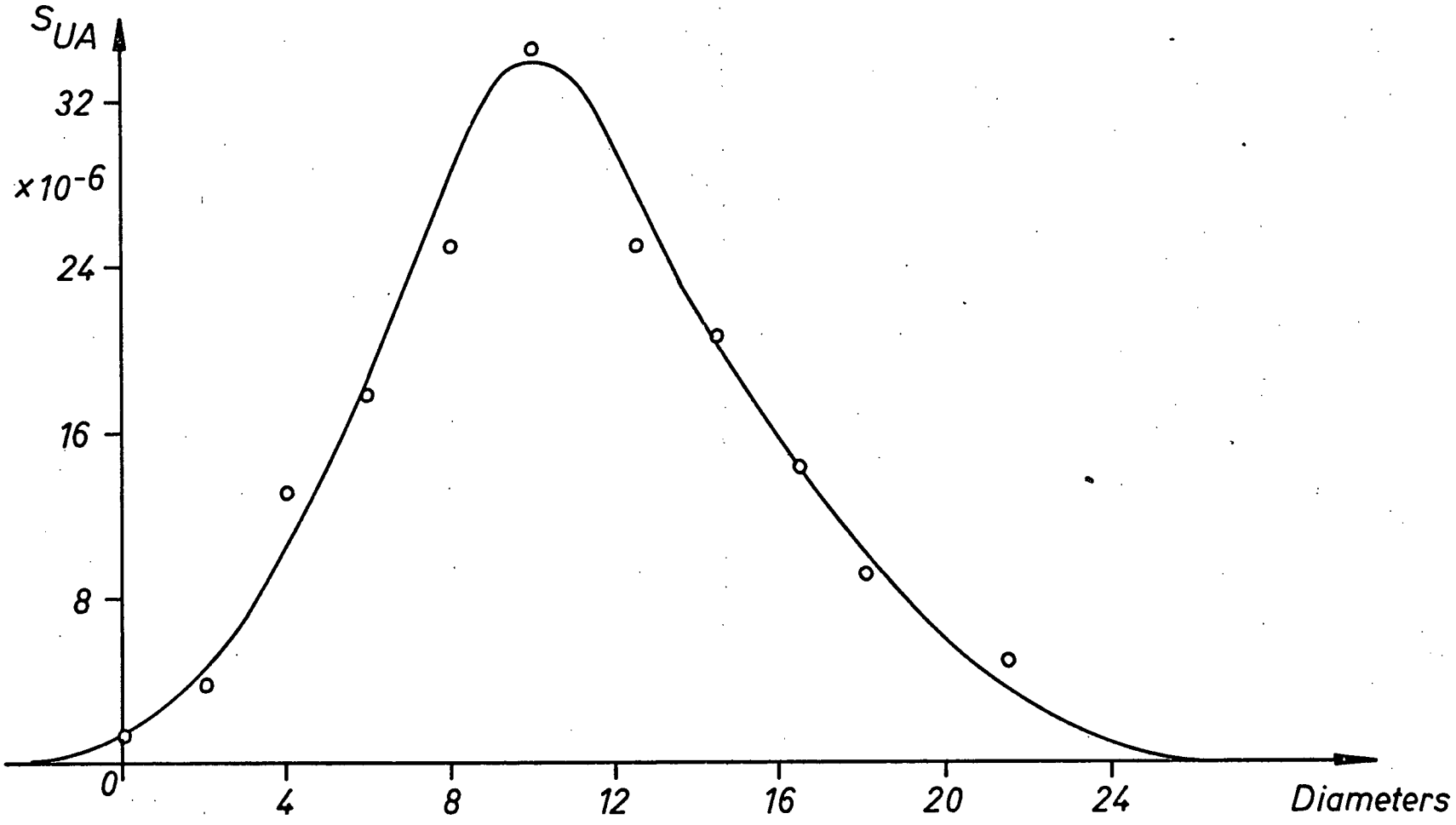

Fig.3-12 "Slicewise" integrated source strength for $\theta=45^{o}$

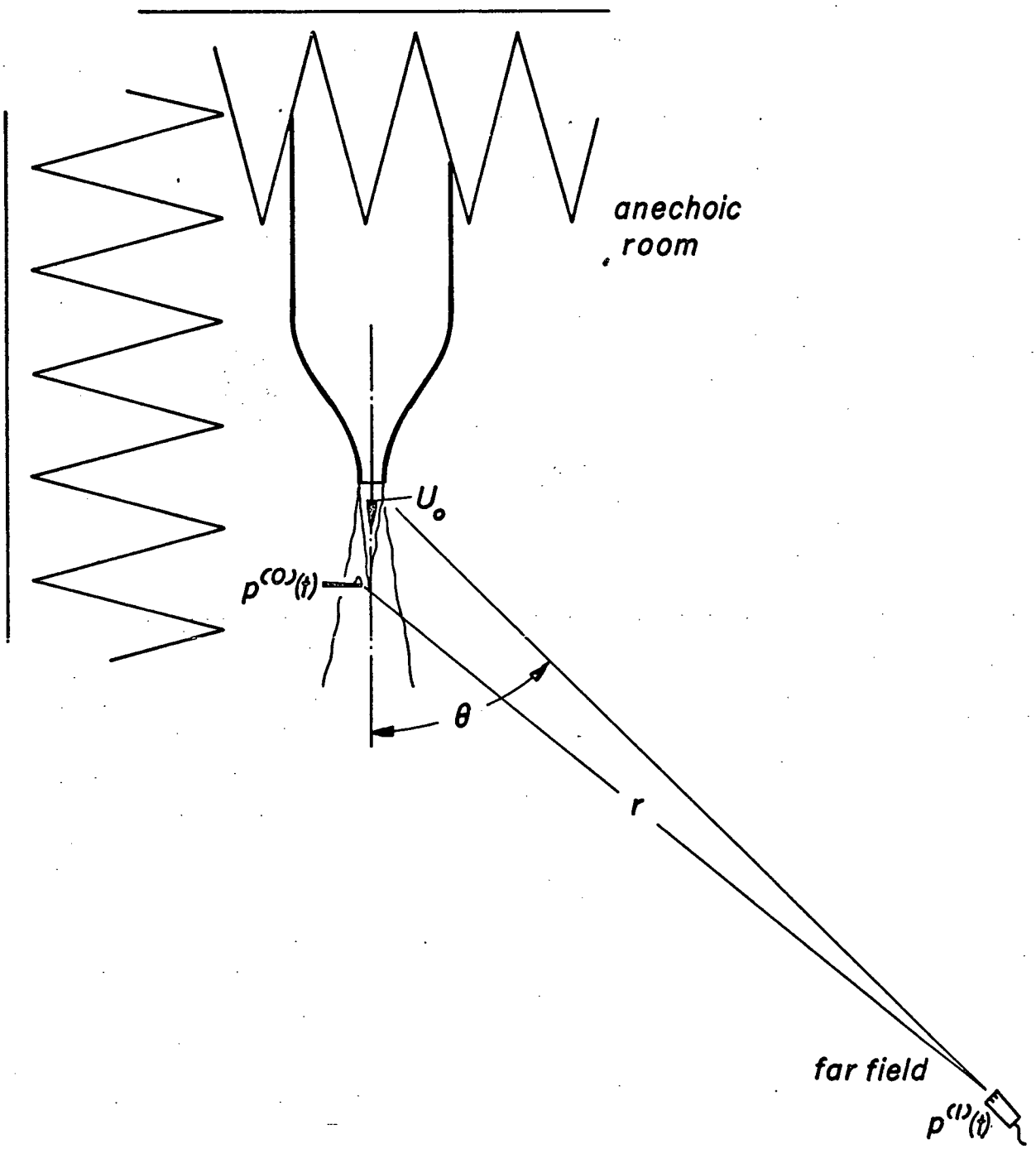

Fig.4-1 Experimental setup of causality correlation technique. Pressure sensor measures $p^{(0)}(t)$, microphone in the far field measures $p^{(1)}(t)$. U_o=exit velocity.

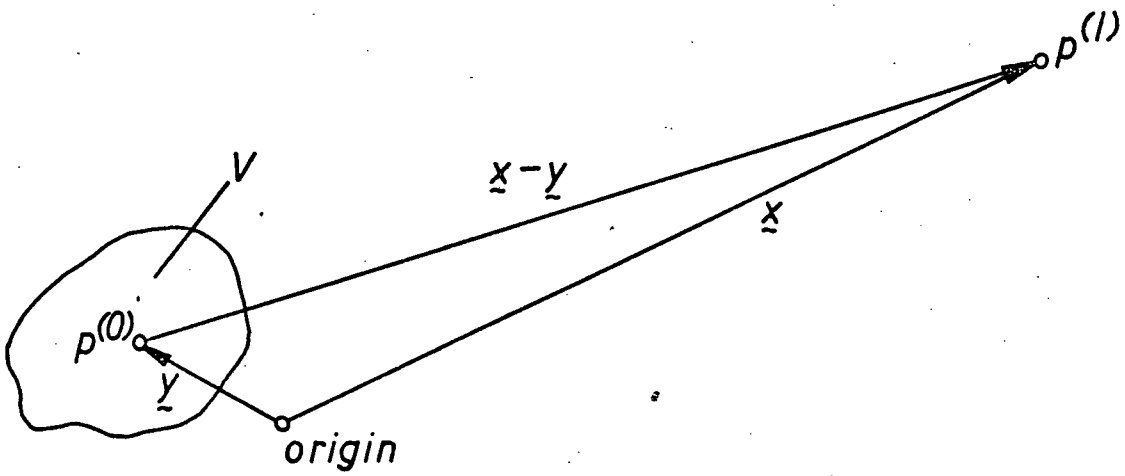

Fig.4-2 Geometry

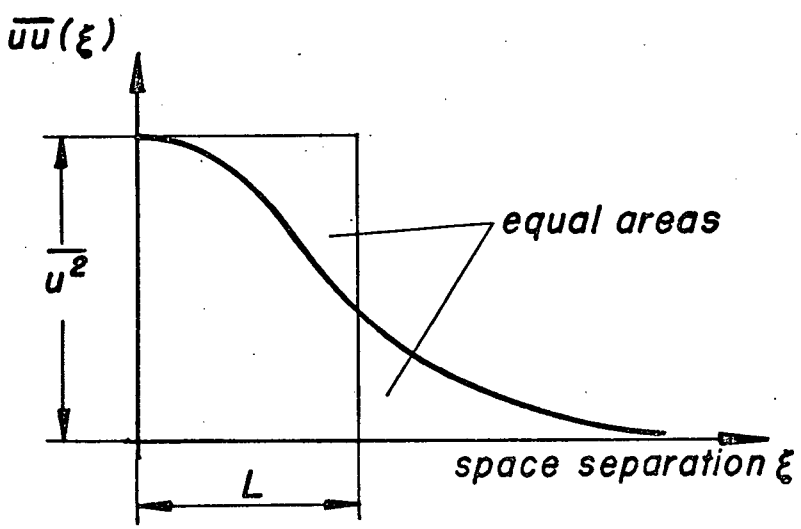

Fig.4-3 Definition of correlation length L

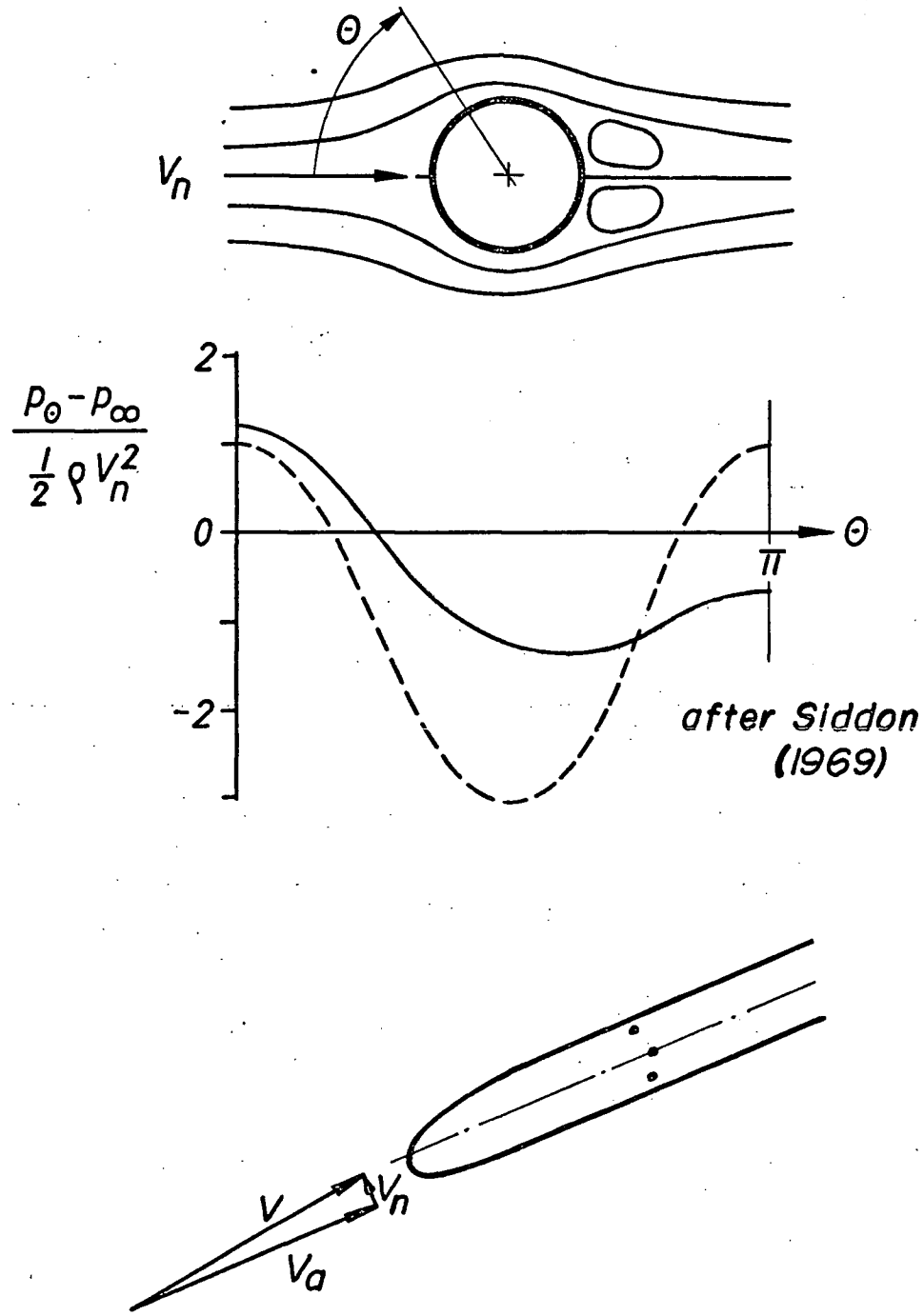

Fig.4-4 Classical cylindrical probe configuration. Upper part: pressure distribution due to cross flow, full line: 40 < Reynolds number < 40000, dashed line: potential flow. Lower part: V instantaneous velocity vector, V_a axial component, V_n cross flow component.

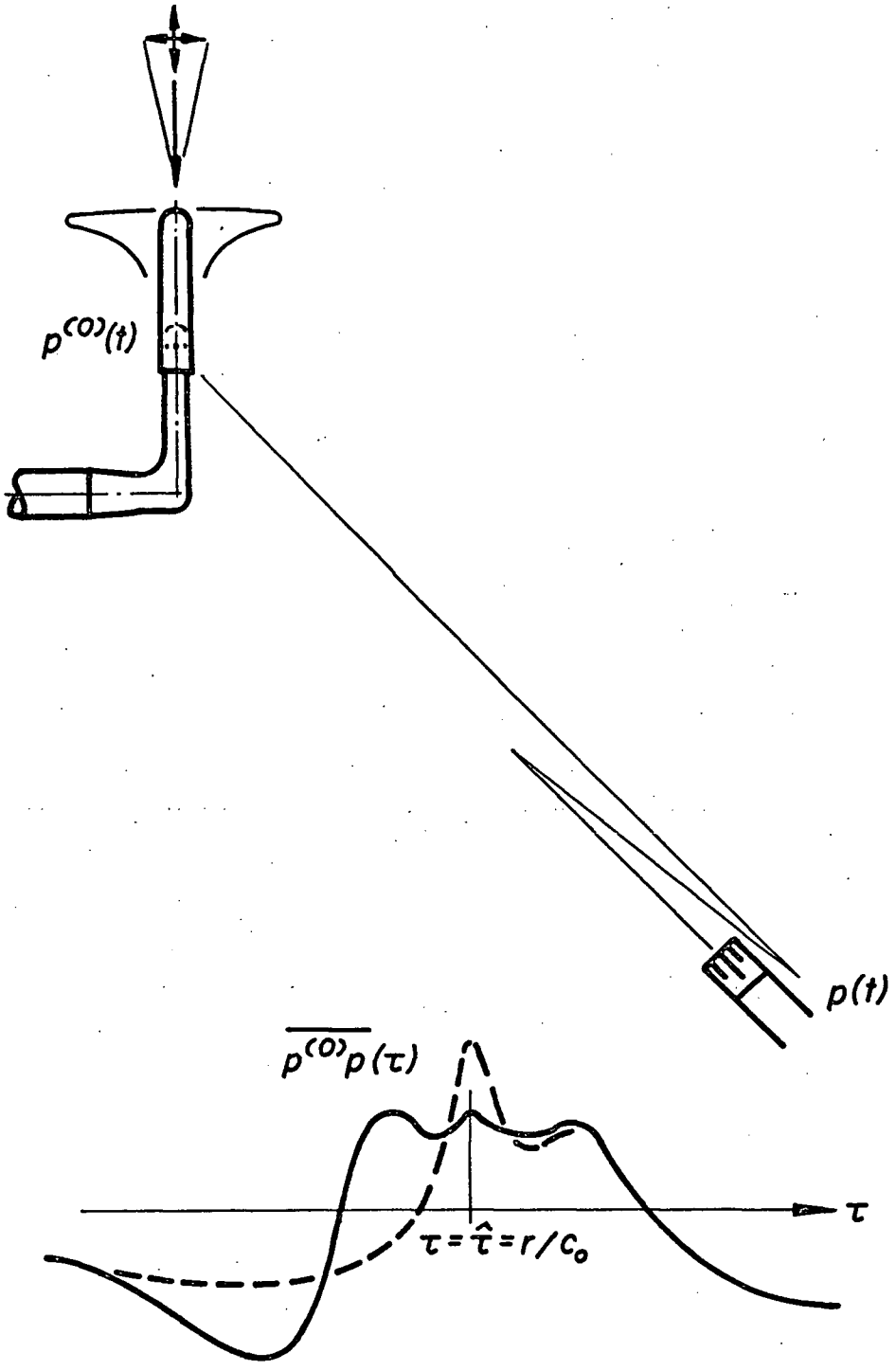

Fig.4-5 Typical cross correlation between fluctuating pressure in the jet $p^{(o)}$ and acoustic pressure p, contaminated by dipole noise: Turbulence induces a fluctuating lift on the nose of the cylindrical probe sending off a dipole pulse. Dashed line: effect of shortening nose piece.

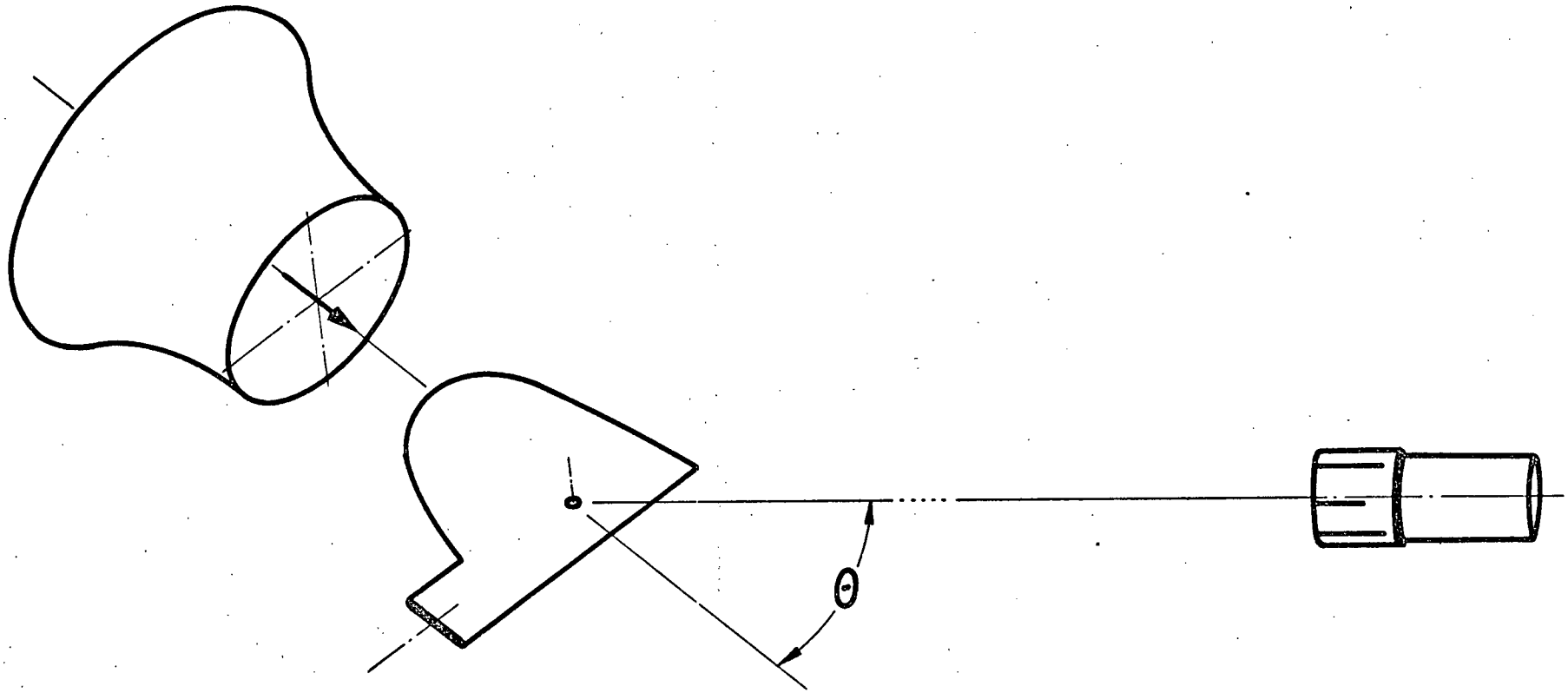

Fig.4-6 Principle of arranging foil probe in the flow (distances and sizes not proportionate): Plane of foil contains mean flow direction and direction of radiation toward far field microphone (right).

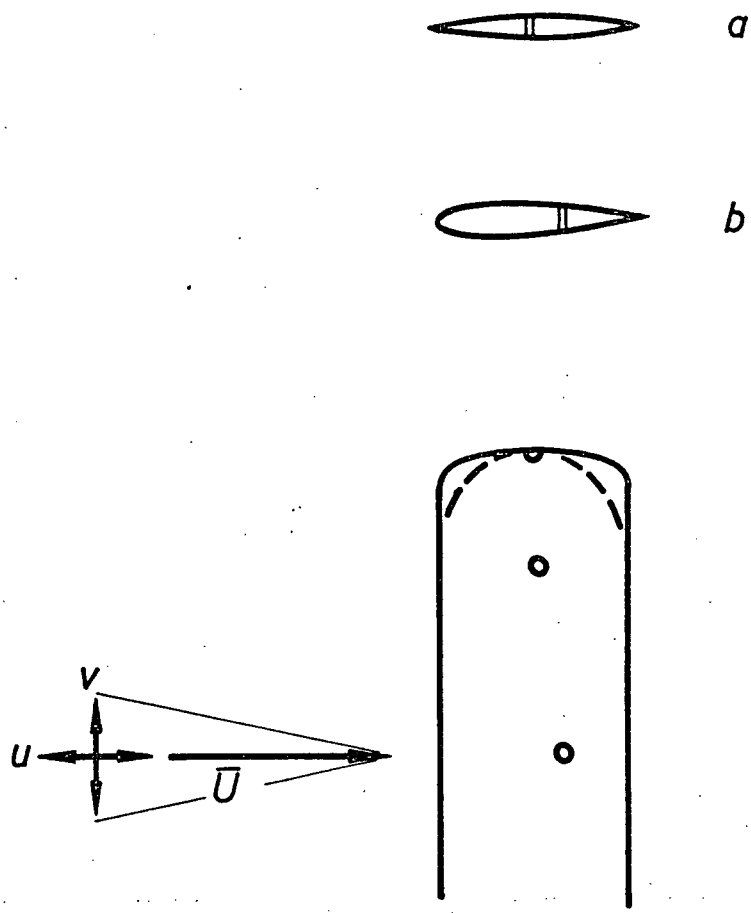

Fig.4-7 Locations of pressure sensing holes on airfoil: (a) supersonic, (b) subsonic. The measured pressure is the average between the pressures on the upper and the lower surface.

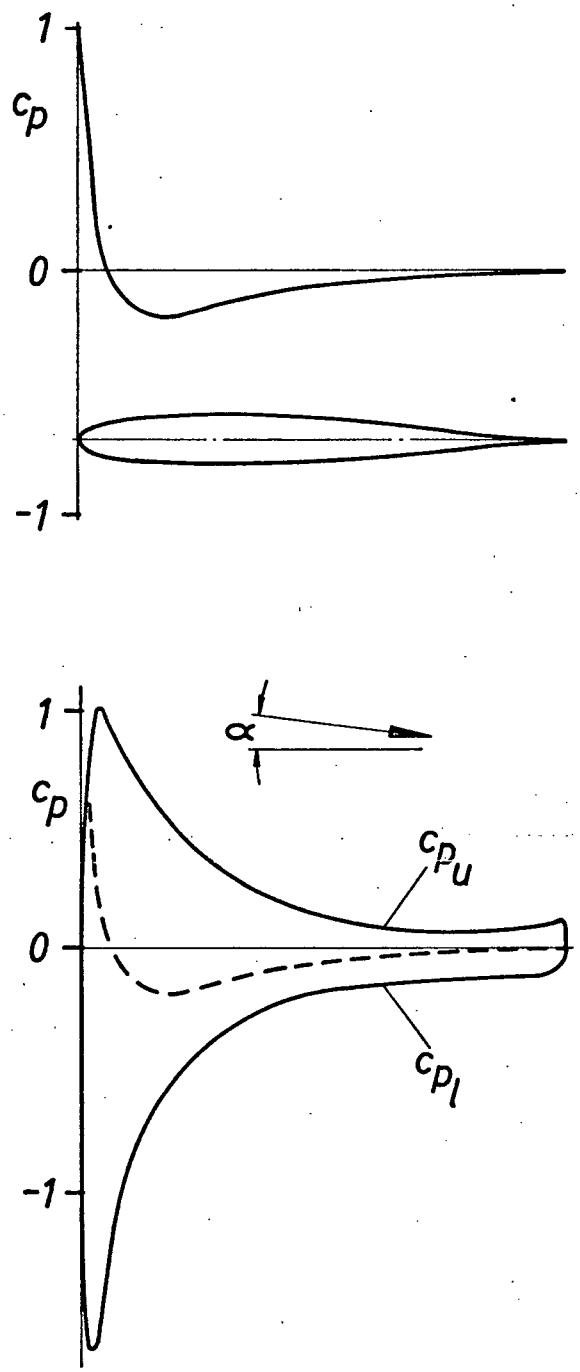

Fig.4-8 Subsonic airfoil. Upper part: foil cross section and distribution of pressure coefficient c_p due to thickness. Lower part: c_p due to thickness and angle of attack. c_{pu}: upper surface, c_{pl}: lower surface.

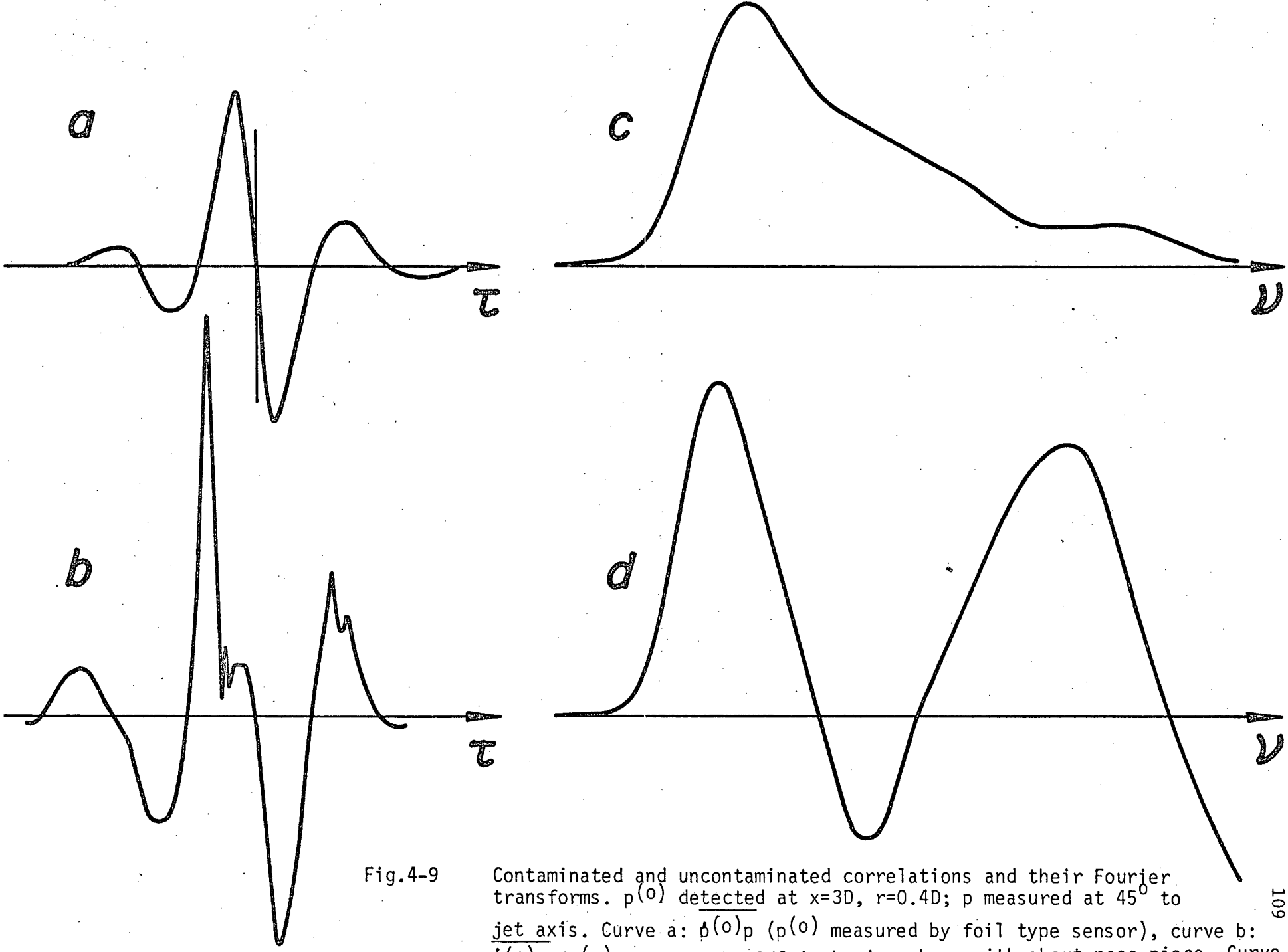

Fig.4-9 Contaminated and uncontaminated correlations and their Fourier transforms. $p^{(o)}$ detected at x=3D, r=0.4D; p measured at 45^{o} to jet axis. Curve a: $\dot{p}^{(o)}p$ ($p^{(o)}$ measured by foil type sensor), curve b: $\dot{p}^{(o)}p$ ($p^{(o)}$ measured by 1/8-inch microphone with short nose piece. Curve c: Fourier transform of a, curve d: F.T. of b. τ time delay, νfrequency.

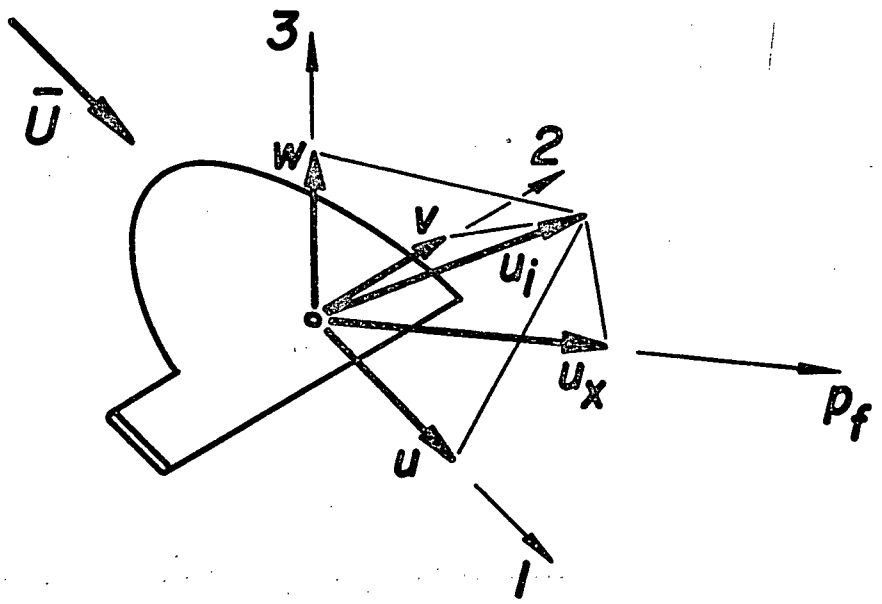

Fig.4-10 Velocity vectors on airfoil probe

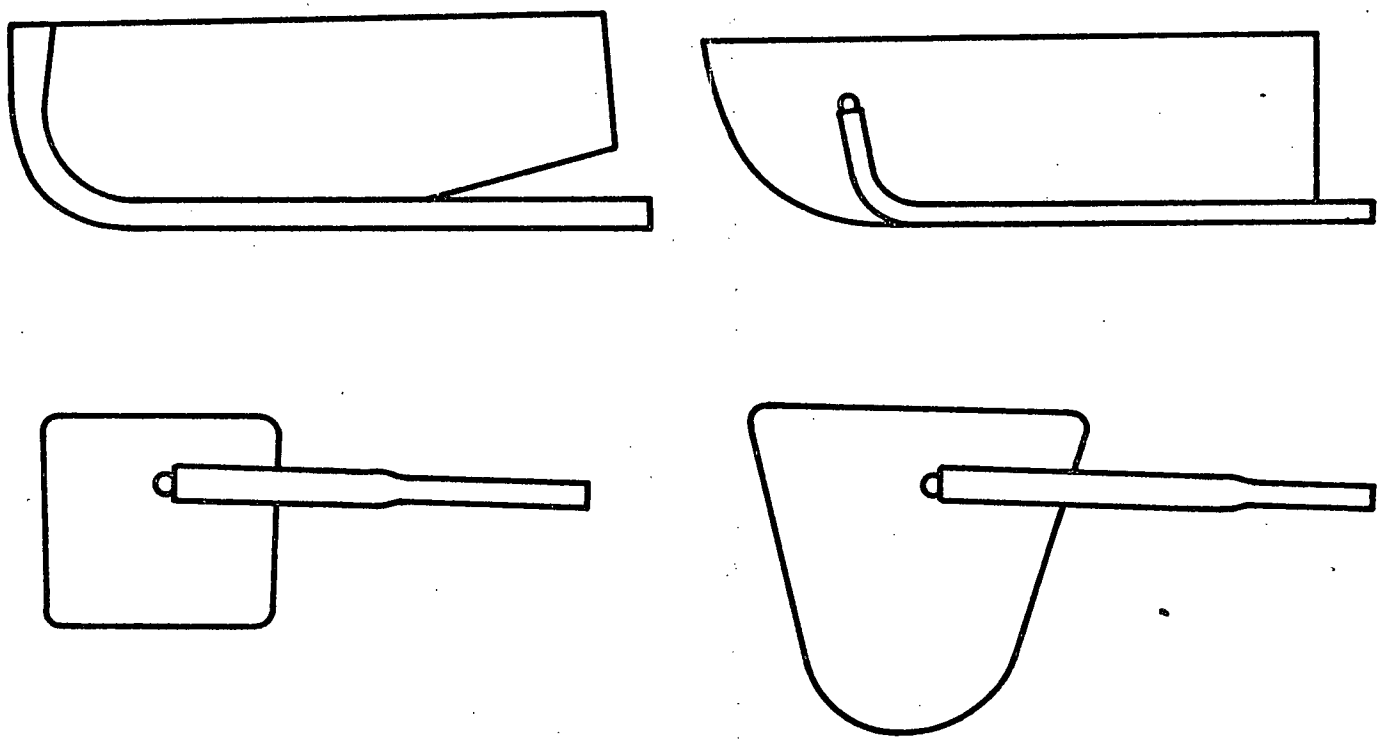

Fig.4-11 Probe shapes tried out but discarded

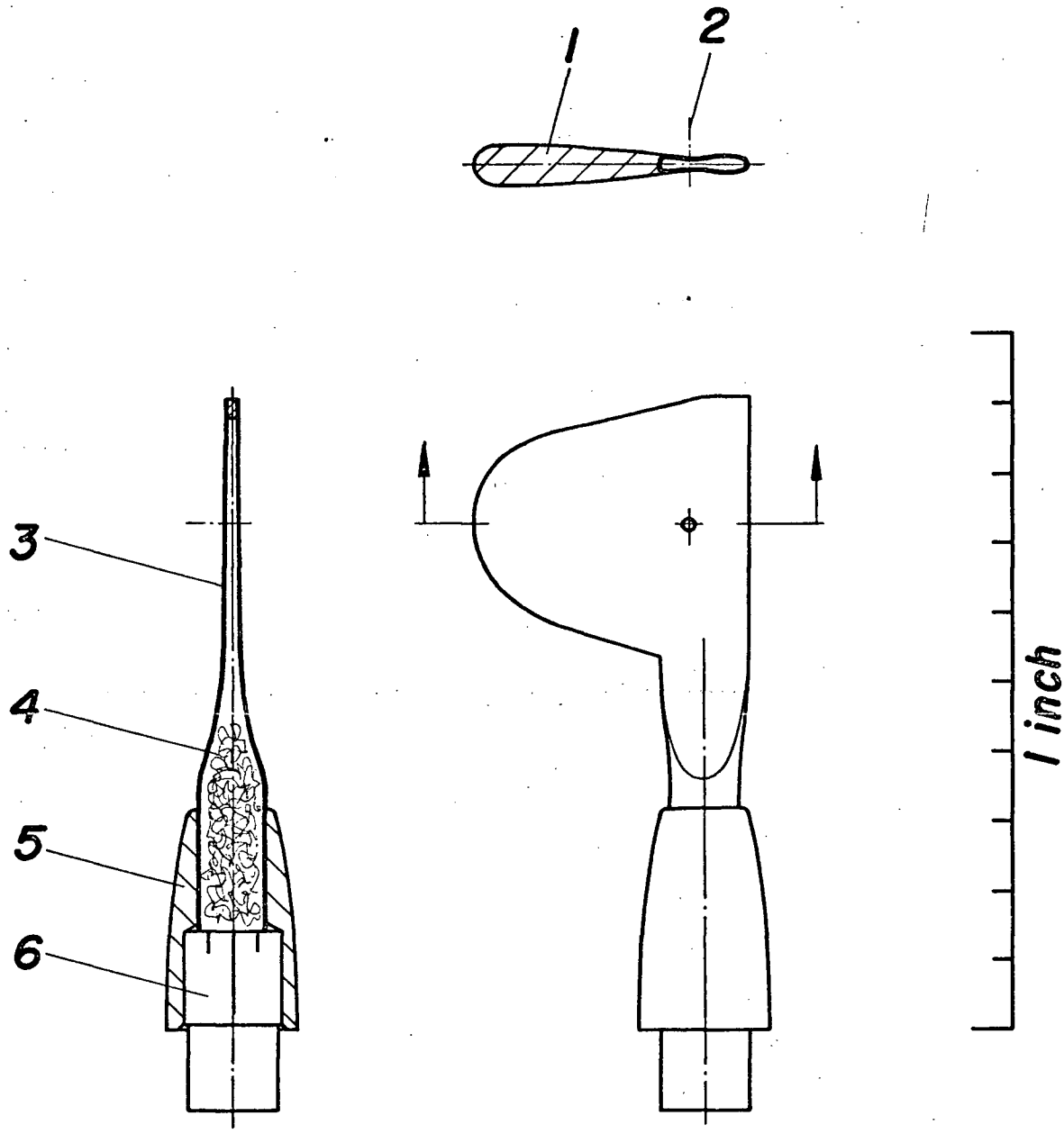

Fig.4-12 Detailed drawing of foil type pressure sensor. 1 balsa leading edge section, 2 sensing hole, 3 stainless steel tubing, 4 cotton wool, 5 teflon connector, 6 1/8-inch Bruel & Kjaer microphone.

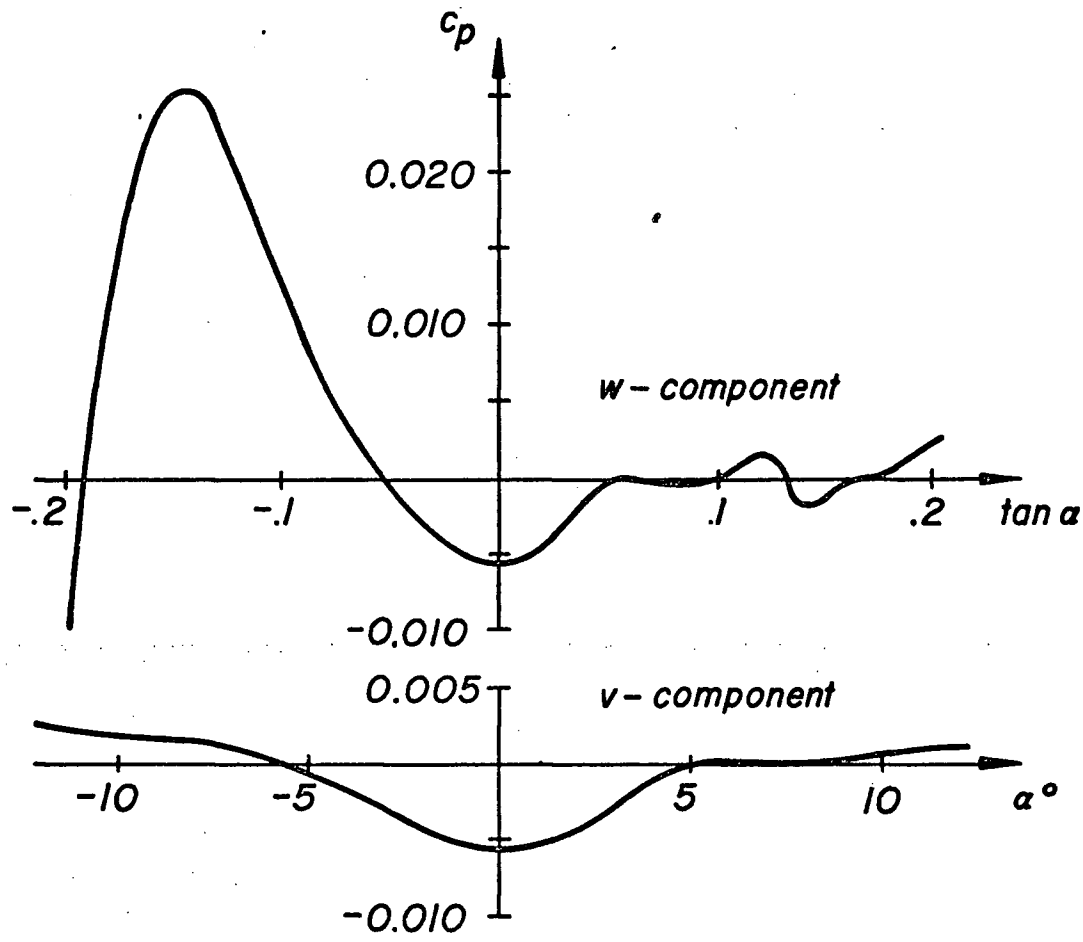

Fig.4-13 Static pressure calibrations of foil type pressure sensor shown in Fig.4-12. $c_p = (P_m - P_t)/(0.5\rho U_o^2)$. v-component: angle of attack α in the plane of the foil. w-component: α perpendicular to plane of foil.

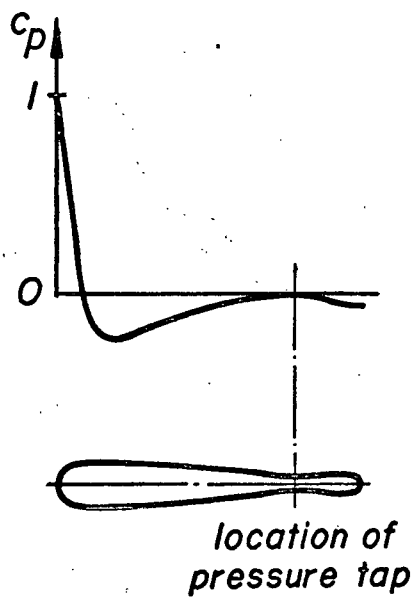

Fig.4-14 Estimated pressure distribution over foil with dip near thickening trailing edge.

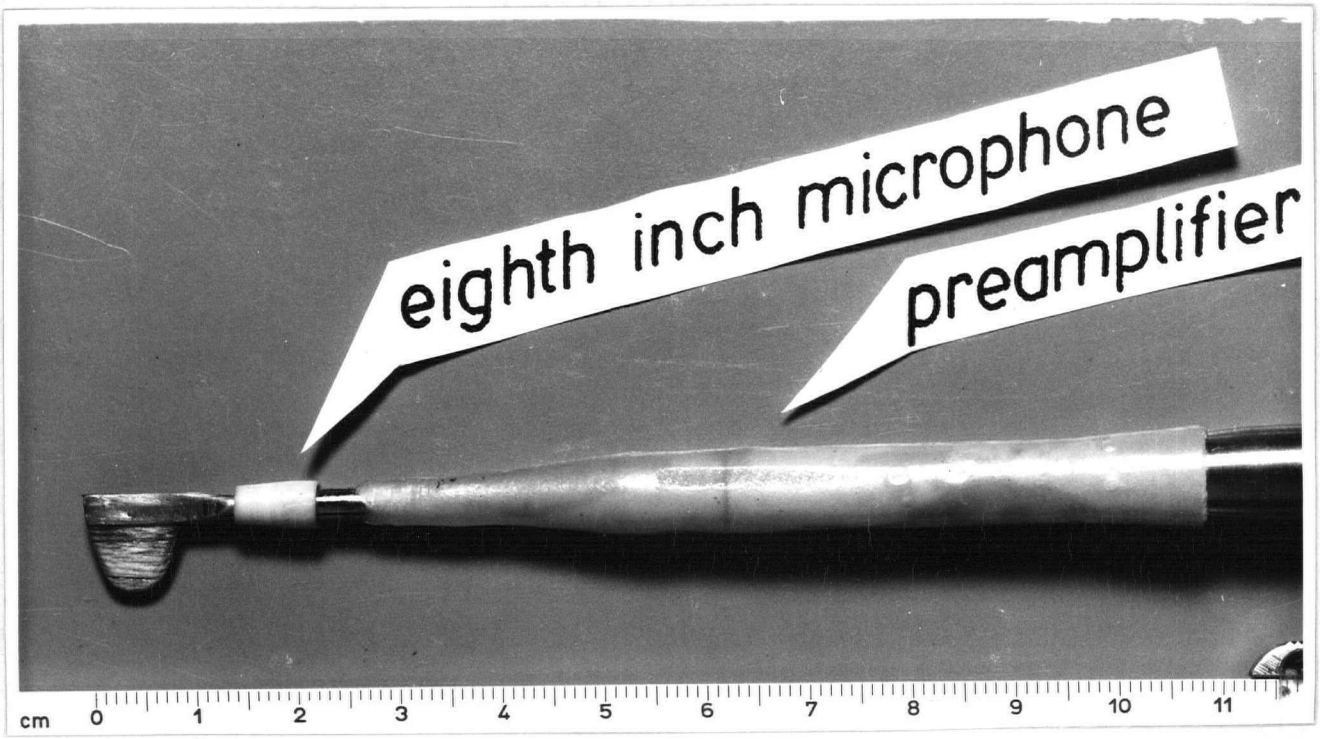

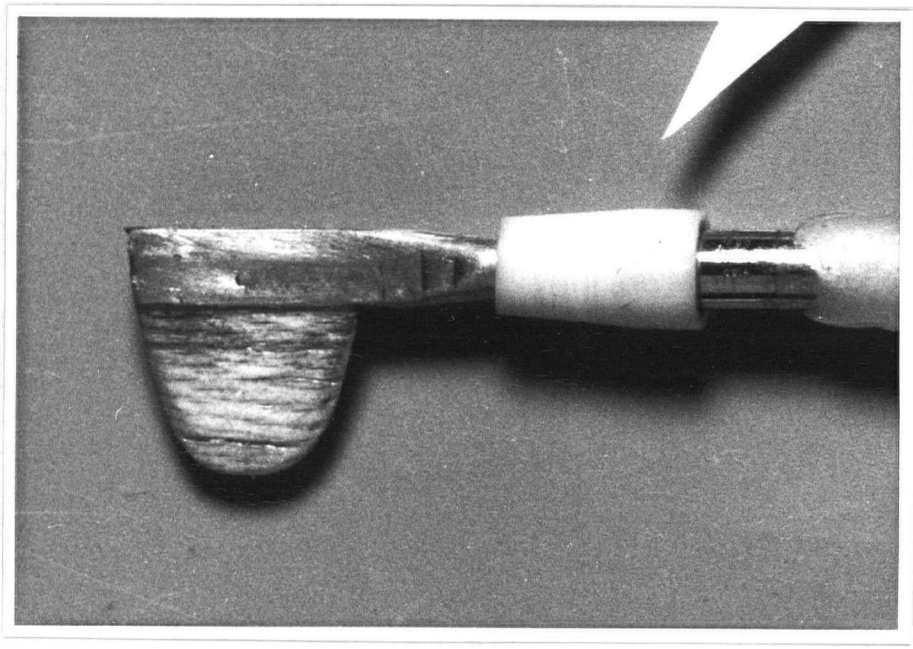

Fig.4-15 Complete foil type pressure sensor

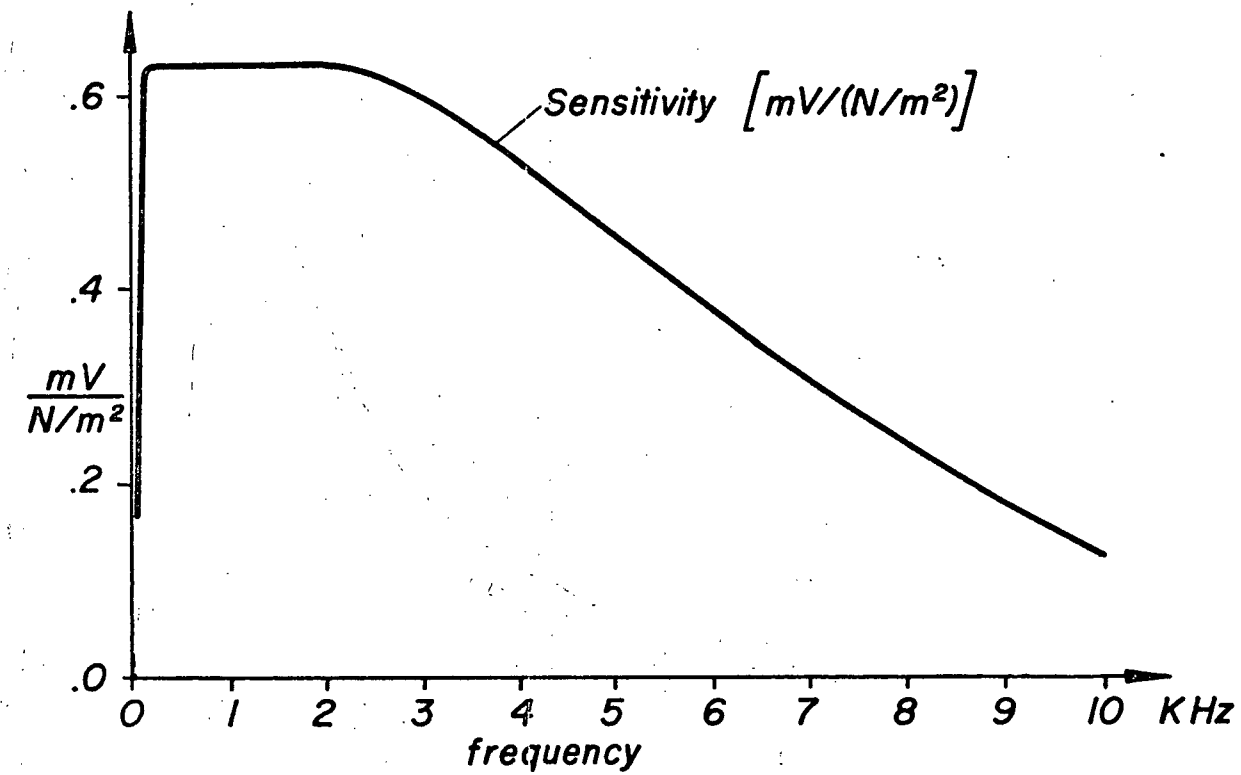

Fig.4-16 Frequency response of foil type pressure sensor.

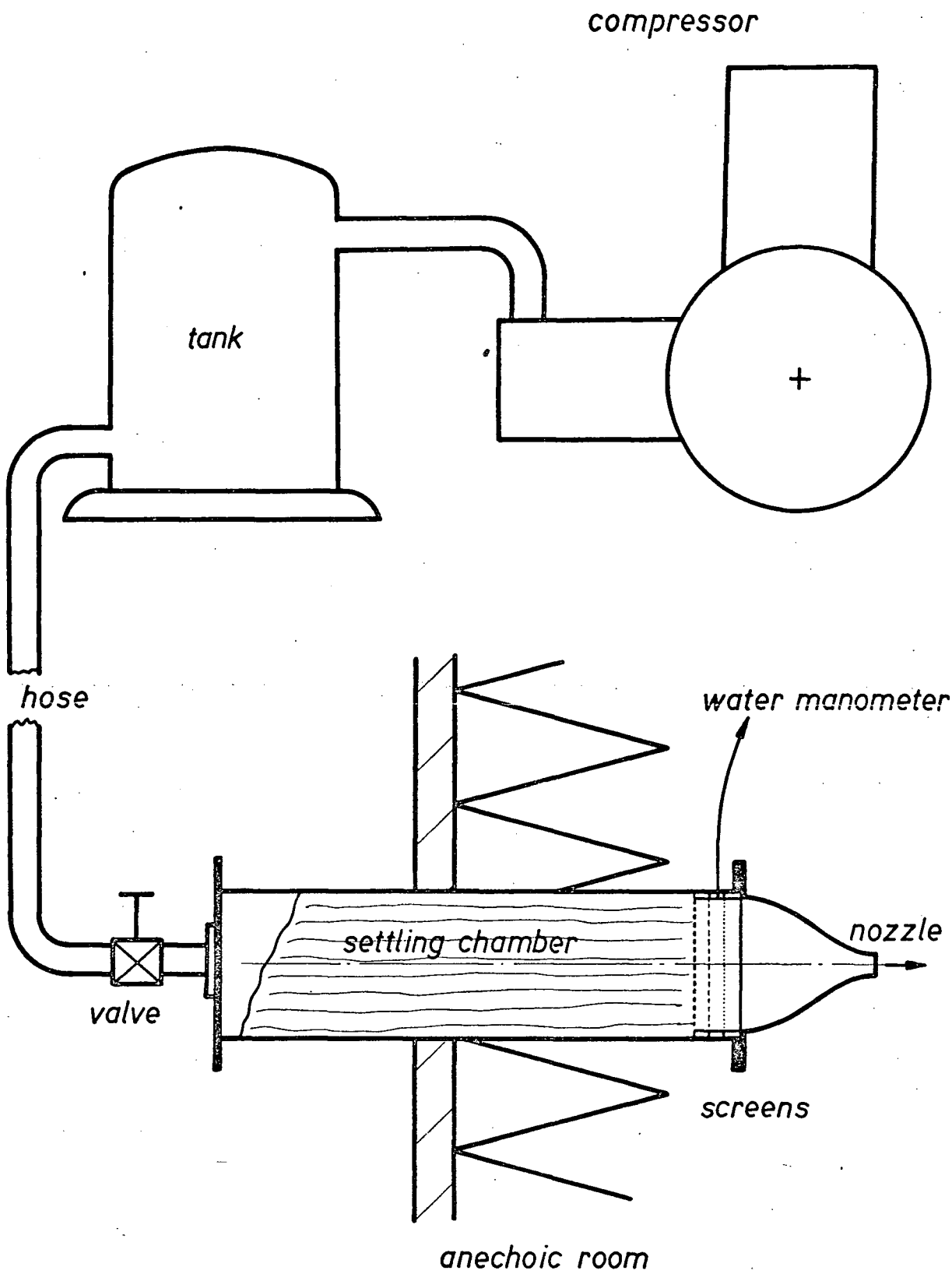

Fig.4-17 Schematic of auxiliary equipment

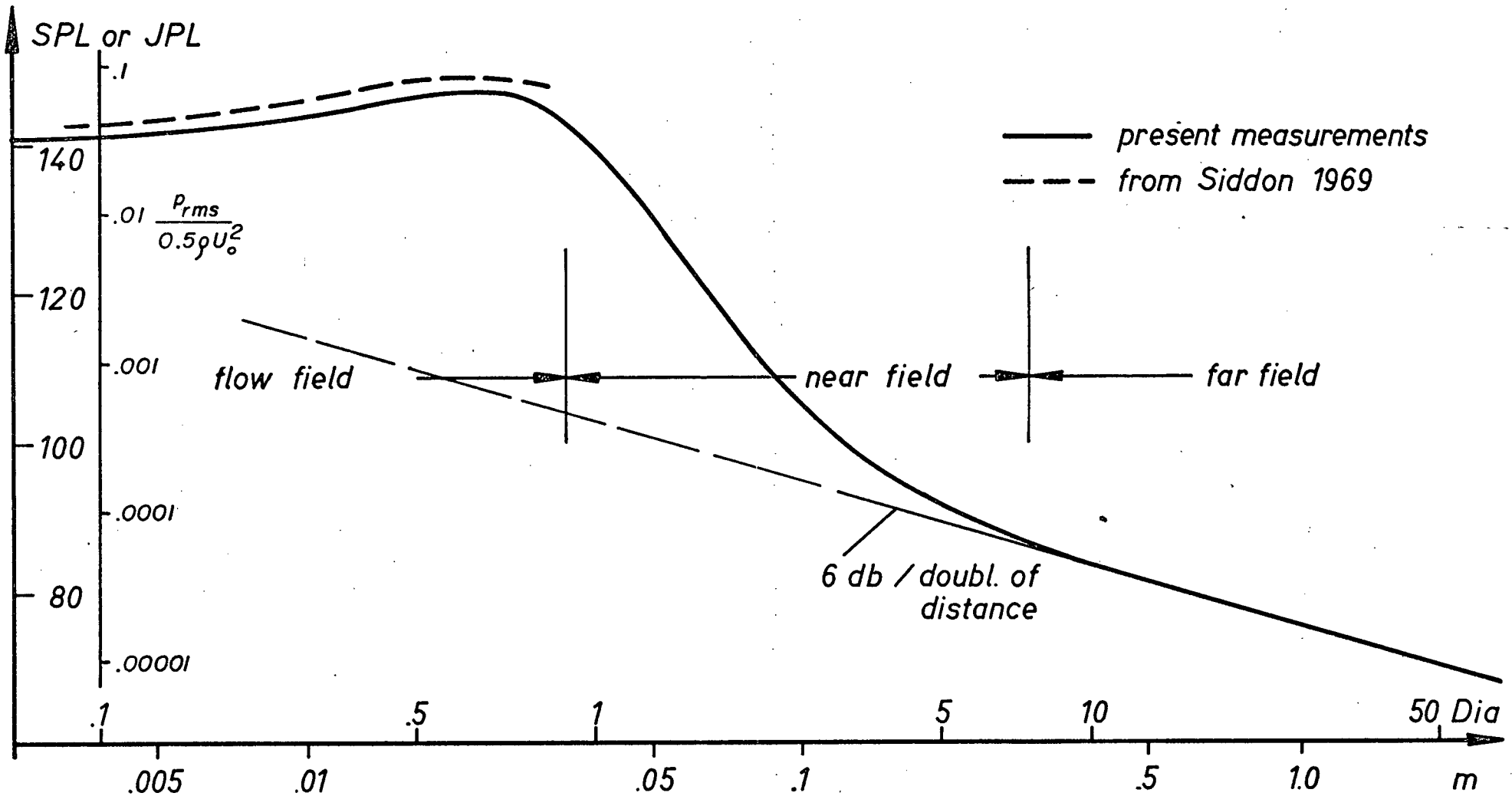

Fig.4-18 Variation of pressure fluctuation with distance from jet, starting at 4 diameters downstream in the jet and proceeding at right angles to the jet axis.

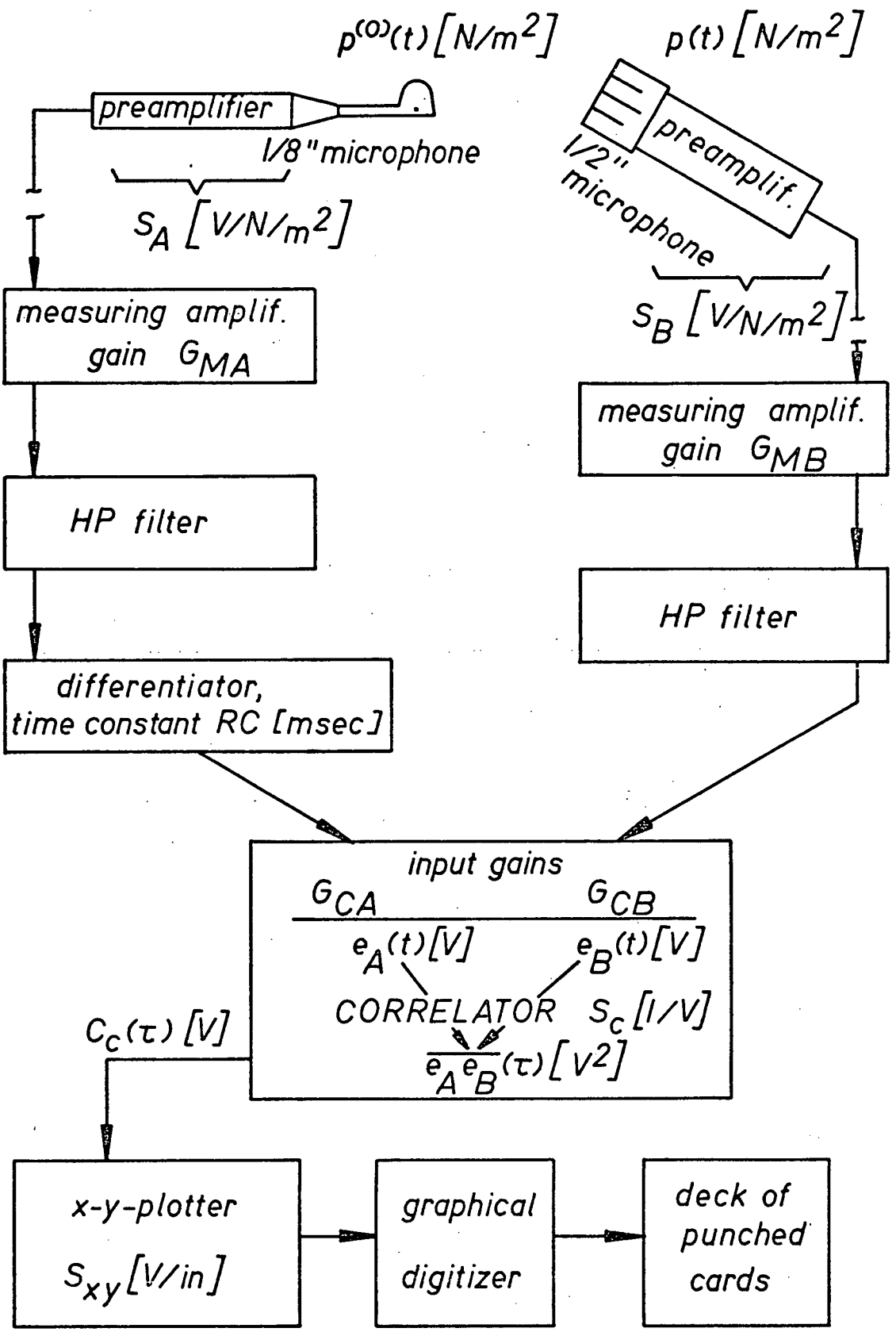

Fig.4-19 Signal flow

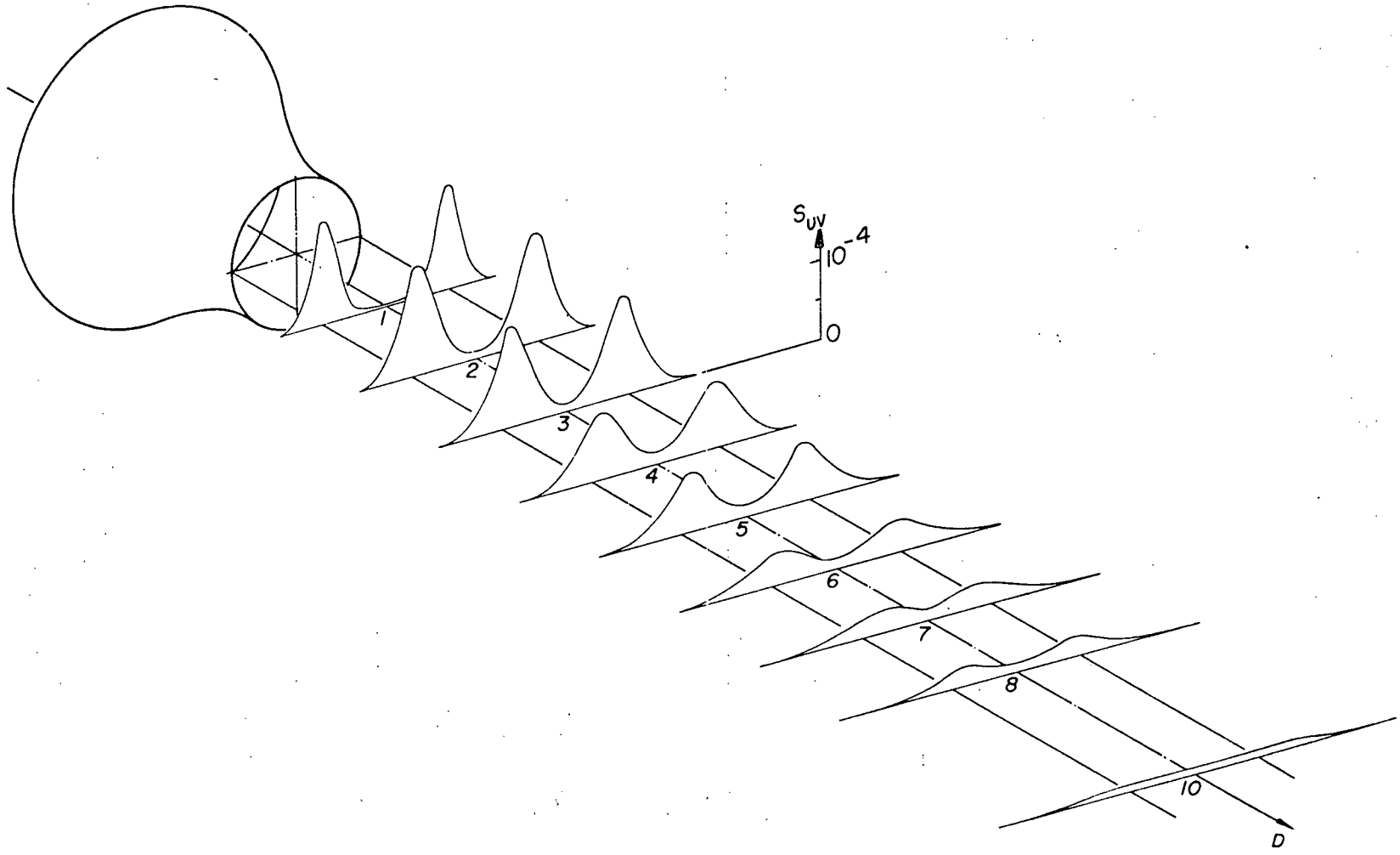

Fig.4-20 Distribution of nondimensionalized source strength per unit volume in subsonic jet for radiation at 45° to jet axis.

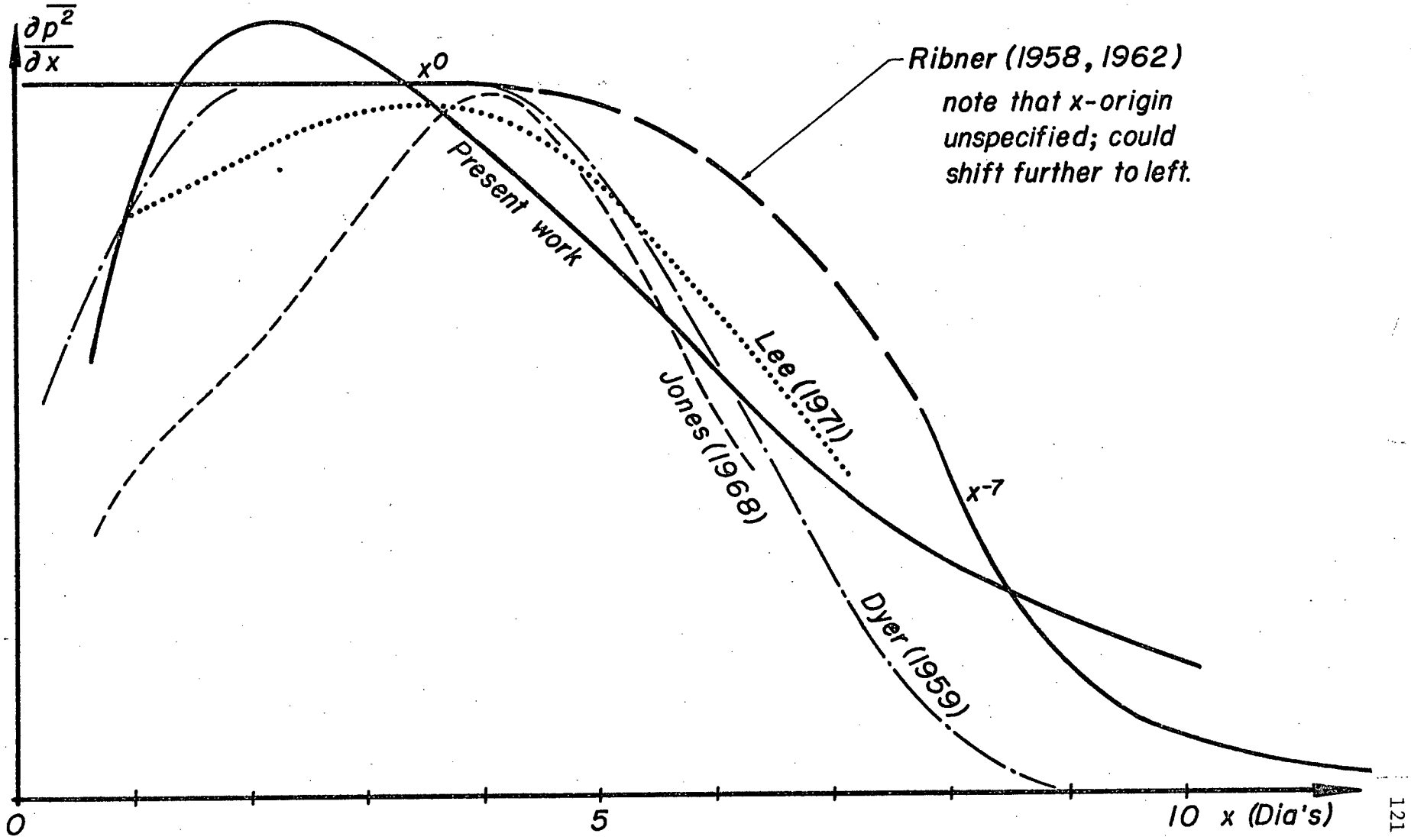

Fig.4-21 "Slicewise" distribution of source strength as integrated from Fig.4-20. Comparison with other results qualitative only.

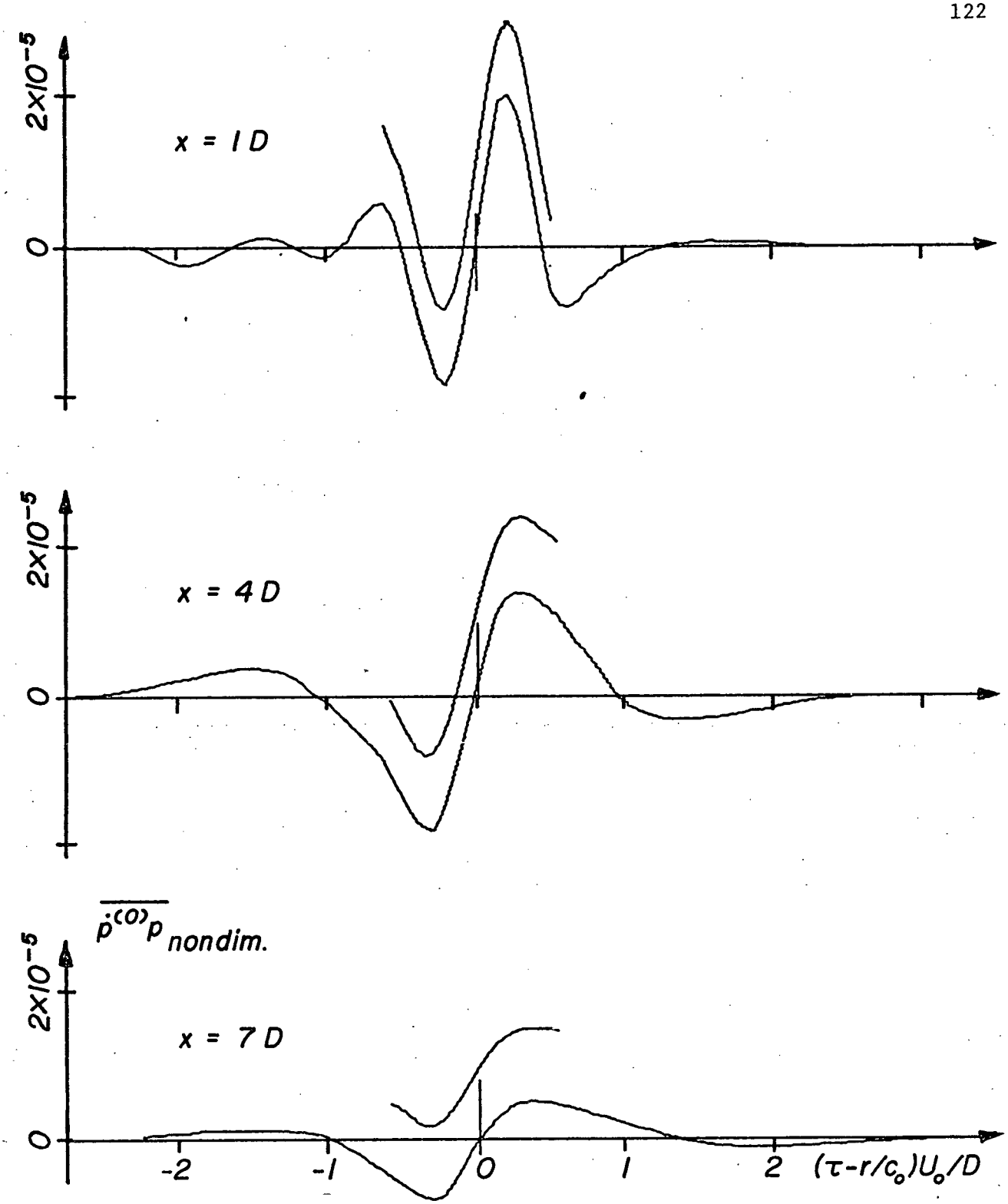

Fig.4-22a Some typical nondimensionalized causality correlation functions $\overline{\dot{p}^{(0)}p}$ at ½ diameter from the jet axis, downstream position x varying. Plotted ½ inch above is fitted 7th order polynomial. (computerplot)

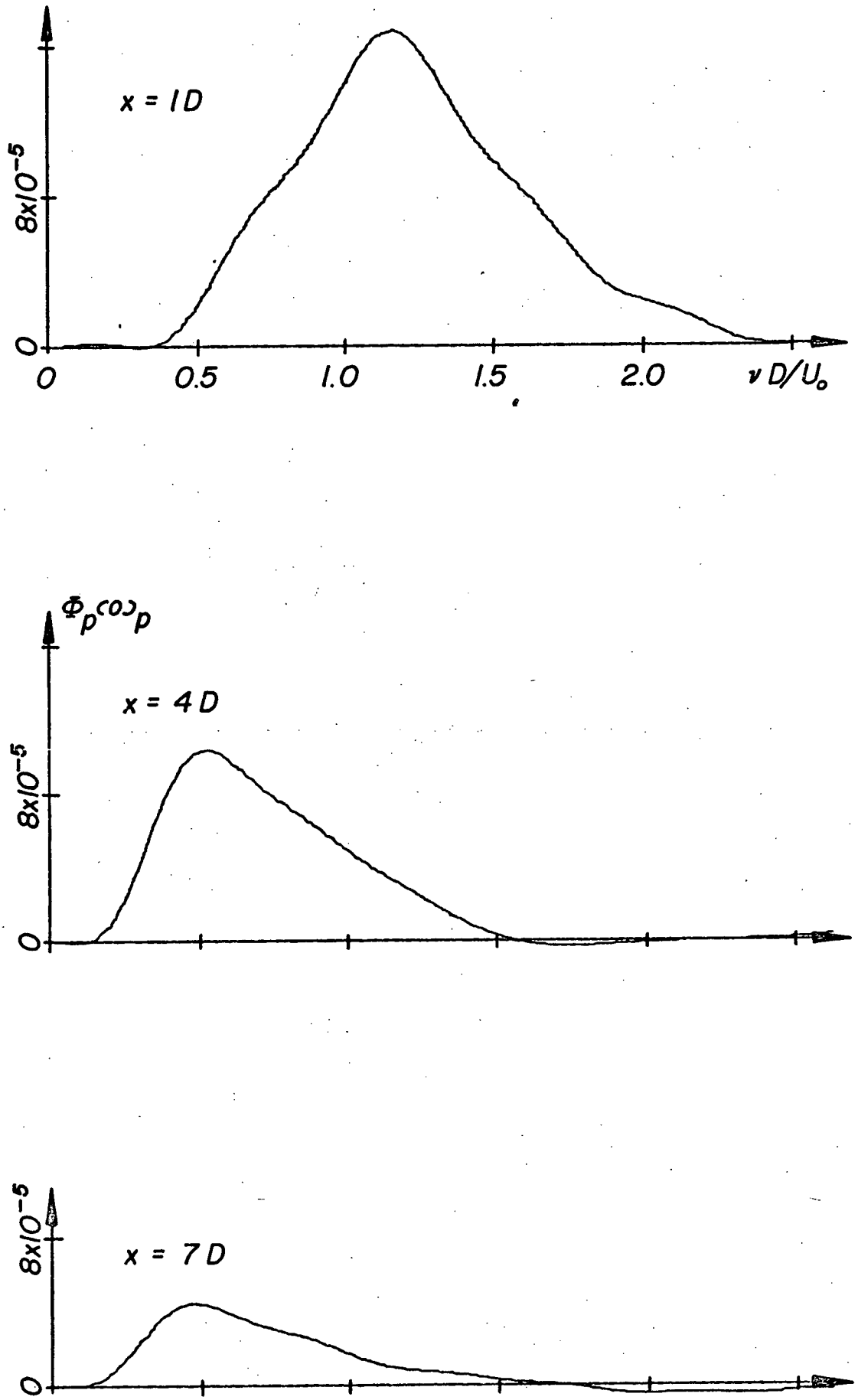

Fig.4-22b Some typical cross spectra (Sine transform of functions shown in Fig.4-22a, multiplied by frequency) (computer plot)

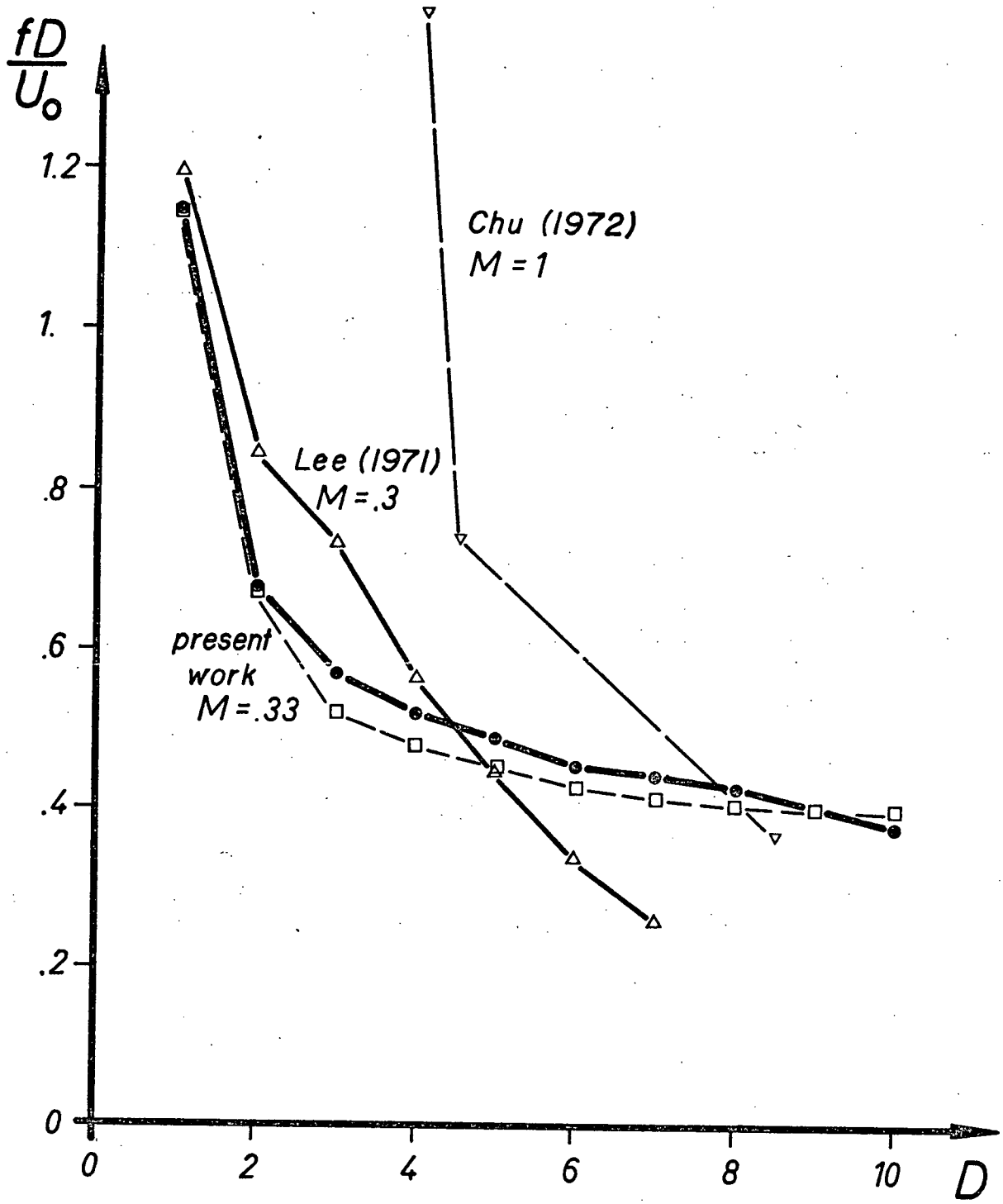

Fig.4-23 Peak frequencies versus downstream position.

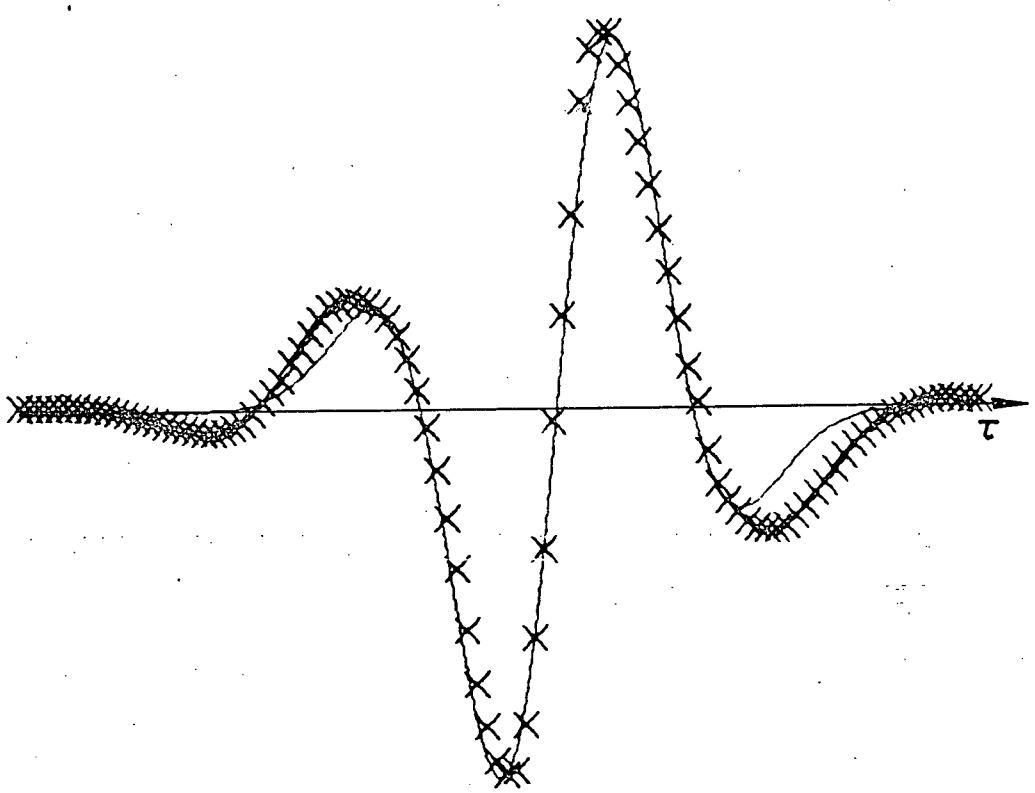

Fig.4-24 Measured causality correlation $\overline{\dot{p}^{(o)}p}$ (crosses) and fitted to it the predicted function.

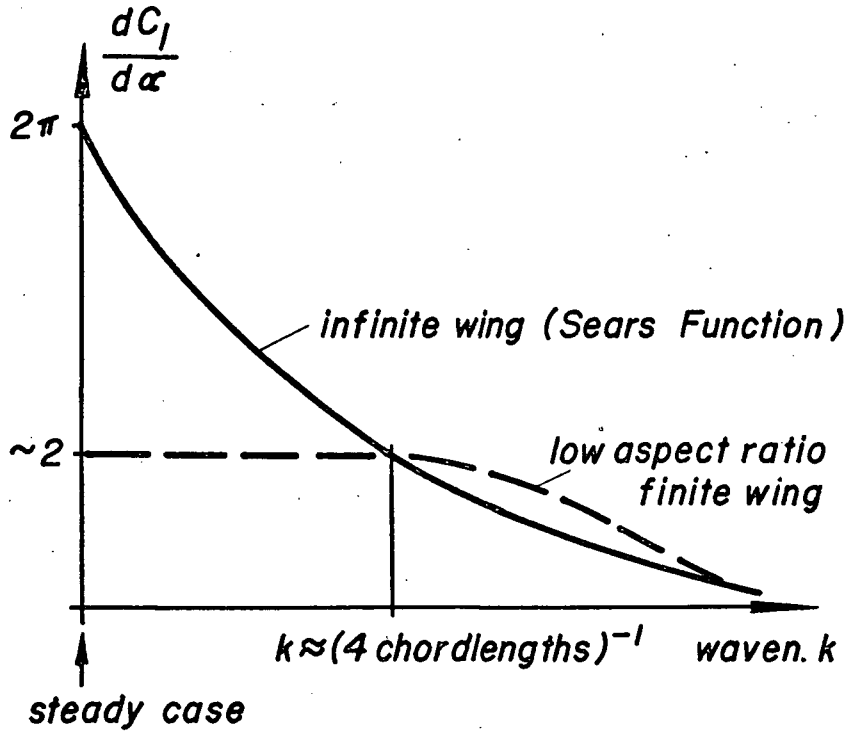

Fig.4-25 Lift curve slope as a function of wave number (Sears function)

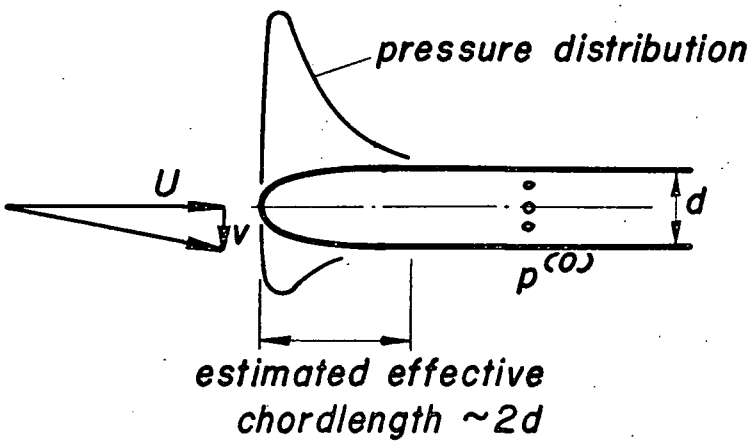

Fig.4-26 Effective chordlength on cylindrical probe.

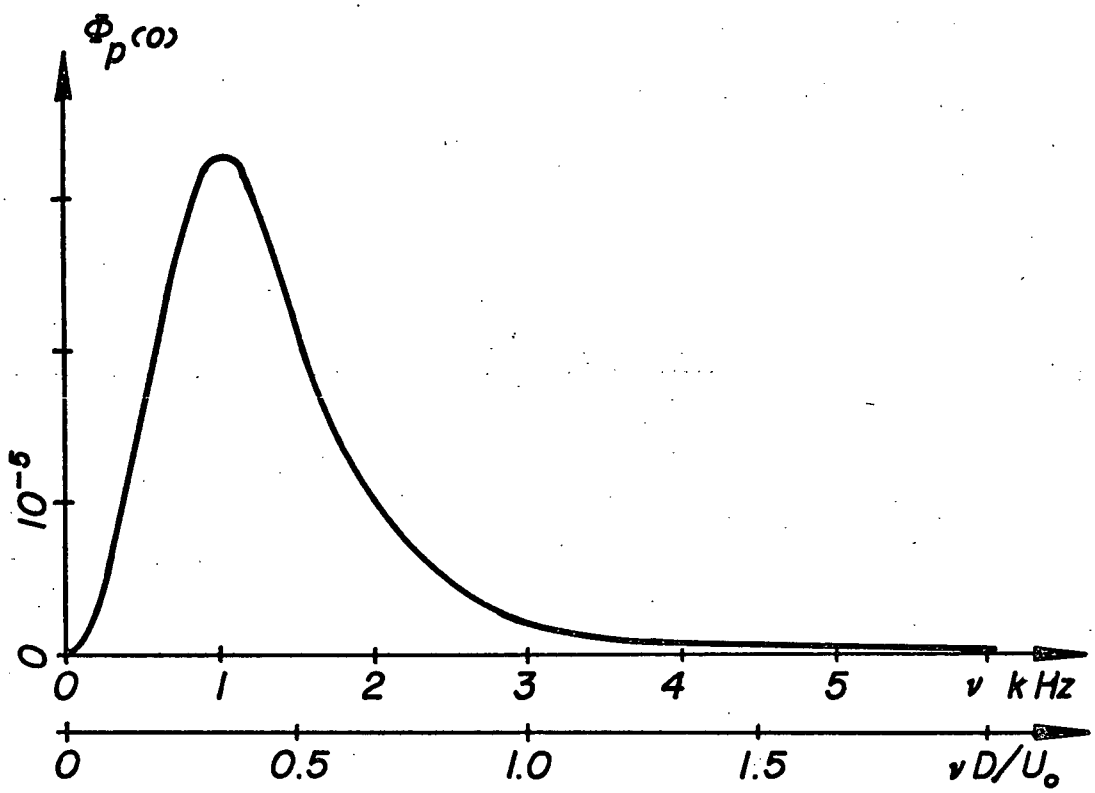

Fig.4-27 Nondimensional spectral density of the "pseudosound" $p^{(o)}$ at 4D downstream, ½D from jet axis, as measured with foil type sensor.

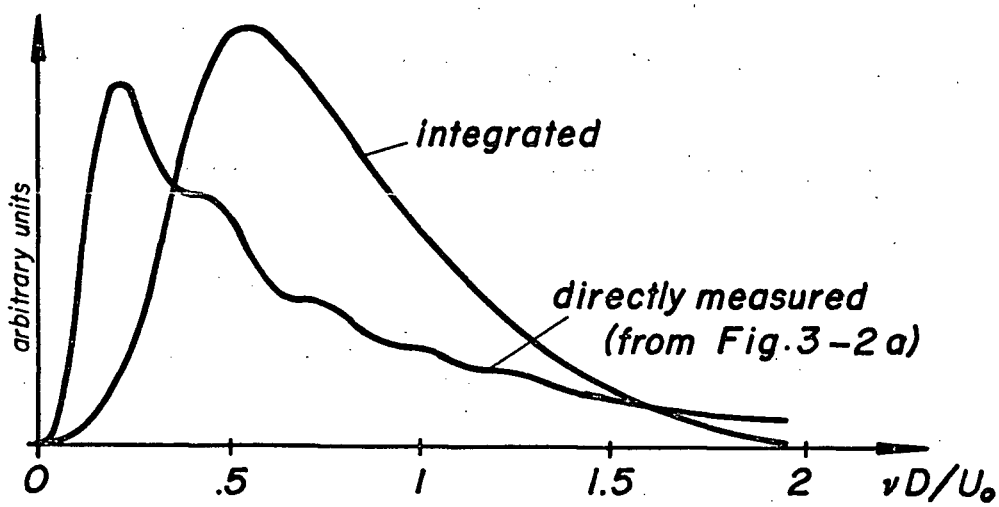

Fig.4-28 Directly measured and integrated spectrum at 45^{o} in the far field. Comparison by shape only.

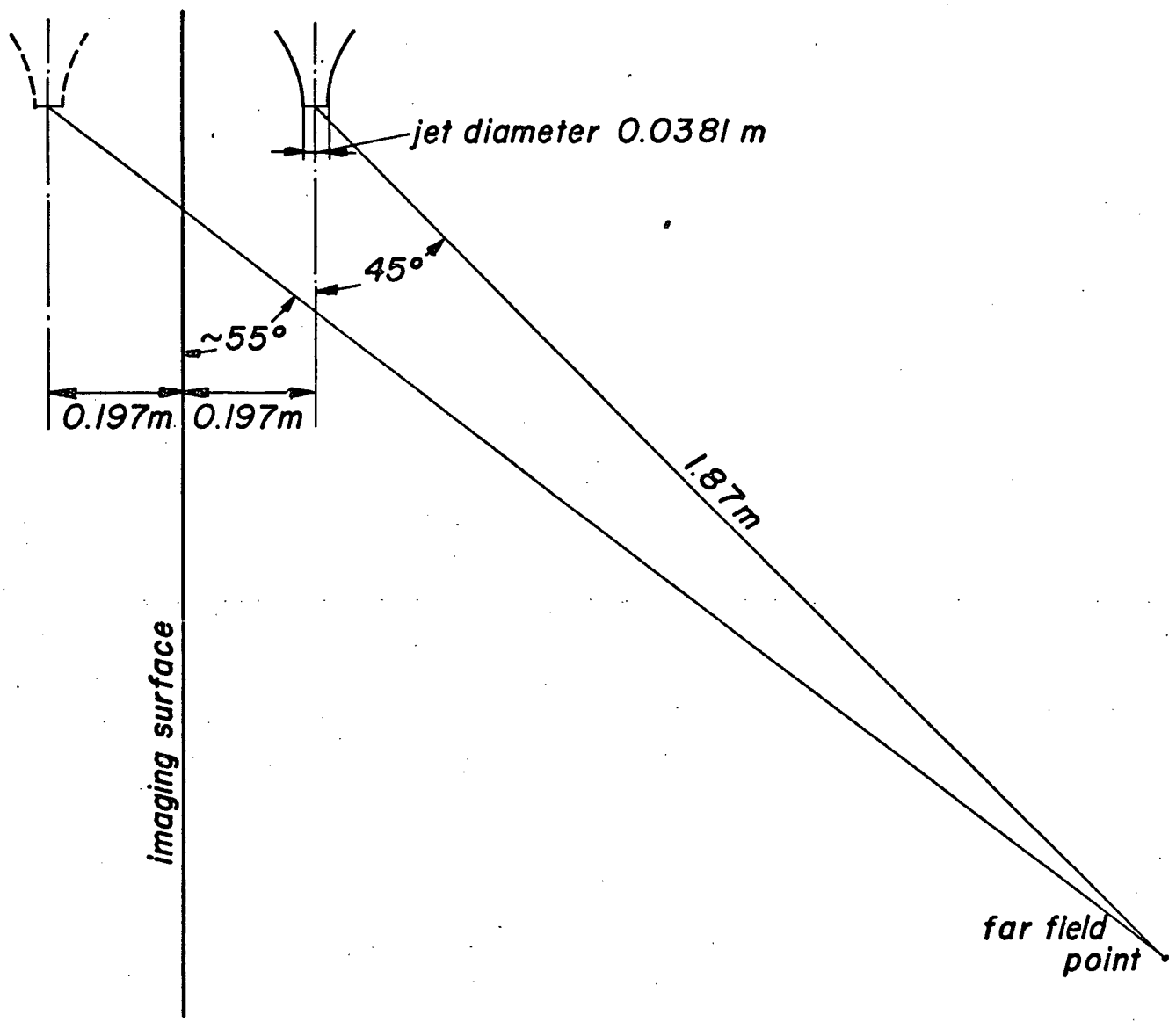

Fig.B-1 Image geometry to scale